MARMARA UNIVERSITY

INSTITUTE FOR GRADUATE STUDIES IN PURE AND APPLIED SCIENCES

DESIGN AND IMPLEMENTATION OF ADAPTIVE CONTROL FOR A NONHOLONOMIC MOBILE MANIPULATOR

GÖKHAN ERDEMİR

Ph.D. THESIS

Department of Electronics and Computer Education

SUPERVISOR

Asst. Prof. Dr. Ahmet Emin Kuzucuoğlu

CO-SUPERVISOR

Prof. Dr. Ning Xi

ISTANBUL, 2013

MARMARA UNIVERSITY

INSTITUTE FOR GRADUATE STUDIES IN PURE AND APPLIED SCIENCES

DESIGN AND IMPLEMENTATION OF ADAPTIVE CONTROL FOR A NONHOLONOMIC MOBILE MANIPULATOR

GÖKHAN ERDEMİR

(141200420060243)

Ph.D. THESIS

Department of Electronics and Computer Education

SUPERVISOR

Asst. Prof. Dr. Ahmet Emin Kuzucuoğlu

CO-SUPERVISOR

Prof. Dr. Ning Xi

ISTANBUL, 2013

MARMARA UNIVERSITY
INSTITUTE FOR GRADUATE STUDIES IN PURE AND APPLIED SCIENCES

GÖKHAN ERDEMİR, a Doctor of Philosophy student of Marmara University Institute for Graduate Studies in Pure and Applied Sciences, defended his thesis entitled "**DESIGN AND IMPLEMENTATION OF ADAPTIVE CONTROL FOR A NONHOLONOMIC MOBILE MANIPULATOR**", on December 05, 2013 and has been found to be satisfactory by the jury members.

Jury Members

Asst.Prof.Dr. Ahmet Emin Kuzucuoğlu Marmara University	(Advisor)	
Prof. Dr. Hakan Temeltaş Istanbul Technical University	(Jury Member)	
Prof.Dr. Ahmet Fevzi Baba Marmara University	(Jury Member)	
Prof. Dr. Serhat Şeker Istanbul Technical University	(Jury Member)	
Assoc.Prof.Dr. Haluk Küçük Marmara University	(Jury Member)	

APPROVAL

Marmara University Institute for Graduate Studies in Pure and Applied Sciences Executive Committee approves that GÖKHAN ERDEMİR be granted the degree of Doctor of Philosophy in Department of Electronics and Computer Education, Computer and Control Education Program on December 30, 2013. (Resolution no:2013/35-03).

Director of the Institute
Prof. Dr. Abdulkerim Kar

ACKNOWLEDGMENT

I would like to express my sincere gratitude to Assist.Prof.Dr. Ahmet Emin Kuzucuoğlu for his guidance and support throughout this research project. His great knowledge and innovative ideas made this dissertation possible. It has been a privilege and a pleasure to work with him. I would like to thank my co-supervisor, Prof. Dr. Ning Xi for providing me with the opportunity to conduct my research in the Robotics and Automation Laboratory (RALAB) in Michigan State University (MSU). It was a great honor to work under direction of him for me. His excellent knowledge and experiences on robotics were my guide during tough days. During my time at RALAB and MSU, I have been helped and influenced by a large number of people. In particular, I would like to thank Mr. Yunyi Jia and Dr. W.C. King Lai. Their presence and knowledge helped promote a friendly and creative environment. And also, I would like to thank to Prof.Dr.Hassan K. Khalil from MSU for his helps.

I also sincerely thank Prof.Dr. Hakan Temeltaş and Assoc. Prof. Dr. Haluk Küçük for their time, helps and valuable suggestions during serving on my dissertation advisory committee and my doctoral jury, and also Prof. Dr. Serhat Şeker, Prof.Dr. A. Fevzi Baba, Prof.Dr. Erol Akata and Assist. Prof. Dr. Erkan Kaplanoğlu for serving as examiners in my dissertation defense. I am also gratefull to Prof.Dr. Zafer Aslan, Mr. Şener Sancar, Mr. Şafak Yüksel, Mr.Birol Gençyılmaz and Ms. Lütfiye Kuşak and for their support during my tough times.

I am very thankful to my wife, Gulfem, for her great support and belief in my ability. She has always been a constant source of love and encouragement while I pursued my education. I would like to thank to my son, Demir, not only for his excellent arts on my notes but also for his vivacious smiles. I also would like to thank all my family and friends.

Finally, I would like to thank The Scientific and Technological Research Council of Turkey (TUBITAK) for their support and funding.

December, 2013 **Gökhan Erdemir**

TABLE OF CONTENTS

Page Nr.

ACKNOWLEDGMENT ..... **i**

TABLE OF CONTENTS ..... **iii**

ABSTRACT ..... **vii**

ÖZET ..... **ix**

CLAIM FOR ORIGINALITY ..... **xi**

SYMBOLS ..... **xiii**

ABBREVIATIONS ..... **xv**

LIST OF FIGURES ..... **xvii**

LIST OF TABLES ..... **xix**

1. INTRODUCTION **1**

1.1. Background and Motivation 1

1.2. Historical Review of Related Studies 4

1.3. Methodology and Contributions 8

1.4. Dissertation Outline 9

2. STRUCTURE OF THE NON-HOLONOMIC MOBILE MANIPULATOR **11**

2.1. Introduction 11

2.2. Schunk LWA3: The 7 DOF Redundant Robot Arm 12

2.2.1. Physical and Geometric Data of the 7 DOF Redundant Robot Arm 15

2.2.1.1. Motors 15

2.2.1.2. Connectors 16

2.3. Segway RMP 400: 4 Wheel – Drive Skid – Steering Mobile Base 17

3. THEORY AND MODELING OF THE NON-HOLONOMIC MOBILE MANIPULATOR 21

3.1. Introduction 21

3.2. The 7 DOF Redundant Robot Arm..... 21

3.2.1. Modeling and Identification 24

3.2.2. Kinematics.....24

3.2.2.1. Forward Kinematics 24

3.2.2.2. Inverse Kinematics 26

3.2.3. Calculation of the Center of Mass of the Whole Arm.....31

3.2.4. Kinetic and Potential Energy of the LWA3 33

3.2.4.1. The Inertia Tensor 33

3.2.4.2. Kinetic Energy for a 7DOF Robot Arm 34

3.2.4.3. Potential Energy for a 7DOF Robot Arm..... 35

3.2.4.4. Equations of Motion 36

3.2.5. Dynamics.....39

3.2.6. Friction Model 39

3.2.7. Control Design.....40

3.2.8. Models Verification.....41

3.3. The 4 Wheel – Drive Skid – Steering Mobile Robot (4WD-MR)..... 46

3.3.1. Modeling of Electrical Drive Subsystem of the RMP400.....48

3.3.2. Kinematics.....50

3.3.3. Dynamics.....56

3.3.4. Control Algorithm 62

3.3.5. Models Verification.....63

3.4. The Nonholonomic Manipulator 67

3.4.1. Redundancy Resolution 67

3.4.2. Feedback Linearization of the Nonholonomic Mobile Manipulator 70

4. ADAPTIVE CONTROL DESIGN FOR THE NON-HOLONOMIC MOBILE MANIPULATOR 73

4.1. Introduction 73

4.2. Model Reference Adaptive Control 74

4.3. Adaptive Tracking Control Design 76

4.3.1. Linearization and decupling 76

4.3.2. Parameter error convergence 78

4.3.3. Tracking control design 80

5. CASE STUDIES AND DISCUSSIONS 81

5.1. Simulation Validation and Results 81

5.2. Real System Experiments 84

5.3. Discussions 86

6. CONCLUSIONS 89

REFERENCES 91

CURRICULUM VITAE 101

ABSTRACT

In recent years there has been observed a growing interest in the mobile manipulation area. Mobile manipulation is usually realized by mobile manipulator which consists of a ground vehicle and a robot arm. This kind of platform can be used in lots of civilian and military areas, including harmful material operation, searching and rescue, demining, explosive ordnance disposal and even battlefield.

A lot of research concentrates on the modeling, control and application of mobile manipulators. One essential requirement for using the mobile manipulator for different applications is the property of stable and reliable mobility, which requires the ground vehicle to move stably, robustly and smoothly under different internal or external uncertainties and disturbances. Thus, the main goal of this study is to design a dynamic controller to control a mobile manipulator with a 4WD ground vehicle to track an assigned desired trajectory under unknown vehicle parameters.

Mobile manipulators offer a dual advantage of mobility and dexterity of a mobile robot and a manipulator. They are composed of a manipulator and a mobile platform. Mobile manipulators have a much larger workspace than fixed–base manipulators. Also, they are more capable than mobile robots. While an on-board manipulator reaches out and performs manipulation tasks, the role of the mobile platform is to adjust a position of the mobile manipulator according to preferred configuration. Mobile manipulators can be used in various military and civilian areas including space exploration, military operations, auto-manufacturing and health-care, etc. In this study, an adaptive tracking controller for a mobile manipulator which consists of a 4-wheel drive(4WD) ground vehicle and a 7-DOF robot arm with unknown vehicle parameters is designed to track an assigned desired trajectory under unknown vehicle parameters. The simulation results are demonstrated the correctness and effectiveness of the performance of the proposed controller.

ÖZET

Son yıllarda, mobil manipülasyon alanında ilginin giderek arttığı görülmektedir. Mobil manipülasyon, robot kolu ve mobil bir robottan oluşan bir mobil manipülatör tarafından gerçekleştirilmektedir. Bu tür platformlar; zararlı maddelerin işlenmesi, arama ve kurtarma, mayın temizleme, patlayıcı madde imha, savaş da dâhil birçok sivil ve askeri uygulamalarda, madencilikte ve uzay araştırmaları gibi birçok alanda kullanılabilmektedir.

Birçok araştırma mobil manipülatörlerin modellenmesi, kontrolü ve uygulaması üzerinde yoğunlaşmaktadır. Farklı uygulamalarda mobil manipülatör kullanımı için temel gereksinim, kararlılık ve güvenli hareketliliğin, farklı iç ve dış belirsizlik ve bozucu etkileri altında da mobil robotun kararlı, düzgün ve dayanıklı olarak sağlanmasıdır. Be nedenlerden, dört tekerden tahrikli bir mobil manipülatörü, bilinmeyen araç parametreleri altında istenilen yörüngeyi takip edebilmesi amacıyla kontrol etmek için dinamik bir denetleyici tasarlamak bu çalışmanın esas amacıdır.

Mobil manipülatörler, mobil robotların yeteneklerini (beceri) ve hareketlilik avantajlarını bir arada sunmaktadır. Bu özellikler, manipülatör ve mobil robotun birleşiminden ortaya çıkan özelliklerdir. Mobil manipülatörler sabit tabanlı manipülatörlere göre çok daha büyük bir çalışma uzayına sahiptirler. Ayrıca, mobil robotlardan daha üstün yeteneklere sahiptirler. Bir mobil robotun görevi, manipülatör bir görevi yerine getirmek için bir noktaya ulaşmaya çalışırken tercih edilen konfigürasyona göre mobil manipülatörün konumunu ayarlamaktır. Bu özelliklerinden ötürü, mobil manipülatörler uzay araştırmaları, askeri operasyonlar, otomatik üretim ve sağlık gibi alanlar dahil olmak üzere çeşitli askeri ve sivil alanlarda kullanılabilir.

Bu çalışmada, bir dört tekerden tahrikli mobil robot ile 7 serbestlik dereceli robot kolundan oluşan bir mobil manipülatör için bilinmeyen araç parametleri tabanlı bir adaptif yörünge takip denetleyicisi tasarlanmıştır. Simülasyon sonuçları önerilen denetleyicinin performansınının doğruluğunu ve etkinliğini göstermiştir.

CLAIM FOR ORIGINALITY

DESIGN AND IMPLEMENTATION OF ADAPTIVE CONTROL FOR A NONHOLONOMIC MOBILE MANIPULATOR

In this dissertation project, modeling and identification of the non-holonomic mobile manipulator are presented. The nonholonomic mobile manipulator consists of two parts: robot arm and mobile base. The Schunk LWA3(LWA3) manipulator is used as robot arm of the mobile manipulator. The Segway RMP 400 4WD skid-steering mobile robot (RMP400) is used as mobile base of the mobile manipulator. This kind of platform can be used in lots of civilian and military areas, including harmful material operation, searching and rescue, demining, space explorations, explosive ordnance disposal and even battlefield. In the first part of this study, full model identification of the LWA3 is performed. The LWA3 is very sensitive manipulator for especially precise manipulation tasks. The high accuracy positioning capabilities, dexterity, back-drivability capability, and zero backlashes of its joints make the LWA3 ideal for not only industrial applications but also scientific researches. Unfortunately, there are not model based experimental studies about dynamics of the LWA3 manipulator in literature. To our knowledge and literature reviews, our work is the first study dynamic model verification and on dynamic based position and velocity control of the LWA3. In the second part of this study, full model identification of the RMP400 is performed. RMP400 are used in lots of civilian and military areas. The aim of this part is to analyze the characteristic behavior of SSMR and to develop the closed-loop controller for RMP400. According to our literature reviews, our work is the first study for full model identification, analysis and control of the RMP400. In the last part of this study, adaptive control algorithm is developed for the non-holonomic mobile manipulator. To our knowledge and literature reviews, our work is the first study for application of adaptive control to this kind of the non-holonomic mobile manipulator. Because of all reasons which are explained in above, this study is original and is not a copy of any work. It will be very important source for robot modeling and control area.

November, 2013	**Supervisors**	**Student**
	Assist.Prof.Dr. A. Emin Kuzucuoğlu	**Gökhan Erdemir**
	Prof.Dr. Ning Xi	

SYMBOLS

μ	Tire – road total friction coefficient
V_x	Longitudinal tire speed
V_y	Lateral tire speed
w	Wheel angular speed
F_z	Normal force
R	Tire radius
μ_0	Tire – road static friction coefficient
V_0	Speed constant
k_x	Tire initial infinitude relative longitudinal stiffness
k_y	Tire initial infinitude relative lateral stiffness
E_y	Tire force characteristic parameter
F_f	Roll friction
F_w	Wind friction
F_x	Longitudinal tire force
F_y	Lateral tire force
m	Mass of vehicle
I_z	Moments of inertia about Z axis
I_f	Distance from front axle to center of gravity
I_r	Distance from rear axle to center of gravity
d	Distance between the left and the right wheel
θ	Yaw angle
M_f	Roll resistance moment
J_w	Moment of inertia

g	Acceleration of gravity
h	Height of center of gravity
C_0	Wind block coefficient
A	Wind area
γ	Yaw rate
f	Roll resistance coefficient
u	Longitudinal speed of center of gravity in fixed reference frame
v	Lateral speed of center of gravity in fixed reference frame
T_d	Electromagnetic torque of induction motor
n_p	Number of poles

ABBREVIATIONS

4WD	Four wheel drive
CG	Center of gravity
COM	Center of mass
DH	Denavit Hartenberg representation
DOF	Degree of freedom
EJ	Extended Jacobian
ICR	Instantaneous center of rotation
LWA3	Schunk LWA3 7 DOF manipulator
PG	Projected Gradient
POS	Products of sum
RG	Reduced Gradient
RMP400	Segway RMP400 mobile robot
SOP	Sum of products
SS	Skid – Steering
SSMR	Skid – Steering mobile robot

LIST OF FIGURES

Page Nr.

Figure 1.1. Different types of mobile manipulators 1

Figure 1.2. Structure and coordinate frame of 4WD mobile manipulator..... 2

Figure 1.3. Developed mobile manipulation platform in different views 3

Figure 2.1. Schunk LWA3 Robot Arm (a), Segway RMP 400 mobile robot (b)..... 11

Figure 2.2 The non-holonomic mobile manipulator..... 12

Figure 3.1. 3D model of the Schunk LWA3 Manipulator..... 23

Figure 3.2. Coordinate frame of 7 DOF manipulator..... 24

Figure 3.3. Chart for Solving $\boldsymbol{\theta 4}$..... 27

Figure 3.4. Definition of Elbow Angle..... 28

Figure 3.5. Rotation of SEW Plane 29

Figure 3.6. Control Law Structure..... 40

Figure 3.7. Desired trajectory and end-effector trajectory tracking performance..... 42

Figure 3.8. Joint angle of joint 1..... 42

Figure 3.9. Joint angle of joint 2..... 43

Figure 3.10. Joint angle of joint 3..... 43

Figure 3.11. Joint angle of joint 4..... 44

Figure 3.12. Joint angle of joint 5..... 44

Figure 3.13. Joint angle of joint 6..... 45

Figure 3.14. Joint angle of joint 7..... 45

Figure 3.15. The Segway RMP400 Mobile Robot..... 46

Figure 3.16. Free body diagram of the SSMR..... 47

Figure 3.17. Block diagram of an electrically driven mobile robot 47

Figure 3.18. Turning model of the SSMR 48
Figure 3.19.Configuration of right side of Segway RMP 400..... 49
Figure 3.20.Velocities and forces of one Wheel 52
Figure 3.21.Wheel velocities 53
Figure 3.22.Active and Resistive Forces of the RMP400 57
Figure 3.23. Motion control for the RMP400..... 63
Figure 3.24. Desired trajectory on the vehicle..... 64
Figure 3.25.Desired trajectories of the three states 64
Figure 3.26. Tracking results of the three states..... 65
Figure 3.27. Tracking errors of the three states..... 65
Figure 3.28. Parameter convergence result 66
Figure 3.29. Step response of x with estimated parameters 66
Figure 4.1. Block diagram of robot control..... 73
Figure 4.2. Block diagram of model reference adaptive control..... 74
Figure 4.3. Adaptive tracking system diagram..... 75
Figure 5.1. Desired trajectory on the 4WD ground vehicle..... 81
Figure 5.2. Desired trajectories and tracking results of the three states 82
Figure 5.3. Tracking errors of the three states..... 83
Figure 5.4. Parameter convergence result 83
Figure 5.5. Step response of x with estimated parameters 84
Figure 5.6. View from path tracking experiment 85
Figure 5.7. View from position and precise trajectory planning experiment 1..... 85
Figure 5.8. View from position and precise trajectory planning experiment 2..... 86
Figure 5.9. View from position and precise trajectory tracking experiment..... 86

LIST OF TABLES

Page Nr.

Table 2.1. The Schunk LWA3 7 DOF Robotic System's Configuration 13

Table 2.2. Specification of joints 13

Table 2.3. Properties of PRL modules 14

Table 2.4. Moment load of PRL modules 14

Table 2.5. Motor weight parameters 15

Table 2.6. COM of the motors relative to their local frames 16

Table 2.7. Connectors weight parameters 16

Table 2.8. Center of mass of the connectors relative to their local frames 17

Table 2.9. Dimensions of RMP 400 17

Table 2.10. Propulsion system properties of RMP 400 18

Table 2.11. Command interface properties of RMP 400 18

Table 2.12. Performance specifications of RMP 400 18

Table 2.13. Battery specifications of RMP 400 19

Table 2.14. Range and energy specifications of RMP 400 19

Table 3.1. DH-Parameters 7DOF Modular Robotic System 25

1. INTRODUCTION

1.1. Background and Motivation

Mobile manipulators offer a dual advantage of mobility and dexterity of a mobile robot and a manipulator. They are composed of a manipulator and a mobile platform. Mobile manipulators have a much larger workspace than fixed–base manipulators. Also, they are more capable than mobile robots. Different types of mobile manipulators are shown in Figure 1.1.

While an on-board manipulator reaches out and performs manipulation tasks, the role of the mobile platform is to adjust a position of the mobile manipulator according to preferred configuration. Mobile manipulators can be used in various military and civilian areas including space exploration, military operations, auto-manufacturing and health-care, etc. In this study, an adaptive tracking controller for a mobile manipulator which consists of a 4-wheel drive(4WD) ground vehicle and a 7-DOF robot arm with unknown vehicle parameters is designed to track an assigned desired trajectory under unknown vehicle parameters. The simulation results are demonstrated the correctness and effectiveness of the performance of the proposed controller.

Figure 1.1. Different types of mobile manipulators

First step of this study, analysis, experimental verification of dynamic models and control of Schunk LWA3 which is a 7-DOF redundant manipulator is presented. The LWA3 is a very sensitive and stable manipulator for especially high accuracy manipulation tasks. The perfect position accuracy, dexterity, back drivability, and redundant joints make the LWA3 ideal for not only industrial applications but also scientific researches. However, there is not enough technical details and information about dynamic modeling of the Schunk LWA3 manipulator in literature. Dynamic models of robots define the relationship between the motion of the robot manipulator and the actuator torques. Dynamic modeling must be expressed by taking into consideration of physical constraints and their details. Unfortunately, robot manufacturers don't provide technical knowledge about all robot parts in detail. This study focuses on the development of the dynamic model of the Schunk LWA3 robot arm, computed torque based PID control and dynamic parameters identification of the robot arm. The stability of the dynamic model is proved by a trajectory tracking experiment by using a PID controller. According to the simulation results, proposed method demonstrates the high accuracy, stability, fast computation and minimum tracking error. In recent years there has been observed a growing interest in the mobile manipulation area. Mobile manipulation is usually realized by mobile manipulator which consist of a mobile base and a manipulator. Structure and coordinate frame of 4WD mobile manipulator is illustrated in Figure 1.2.

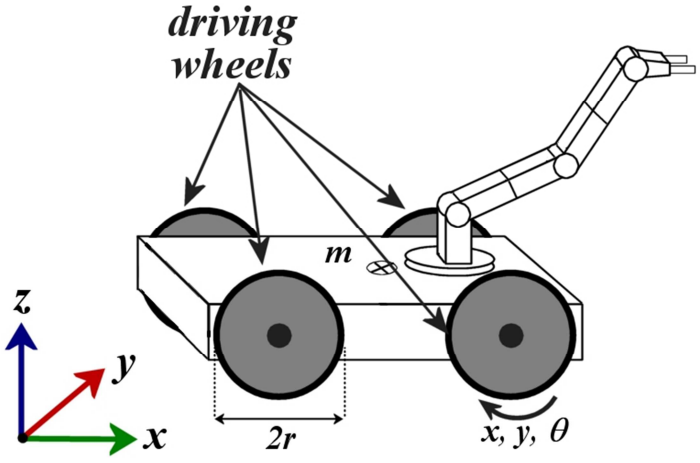

Figure 1.2. Structure and coordinate frame of 4WD mobile manipulator.

This kind of platform can be used in lots of civilian and military areas, including harmful material operation, searching and rescue, demining, explosive ordnance disposal and even battlefield.

A lot of research concentrates on the modeling, control and application of mobile manipulators [1-3]. One essential requirement for using the mobile manipulator for different applications is the property of stable and reliable mobility, which requires the mobile base to move stably, robustly and smoothly under different internal or external uncertainties and disturbances. Thus the motivation of this paper is to design a dynamic controller to control a mobile manipulator with a 4-wheel drive vehicle to track an assigned desired trajectory under unknown vehicle parameters and terrain parameters. Developed mobile manipulation platform is shown in Figure 1.3.

Figure 1.3. Developed mobile manipulation platform in different views

In this study, we firstly focused on dynamic modelling and parameter identification of the LWA3 [1-14]. A new simulation tool was developed for model verification of the LWA3 [1-20]. In the second step, we focused on mathematical modeling of the RMP400 mobile robot [16-19, 21-33]. Next step is to develop mathematical model of mobile manipulator [34-59]. After the full model identification of the mobile manipulator, we developed model based adaptive control for mobile manipulator [60 – ##89]. Finally, model and control verification were done by using simulation tool and in real environment both.

1.2. Historical Review of Related Studies

Dynamic models of robots are required in the implementation of the most advanced model and force based control [1, 2]. The dynamic model can be used to linearize the nonlinear system for not only joint space but also task space [1-5]. It is very difficult to identify and estimate dynamic parameters because of the lack of any technical knowledge on the dynamic parameters of manipulators. Dynamic model of robot contains uncertainties in many parameters such as lack of technical knowledge on robot parameters, effects of disturbances, unknown environmental conditions and parameters, etc. And also, many control methods are sensitive to their values [6]. Dynamic parameter identification methods have gained importance for developing model based controllers [6]. In general, a standard robot identification procedure consists of modeling, experiment design, data acquisition, signal processing, parameter estimation and model verification [1, 5-7]. There are two common methods to obtain identification of dynamic parameters and formulation of dynamic model [6]. First method is to identify friction parameters for each joint and then to continue to identify the rigid body dynamic parameters using identified friction parameters. Second method is to identify joint frictions and the rigid body dynamics at the same time. In general, second method is used commonly.

Swevers et al presented dynamic model identification for industrial robots in [1]. In [1], programming types of robots and task optimization problem were presented. Swevers et al mentioned about offline and online programming of industrial robots. According to [1], dynamic models are a key point to develop advanced offline

programming tools and controllers to improve productivity and accuracy. Because, dynamic model based control offers high accuracy, stability and force efficiency [1 – 7, 9, 12, and 14].

Tarn, Wu, Xi and Isidori present a sensor based control method for force regulation and robot impact control [2]. They used nonlinear feedback linearization method for dynamic model linearization. The most important part of dynamic modeling is feedback linearization [2, 5].

Wu et al presented dynamic parameter identification of robots in [6]. Parameter selection and identification are most important point for dynamic model based control [6 -12, 14]. In [6], off-line and on-line identification methods are defined in detail. As described in [6], a robot identification procedure consists of modeling, experiment design, data acquisition, signal processing, parameter estimation and model validation [6].

Wang et al developed an online motion planning algorithm for a 7 DOR redundant manipulator in [8]. The LWA3 manipulator was used as a 7DOF redundant manipulator in [8]. Forward and inverse kinematics were described in the Wang's study. PD control was developed for online motion planning of the LWA3. All technical details for the LWA3 can be found in [13].

In other study, Voung and Ang presented dynamic model identification for Mitsubishi PA10 industrial robot arm [9]. Friction models, model – based control and dynamic model of PA10 are presented. In [9], two methods are explained for robot identification. The first one is dismantlement method which is used to measure and to identify robot arm link by link. But, in practice, this method is not feasible. Genetic algorithm is used to identify dynamic parameters in [9]. In practice, uncertainties can also occur in the motion data which is presented $M(q, \dot{q}, \ddot{q})$ form. $q, \dot{q}, \ddot{q}$ are joint position, velocity and acceleration, respectively [1-9, 14-20].

Developing controller for manipulators is another important point for robot control. Astrom and Hagglund described PID control not only for robot control but also for industrial applications[15]. And also, they explained future of PID control in [15]. PID control is the commonly used control method. It is simple and robust. Many control algorithms were derived from PID. Nokleby and Podhorodeski developed new

methodology for identifying multi-DOF singular configurations of redundant manipulators [20]. Several methodologies were explained and compared in [20].

Kozlowski and Pazderski developed mathematical model of a skid – steering mobile robot (SSMR) and controller [23]. In [23], SSMR was divided into three parts. These are kinematics, dynamics and drive subsystem. Kozlowski's model was used in many studies [21-29]. In another study, Shuang et al applied Kozlowski's methodology to another robot platform [21]. Yu and Chuy present dynamic modeling of 4WD SSMR with PID control. Dynamic model of 4WD SSMR are verified not only in simulation environment but also in real environment. Stability of PID control is verified experimentally in xyz plane axes.

The united semi-empirical tire model was used in Shuang's study [21]. Arslan and Temeltas developed robust motion control for 4WD SSMR [25]. Control problem was deal with in two parts [25]. These are tracking control and velocity control. Pazderski et al preset practical stabilization method for 4WD SSMR by using back stepping method and Lyapunov stability analysis in [26].

The mobile manipulator is shown in Figure 1.3. It contains a 4-wheel drive Segway vehicle and a 7-DOF Schunk manipulator. Many papers have researched on the tracking control design for a 4-wheel drive vehicle by using different methods including Lyapunov based control [20, 24-27], sliding mode control [21], robust QFT control [22], adaptive control [23], etc. Most of these papers assume that the vehicle parameters including mass and inertia moment are all known. However, in the real case, one of the uncertainties of the vehicle, especially for the mobile manipulator we consider, is just the mass and inertia moment of the vehicle. When the mobile manipulator is running, especially when it is doing some manipulation, it will put some loads on it or take some loads off itself. Thus the mass of the mobile manipulator will change and become unknown. And also, during the mobile manipulation, the manipulator will change its configuration frequently, so the inertia moment of the system will also change and become unknown. Besides, when it is doing manipulation, the ways it put or take the loads on or off the mobile manipulator will also change the inertia moment of the system. So how to design a controller to make the mobile manipulator be able to track a desired trajectory under the unknown vehicle parameters will be a problem. The second

part of this study applies an adaptive control method to realize the tracking controller and deal with the unknown parameters. Model reference adaptive control is used to design the tracking controller and gradient algorithm based adaption law is used to estimate the unknown vehicle parameters on line.

One of the most important topics to control of mobile manipulators is a redundancy resolution. Mobile manipulators offer dual advantages of manipulators and mobile robots at the same time. But, this situation is a cause of some control problems. Mobile manipulators have multi-DOF. It is too difficult to control mobile manipulators under nonholonomic constraints. Several redundancy resolution methods have been proposed such as Extended Jacobian (EJ), Reduced Gradient(RG) and also Projected Gradient (PG)[36, 41 – 44]. Zhang et al present sensor based approach to solve redundancy problem in [36]. The paper contributes to literature about three major topics. These are (i) to develop redundancy resolution method for online trajectory by using real-time sensor data, (ii) application of developed method to the high-DOF nonholonomic mobile manipulator [36]. In another work, Zhang et al developed redundancy resolution based obstacle avoidance method for the high-DOF mobile manipulator [41].

Andaluz et al present robust control with redundancy resolution and dynamic compensation for mobile manipulators [42]. Lyapunov's method used to prove stability of proposed control law in [42]. De Luca et al present kinematic modeling and redundancy resolution for nonholonomic mobile manipulators in [44]. EJ, RG and PG redundancy resolution methods are compared in [44]. Dynamic model based redundancy resolution and control are presented by Chung and Velinsky [45].

In addition, traction control is another important vehicle control fields. Particularly for the motor in wheel drive vehicles, no matter in acceleration [20-24] or deceleration braking [21], they are always expected to provide fast and precise torque response. Many design approaches to the traction control have been provided at the driving torque level. The vehicle traction control is mainly to deal with the high nonlinear characteristic of the relation between the friction coefficients and slip ratio, which drastically varies depending on the condition of a road surface, which, in most cases, is unknown or uncertain. In order to cope with the uncertain friction effect, some

estimation methodologies have been studied, and they are mainly categorized into three methods (i) the parameters of the approximation function of the friction effect, (ii) the maximum values of the friction effect and (iii) the gradient of the friction function.

The main aim of this study is to design and implement an adaptive control to make the mobile manipulator be able to track a desired trajectory and velocity. First, this study applies an adaptive control method to realize the tracking controller and deal with the unknown parameters. Model reference adaptive control is used to design the tracking controller and gradient algorithm based adaption law is used to estimate the unknown vehicle parameters on line. Second, for the purpose of keeping the vehicle right on the track with unknown terrain conditions, a direct model reference adaptive controller was proposed for the vehicle traction control based upon a simplified road/tire friction model.

1.3. Methodology and Contributions

In this dissertation project, modeling and identification of the non-holonomic mobile manipulator are presented. The nonholonomic mobile manipulator consists of two parts: robot arm and mobile base. The Schunk LWA3(LWA3) manipulator is used as robot arm of the mobile manipulator. The Segway RMP 400 4WD skid-steering mobile robot (RMP400) is used as mobile base of the mobile manipulator. This kind of platform can be used in lots of civilian and military areas, including harmful material operation, searching and rescue, demining, space explorations, explosive ordnance disposal and even battlefield.

In the first part of this study, full model identification of the LWA3 is performed. The LWA3 is very sensitive manipulator for especially precise manipulation tasks. The high accuracy positioning capabilities, dexterity, back-drivability capability, and zero backlashes of its joints make the LWA3 ideal for not only industrial applications but also scientific researches. Unfortunately, there are not model based experimental studies about dynamics of the LWA3 manipulator in literature. To our knowledge and literature reviews, our work is the first study dynamic model verification of the LWA3 and on dynamic based position and velocity control of the LWA3.

In the second part of this study, full model identification of the RMP400 is performed. RMP400 are used in lots of civilian and military areas. The aim of this part is to analyze the characteristic behavior of SSMR and to develop the closed-loop controller for RMP400. According to our literature reviews, our work is the first study for full model identification, analysis and control of the RMP400.

In the last part of this study, adaptive control algorithm is developed for the non-holonomic mobile manipulator which is a combination of LWA3 and RMP400. To our knowledge and literature reviews, our work is the first study for application of adaptive control to this kind of the non-holonomic mobile manipulator.

1.4. Dissertation Outline

The dissertation is organized as follows. Introduction, related works and common information about the mobile manipulators are presented in Chapter 1. In Chapter 2, structure of the LWA3 robot manipulator and the RMP400 are explained. Properties are given.

In Chapter 3, kinematic models, DH Table, dynamic model, friction model are emphasized in this chapter. It presents the formulation of the vehicle dynamic model with unknown vehicle parameters, as well as the proposed adaptive controller; The wheel dynamic model with the unknown terrain and its adaptive traction controller are presented.

Control design and stability analysis for model verification are presented in Chapter 4. The system integration and testing results are shown in Chapter 5. Finally, our conclusions and future works are presented in Chapter 6.

2. STRUCTURE OF THE NON-HOLONOMIC MOBILE MANIPULATOR

2.1. Introduction

In this chapter, structure of the non-holonomic mobile manipulator is presented. Our underlying robot parts are stated, which will hold throughout the dissertation. The Schunk's lightweight arm LWA3 was used as a manipulator which is shown in Fig. 2.1a [13]. Segway's four wheel-drive (4WD) skid-steering ground vehicle RMP400 was used as a mobile part of the non-holonomic mobile manipulator which is shown Fig. 2.1b. The combination of LWA3 and RMP400 is shown in Figure 2.2.

Figure 2.1. Schunk LWA3 Robot Arm (a), Segway RMP 400 mobile robot (b)

The redundant 7 DOF robot arm (LWA3) is presented in detail in the first. Technical and operational properties of LWA3 are showed in Table 2.1 – 2.4. Table 2.1 – 2.4 present the Schunk LWA3 7 DOF modular robotic system in RPRPRPR configuration, specification of joints, properties of PRL modules and moment load of PRL modules, respectively. All data of tables are supported from [13]. Table 2.5. – 2.8. present motor weight parameters, center of mass (COM) of the motors relative to their local frames, connectors weight parameters and center of mass of the connectors relative to their local frames, respectively.

Secondly, mobile base of the non-holonomic mobile manipulator will be presented, which is four-wheel drive skid-steering ground vehicle of Segway. It is shown in Figure 2.1(b) [19]. Technical and operational properties of the RMP400 are listed in Table 2.9 to 2.14. Operational properties of the RMP400 are listed in Table 2.9. and Table 2.10. Technical properties of the RMP400 are listed in Table 2.11. through Table 2.14.

Figure 2.2 The non-holonomic mobile manipulator

2.2. Schunk LWA3: The 7 DOF Redundant Robot Arm

In this section, general structure and properties of the LWA are presented. The Schunk LWA3 robot arm is used for experimental studies as an arm of non-holonomic mobile manipulator in this study. The LWA3 is very sensitive manipulator for especially precise manipulation tasks. The high accuracy positioning capabilities, dexterity, back-drivability capability, and zero backlashes of its joints make the LWA3 ideal for not only industrial applications but also scientific researches. However, the lack of any technical knowledge on the dynamic parameters of its links makes the development of an accurate dynamic model of the robot extremely challenging. In section 3.2, the modeling, dynamic model verification and control of the Schunk LWA3 manipulator is implemented.

System configuration of the LWA3 is listed in Table 2.1 [13]. As seen in Table 2.1., the LWA3 has high repeat accuracy and high pay load capacity. The LWA3 has dexterity and maneuverability for precise operation because of redundant joints of the LWA3.

Table 2.1. The Schunk LWA3 7 DOF Robotic System's Configuration

Property	Value
Axes/DOF	7 (roll-pitch-roll-pitch-roll-pitch-roll)
Operation range	1870 x 1650 x 1870 mm^3
Envelope	3350 dm^3
Payload	10 kg
Repeated accuracy	0.1 mm
Power supply	24V DC / max. 20 A
Control	PC control (Linux or Windows) using CAN-Bus interface
Fail safeness	All joints equipped with permanent magnet brakes

Specification of joints of the LWA3 is listed in Table 2.2. PRL120 modules are used as joint 1 and joint 2. PRL100 modules are used as joint 3 and joint 4. PRL80 modules are used as joint 5 and joint 5. And, PRL60 module is used as joint 7. Maximum and nominal force/torque values of each joint are listed in Table 2.2.

Table 2.2. Specification of joints

Module	Force/Torque nom.	Force/Torque Max.	Weight [kg]	Accuracy
Joint 1 (PRL120)	210 Nm	370 Nm	3.6	± 2 arc sec
Joint 2 (PRL120)	210 Nm	370 Nm	3.6	± 2 arc sec
Joint 3 (PRL100)	81.5 Nm	176 Nm	2	± 2 arc sec
Joint 4 (PRL100)	81.5 Nm	176 Nm	2	± 2 arc sec
Joint 5 (PRL080)	20.1 Nm	41.6 Nm	1.2	± 2 arc sec
Joint 6 (PRL080)	20.1 Nm	20.1 Nm	1.2	± 2 arc sec
Joint 7 (PRL060)	4.5 Nm	9.6 Nm	1	± 2 arc sec

Properties of each PRL module are shown in Table 2.3 [13]. In Table 2.4, moment loads of PRL modules are presented. As seen in Table 2.3 and 2.4, each joint of the LWA3 produces high torque value.

Table 2.3. Properties of PRL modules

Property	PRL60	PRL80	PRL100	PRL120
Nominal Torque (Nm)	4.5	20.7	81.5	216
Peak Torque (Nm)	9.6	41.4	176	372
Rotating Angle (>)(°)	360	360	360	360
Weight (kg)	1	1.2	2	3.6
Swiveling time (90°) with mean attached load (s)	2.55	4.25	4.25	4.25
Min. ambient temperature (°C)	5	5	5	5
Max. ambient temperature (°C)	55	55	55	55
Repeat accuracy (°)	0.02	0.02	0.02	0.02
Max. angular velocity (°/s)	50	25	24	25
Max. acceleration ($°/s^2$)	200	100	96	100
Gear ratio	300:1	552:1	625:1	596:1
Nominal voltage (VDC)	24	24	24	24
Nominal power current (A)	2	3	4	5
Max. Current (A)	4	6	8	10
Resolution (arcsec)	2	1	1	1

Table 2.4. Moment load of PRL modules

Module	F_x (N) max.	F_z (N) max.	M_y (Nm) max.
PRL60	160	120	20
PRL80	520	300	60
PRL100	850	500	100
PRL120	2800	800	320

2.2.1. Physical and Geometric Data of the 7 DOF Redundant Robot Arm

In this section, physical and geometric information of the LWA3 are presented. Each PRL module is divided into two parts as motor and connector. Motor parameters and the COM properties of each module are listed in Table 2.5 and Table 2.6, respectively. Connector parameters and the COM properties of each connector are listed in Table 2.7 and Table 2.8, respectively. Calculation of the COM of the whole arm is shown in section 3.2 in detail.

2.2.1.1. Motors

Using the information for the PRL modules, motor weight parameters are gathered which is shown Table 2.5 and COM of the motors relative to their local frames is shown Table 2.6.

Table 2.5. Motor weight parameters

Designation	Motor Weight (kg)
M_{m1}	3.6
M_{m2}	3.6
M_{m3}	2.0
M_{m4}	2.0
M_{m5}	1.2
M_{m6}	1.2
M_{m7}	1.0

Table 2.6. COM of the motors relative to their local frames

COM	x(m)	y(m)	z(m)	Joint
CM_{m1}	0	0	(0.110 + 0.0821 – 0.008)	J1
CM_{m2}	0	0	0	J2
CM_{m3}	0	0	(0.110 + 0.059 – 0.008)	J3
CM_{m4}	0	0	0	J4
CM_{m5}	0	0	(0.080 + 0.0535 – 0.008)	J5
CM_{m6}	0	0	0	J6
${}^{7}CM_{m7}$	0	0	(0.050 – 0.0068)	J7

2.2.1.2. Connectors

For the calculation of the COM of connectors of joints, the effect of the metallic connectors must be considered between the motors. In Table 2.7, connectors' weight parameters are listed. Total weight of each connector is 3.312 kg. Connectors' total weight must be added to whole arm. The COM of the connectors relative to their local frames is shown in Table 2.8.

Table 2.7. Connectors weight parameters

Designation	Motor Weight (kg)
MC_{01}	0.635
MC_{12}	0.636
MC_{23}	0.576
MC_{34}	0.471
MC_{45}	0.420
MC_{56}	0.302
MC_{67}	0.273

Table 2.8. Center of mass of the connectors relative to their local frames

COM	x(m)	y(m)	z(m)	Joint
CM_{m01}	0	0	(0.110 + 0.0821 – 0.008)	J1
CM_{m02}	0	0	0	J2
CM_{m03}	0	0	(0.110 + 0.059 – 0.008)	J3
CM_{m04}	0	0	0	J4
CM_{m05}	0	0	(0.080 + 0.0535 – 0.008)	J5
CM_{m06}	0	0	0	J6
CM_{m07}	0	0	(0.50 – 0.0068)	J7

2.3. Segway RMP 400: 4 Wheel – Drive Skid – Steering Mobile Base

The Segway RMP400 is the one of the powerful mobile robot platform [19]. The RMP400 is powered by four lithium-ion battery packs and also it has rolling on four ATV tires [19]. Dimensions, propulsion system properties, command interface properties, performance specifications, battery specifications, range and energy specification are listed in Table 2.9 through Table 2.14, respectively. The RMP400 is used in many different applications such as rescue robotics, farm robotics, etc. Detailed information about application of the RMP400 can be found in [19].

Table 2.9. Dimensions of RMP 400

Dimensions	Value
Overall width	79 cm (31 in)
Overall height	53 cm (21 in)
Overall length	111 cm (43.5 in)
Weight	100 kg (220 lb.)

Table 2.10. Propulsion system properties of RMP 400

Propulsion System	**Value**
Motor torque constant @ motor shaft	0.071 Nm/amp
Motor drive peak current, per wheel	70 amp
Motor drive continuous current, per wheel	24 amp
Gearbox ratio	24:1
Battery pack capacity (total)	1600 watt-hours
Battery pack voltage (nominal)	72 Volts
Tire diameter	53 cm (21 in)
Wheel track width	62 cm (24.5 in)

Table 2.11. Command interface properties of RMP 400

Command Interface	**Value**
Communications link	USB external, CAN available via internal connector
Control	Pushbutton interface for power and mode select
Data update rate	100 Hz

Table 2.12. Performance specifications of RMP 400

Performance	**Value**
Top Speed	29 km/h (18 m/h)
Payload	90 kg. (200 lbs.)
Turning radius	Zero (load dependent)
Turning envelope	127 cm (50 in)
Maximum climbing and descending capacity	45 degrees
Controller modes	Statically stable control mode only

Table 2.13. Battery specifications of RMP 400

Battery	**Value**
Battery Chemistry	Li
Acceptable current	90 to 260 Volts; 50 to 60 Hz.
Charge rate	600 mA per battery
Operating temperature range	-10^{o}C to 50^{o}C (14^{o}F to 122^{o}F)
Charging temperature range	-10^{o}C to 50^{o}C (14^{o}F to 122^{o}F)
Battery weight (total)	20.6 kg. (46 lbs.)

Table 2.14. Range and energy specifications of RMP 400

Range and Energy	**Value**
Range under Optimal Test conditions	24 km (15 mi)
Range under Good conditions	19 km (12 mi)
Range under Severe conditions	10 km (6 mi)
Run time, stationary	8 hours
Recharge Time (from empty)	~ 8 hours

3. THEORY AND MODELING OF THE NON-HOLONOMIC MOBILE MANIPULATOR

3.1. Introduction

In this chapter, modeling and identification of the non-holonomic mobile manipulator are presented. The nonholonomic mobile manipulator consists of two parts: robot arm and mobile base. The Schunk LWA3 manipulator is used as robot arm of the mobile manipulator. Technical and operational properties of the LWA3 are presented in section 2.2 in detail. And also, more information can be found in [13]. The Segway RMP 400 4WD skid-steering mobile robot is used as mobile base of the mobile manipulator. Technical information of the RMP400 can be found in previous chapter and [19].

This chapter is organized as follows. In section 3.2, kinematics, dynamics, control and analysis of the LWA3 are presented. Stability analysis of the developed controller is examined by motion control experiments. Experimental validation of the system is graphically presented at the last part of the section 3.2. Results are discussed at the same part. In section 3.3, the mathematical model of RMP400 is systematically presented in detail. The RMP 400 is considered as three subsystems consisting of electrical drive, kinematic and dynamic [20 – 29]. Experimental verification of the mathematical models of the RMP 400 is planned with two experiments. These experiments are trajectory tracking control which based on kinematic model and velocity control which based on dynamic model. Obtained results from simulation are discussed at the end of the section 3.3.

3.2. The 7 DOF Redundant Robot Arm

The LWA3 is a high-accuracy robotic arm for precise manipulation tasks in both industrial applications and scientific researches. However, there are no enough technical details and information about the dynamic modeling of the LWA3 from literature review. Dynamic models of robots define the relationship between the motion of the robot and the actuator torques, which is very important for precise control of manipulators. This section is focused on the development of the dynamic model of the

LWA3 robot arm, identification of unknown dynamics parameters and the dynamic control design for the arm. The dynamic model and desired dynamic controller are verified by a trajectory tracking test through simulation.

Dynamic models of manipulators are required in the implementation of the most advanced model and force based control [1-2, 4]. The dynamic model can be used to linearize the nonlinear system for not only joint space but also task space [1-5]. It is very difficult to identify and estimate dynamic parameters. Dynamic model of robot contains uncertainties in many parameters such as lack of technical knowledge on robot parameters, effects of disturbances, unknown environmental conditions and unknown parameters, etc. And also, many control methods are sensitive to these values [6]. Dynamic parameter identification methods have gained importance for developing model based controllers [6]. In general, a standard robot identification procedure consists of modeling, experiment design, data acquisition, signal processing, parameter estimation and model verification [1, 5-7]. There are two common methods to obtain identification of dynamic parameters and formulation of dynamic model [6]. First method is to identify friction parameters for each joint and then to continue to identify the rigid body dynamic parameters using identified friction parameters. Second method is to identify joint frictions and the rigid body dynamics at the same time. In general, second method is used commonly.

Tarn, Wu, Xi and Isidori present a sensor based control method for force regulation and robot impact control [2] by using dynamic model of robot manipulator. They used nonlinear feedback linearization method for dynamic model linearization. According to [2], the most important part of dynamic modeling is feedback linearization [2, 5].

Featherstone and Orin [14] present reviews some of the accomplishments in the field of robot dynamics research. Wu, Wang and You [6] present two different methods for dynamic parameter identification. These are described as Off-line and On-line identification methods [6]. After parameter identification stage, they perform optimal trajectory calculation and model verification [6]. In [12], the modeling, identification and control of the 7 DOF Mitsubishi PA10 robot arm are presented in detail. PID control is performed for model verification in this work. Voung and Ang[9] present

dynamic modeling, model identification, friction models and model-based control of Mitsubishi PA10 [9]. Torque reconstruction, computed torque control and optimal trajectory planning are performed by using Matlab Genetic algorithms toolbox in [9]. And also, joint tracking error between kinematic and dynamic control are compared for Mitsubishi PA10 robot arm at [9]. In [9] and [12], performed experiments and methodologies are different, but structures of robots are the same. Mitsubishi PA10 is used in both studies. Unfortunately, there are not model based experimental studies about dynamics of the LWA3 manipulator in literature.

Dynamic modeling and dynamic parameter identification are more difficult to state [5]. Dynamic modeling, analysis and control design should be performed on different kind of robots for the enrichment of literature on robot dynamics. To our knowledge and reviews, our work is the first study on dynamic model verification of the LWA3. In this section, the modeling, dynamic model verification and control of the LWA3 is implemented. The goal of this section is to present full identification of the LWA3 and to design dynamic parameter based controller for the LWA3. 3D model of the Schunk LWA3 is shown in Figure 3.1.

Figure 3.1. 3D model of the Schunk LWA3 Manipulator

The section is organized as follows. In section 3.2.1, structure of a 7 DOF robot manipulator is explained. Kinematic models, DH Table, dynamic model, friction model are emphasized in this section. Control design and stability analysis for model verification are presented in section 3.2.2. The system integration and testing results are shown in section 3.2.4.

3.2.1. Modeling and Identification

3.2.2. Kinematics

3.2.2.1. Forward Kinematics

The coordinate frame of the redundant 7 DOF manipulator is shown in Figure 3.2. It has 7 rotational degrees of freedoms. 2 DOFs are used as the shoulder, 2 DOFs are used as the elbow and 3 DOFs are used as the wrist. The end-effector of the manipulator is attached to as the 7^{th} link of it.

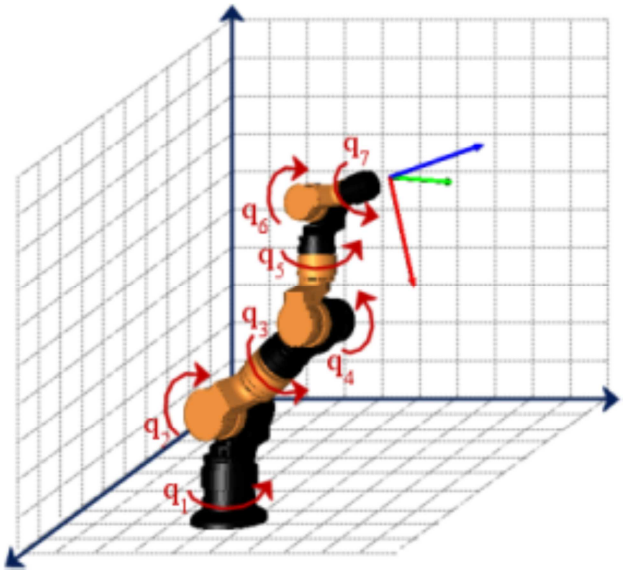

Figure 3.2. Coordinate frame of 7 DOF manipulator

The forward kinematic of the manipulator is defined by using Denavit-Hartenberg representation [8-10]. Denavit-Hartenberg notation is listed in Table 3.1.

Table 3.1. DH-Parameters 7DOF Modular Robotic System

DH-Parameters	θ_i	d_i	a_i	α_i
Joint 1 (PRL120)	q_1	300	0	-90
Joint 2 (PRL120)	q_2	0	0	90
Joint 3 (PRL100)	q_3	328	0	-90
Joint 4 (PRL100)	q_4	0	0	90
Joint 5 (PRL080)	q_5	276.5	0	-90
Joint 6 (PRL080)	q_6	0	0	90
Joint 7 (PRL060)	q_7	385.7	0	0

In Table 3.1, d_i, a_i and α_i are all DH model parameters and they have constant values. θ_i is a joint angle and its value is variable [8]. The corresponding homogeneous transformation matrices are:

$$A_1^0 = \begin{bmatrix} c_1 & 0 & -s_1 & 0 \\ s_1 & 0 & c_1 & 0 \\ 0 & -1 & 0 & d_1 \\ 0 & 0 & 0 & 1 \end{bmatrix}, A_2^1 = \begin{bmatrix} c_2 & 0 & s_2 & 0 \\ s_2 & 0 & -c_2 & 0 \\ 0 & 1 & 0 & 0 \\ 0 & 0 & 0 & 1 \end{bmatrix},$$

$$A_3^2 = \begin{bmatrix} c_3 & 0 & -s_3 & 0 \\ s_3 & 0 & c_3 & 0 \\ 0 & -1 & 0 & d_3 \\ 0 & 0 & 0 & 1 \end{bmatrix}, A_4^3 = \begin{bmatrix} c_4 & 0 & s_4 & 0 \\ s_4 & 0 & -c_4 & 0 \\ 0 & 1 & 0 & 0 \\ 0 & 0 & 0 & 1 \end{bmatrix}, \quad (3.1)$$

$$A_5^4 = \begin{bmatrix} c_5 & 0 & -s_5 & 0 \\ s_5 & 0 & c_5 & 0 \\ 0 & -1 & 0 & d_5 \\ 0 & 0 & 0 & 1 \end{bmatrix}, A_6^5 = \begin{bmatrix} c_6 & 0 & s_6 & 0 \\ s_6 & 0 & -c_6 & 0 \\ 0 & 1 & 0 & 0 \\ 0 & 0 & 0 & 1 \end{bmatrix},$$

$$A_7^6 = \begin{bmatrix} c_7 & -s_7 & 0 & 0 \\ s_7 & c_7 & 0 & 0 \\ 0 & 0 & 1 & d_7 \\ 0 & 0 & 0 & 1 \end{bmatrix}$$

The relationships between each joint are given by (3.1)[8]. The transformation matrix form the end-effector to the base is defined by (3.2). In equation (3.1), s_i and c_i denote $sin\theta_i$, $cos\theta_i$ respectively. According to (3.1), forward kinematic can be expresses as [8]:

$$A_7^0 = \prod_{i=1}^{7} A_i^{i-1} \tag{3.2}$$

The position and orientation of the end-effector can be get by using (3.2) with joint angles $Q = [q_1 \dots q_7]^T$.

3.2.2.2. Inverse Kinematics

The problem of inverse kinematics is to find the joint angles, given the end effector position and orientation [5, 7, 10]. In general, inverse kinematics is much harder than forward kinematics. Especially, the solution of inverse kinematics of redundant manipulators is more complex and it contains too many constraints. Definition of inverse kinematics problem is to find the Cartesian position and orientation of the end-effector in the form of the (4x4) homogeneous transformation matrix A_7^0, determine the joint variable $(\theta_1, \dots, \theta_7)$.

Solving joint angle $\boldsymbol{\theta_4}$

To the 7-DOF redundant manipulator discussed in this chapter, for a specific Destination Matrix A_7^0 of it, the origin of coordinate system Σ_6 can be verified solely. Because the joint angle value θ_7 just change the orientation relationship of coordinate system Σ_6 and coordinate system Σ_7 while it have no effect on the position relationship of the two coordinates systems. Then the origin of the coordinate system Σ_6 can be calculated:

$$P_6^0 = A_7^0 \begin{bmatrix} 0 \\ 0 \\ -d_7 \\ 1 \end{bmatrix} = \begin{bmatrix} P_{6x} \\ P_{6y} \\ P_{6z} \\ 1 \end{bmatrix} \tag{3.3}$$

The same case, the joint angle θ_1 will not affect the position relationship of coordinate system Σ_2 and coordinate system Σ_0 which means that the origin of coordinate system Σ_2 is $P_2^0 = [0 \quad 0 \quad d_1 \quad 1]^T$. Based on the analysis above, it is obvious that when the Destination Matrix is fixed, the position of P_6^0 and P_2^0 are also verified. Then the distance of these two points can be calculated:

$$L_{26} = \|P_6^0 \quad P_2^0\| \tag{3.4}$$

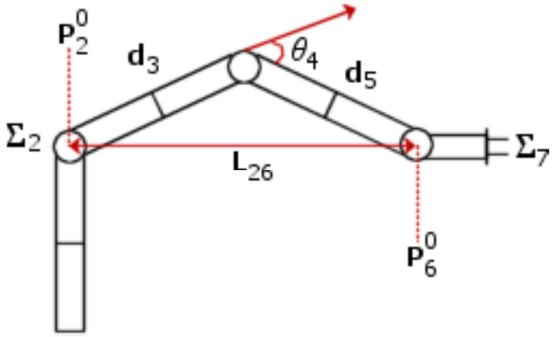

Figure 3.3. Chart for Solving $\boldsymbol{\theta_4}$

Based on the physic structure of the manipulator, it is easy to find that joint 2, joint 4 and joint 6 form a triangle. The distance from joint 2 to joint 4 and from joint 4 to joint 6 are constant which are d_3 and d_5. Since the length of the three sides has been identified, θ_4 is calculated with cosine theorem:

$$\theta_4 = \pm\left(\pi - \cos^{-1}\left(\frac{{d_3}^2 + {d_5}^2 - {L_{26}}^2}{2d_3d_5}\right)\right) \tag{3.5}$$

Definition of extra constraint

This 7DOF redundant manipulator has an interesting feature that the rotation axis of the first three joints perpendicular to each other and cross in one point. Korein has proved this type of structure is equal to a spherical joint and it can rotate through *x*, *y*, *z* axis simultaneously.

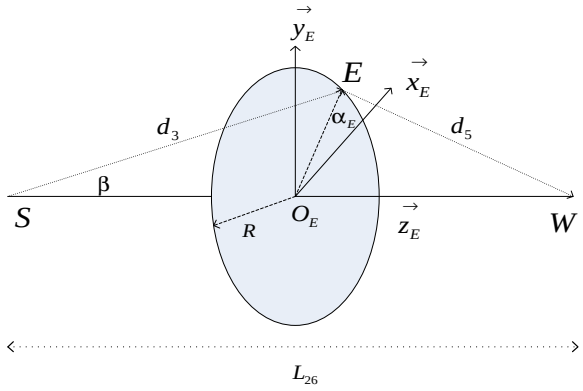

Figure 3.4. Definition of Elbow Angle

As shown in Figure 3.4, the structure composed by the first three joints is defined as Shoulder (S) like human arm and the similarly the structure composed by the last three joints is defined as Wrist (W). Since the Shoulder and Wrist are both equal to spherical joints, the Elbow (E) can rotate around the virtual axis SW. The path of the Elbow is a circular. In order to calculator the position of Elbow, a mathematical expression of this circular is deduced below. The coordinate system of Elbow rotation plane is defined as $\left(\vec{x}_E, \vec{y}_E, \vec{z}_E, O_E\right)$ $(\vec{x}_E, \vec{y}_E, \vec{z}_E, \vec{o}_E)$, in which o_E is the origin and $\vec{x}_E, \vec{y}_E$ and $\vec{z}_E$ are three axis respectively. Based on base coordinate system Σ_0:

$$\vec{z}_E = \frac{P_6^0 \quad P_2^0}{\|P_6^0 \quad P_2^0\|}, \vec{x}_E = \frac{\vec{z}_0 \times \vec{z}_E}{\|\vec{z}_0 \times \vec{z}_E\|}, \vec{y}_E = \frac{\vec{z}_E \times \vec{x}_E}{\|\vec{z}_E \times \vec{x}_E\|} and\ o_E = \cos(\beta) \times d_3 \times \vec{z}_E \tag{3.6}$$

where, $z_0 = [0 \quad 0 \quad 1]^T$, $\beta = \cos^{-1}\left(\frac{{d_3}^2 - {d_5}^2 + {L_{26}}^2}{2 d_3 L_{26}}\right)$ and radius of this circular $R = \sin(\beta) \times d_3$. After the definition of rotation plane coordinator system, an angle that express the elbow rotating through $\vec{z}_E$ can be defined as Elbow Angle α_E :

$$\alpha_E = \langle E o_E \vec{x}_E \tag{3.7}$$

Based on the analysis in last chapter, it can be found that the ideal range of the elbow Angle α_E is from 0 to 2π. For any specific value of Destination Matrix H_7^0 and Elbow α_E Angle, the position of the elbow is fixed and can be calculated as:

$$E(\alpha_E) = o_E + R(\cos(\alpha_E) \times \vec{x}_E + \sin(\alpha_E) \times \vec{y}_E) \tag{3.8}$$

Solving $\theta_1, \theta_2, \theta_3$ and $\theta_5, \theta_6, \theta_7$

In this kind of 7-DOF redundant manipulator, the values of joint angle $\theta_5, \theta_6, \theta_7$ do not affect the position of *S*, *E* and *W*, which means that the plane composed by *S*, *E* and *W* is solely verified by $\theta_1, \theta_2, \theta_3$.

As shown in Figure 3.5, we define the origin position of *SEW* plane as Σ_{origin} and destination position of this plane is Σ_{dest} . The origin position is when $\theta_1, \theta_2, \theta_3$ are equal to 0 and the destination position is when $W = P_6^0$ and $E = E(\alpha_E)$.

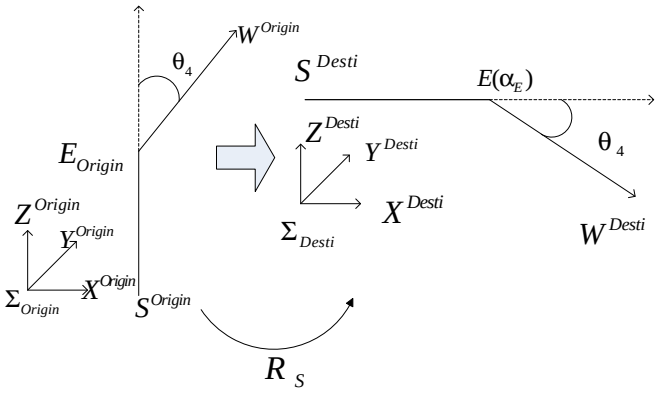

Figure 3.5. Rotation of SEW Plane

Σ_{origin} can be defined as:

$$Z_{origin} = \frac{E_{origin} - S_{origin}}{\|E_{origin} - S_{origin}\|} \tag{3.9}$$

$$X_{origin} = \frac{(W_{origin} - S_{origin}) - \left((W_{origin} - S_{origin}) + Z_{origin}\right) \times Z_{origin}}{\left\|(W_{origin} - S_{origin}) - \left((W_{origin} - S_{origin}) + Z_{origin}\right) \times Z_{origin}\right\|}$$

$$Y_{origin} = Z_{origin} \times X_{origin}$$

Similarly, Σ_{dest} is defined as:

$$Z_{dest} = \frac{E(\alpha_E) - S_{dest}}{\|E(\alpha_E) - S_{dest}\|}$$

$$X_{dest} = \frac{(W_{dest} - S_{dest}) - \left((W_{dest} - S_{dest}) + Z_{dest}\right) \times Z_{dest}}{\left\|(W_{origin} - S_{origin}) - \left((W_{dest} - S_{dest}) + Z_{dest}\right) \times Z_{dest}\right\|} \tag{3.10}$$

$$Y_{dest} = Z_{dest} \times X_{dest}$$

Then the rotation matrix of Shoulder from Σ_{origin} to Σ_{dest} is

$$R_S = [X_{dest} \quad Y_{dest} \quad Z_{dest}] \times [X_{origin} \quad Y_{origin} \quad Z_{origin}]^T \tag{3.11}$$

There is another expression of this rotation matrix. Because $\theta_1, \theta_2, \theta_3$ are the ZYZ Euler angle of spherical joint *S*, R_S can be rewritten as:

$$R_S(\theta_1, \theta_2, \theta_3) = \begin{bmatrix} c1 & -s1 & 0 \\ s1 & c1 & 0 \\ 0 & 0 & 1 \end{bmatrix} \begin{bmatrix} c2 & 0 & s2 \\ 0 & 1 & 0 \\ -s2 & 0 & c2 \end{bmatrix} \begin{bmatrix} c3 & -s3 & 0 \\ s3 & c3 & 0 \\ 0 & 0 & 1 \end{bmatrix} \tag{3.12}$$

So let $R_S(\theta_1, \theta_2, \theta_3) = R_S$, then $\theta_1, \theta_2, \theta_3$ can be calculated.

The solving for $\theta_5, \theta_6, \theta_7$ is extremely similar with $\theta_1, \theta_2, \theta_3$. First, Destination matrix is rewritten as $H_7^0 = \begin{bmatrix} R_7^0 & p_7^0 \\ 0 & 1 \end{bmatrix}$, in which R_7^0 is the destination rotation matrix. It is easy to get

$$R_W = \left(R_S R(\theta_4)\right)^{-1} R_7^0 \; and \; R(\theta_4) = \begin{bmatrix} c4 & 0 & s4 \\ 0 & 1 & 0 \\ -s4 & 0 & c4 \end{bmatrix} \tag{3.13}$$

$\theta_5, \theta_6, \theta_7$ are also the ZYZ Euler angle of spherical joint. W and R_W can also be rewritten as:

$$R_S(\theta_5, \theta_6, \theta_7) = \begin{bmatrix} c5 & -s5 & 0 \\ s5 & c5 & 0 \\ 0 & 0 & 1 \end{bmatrix} \begin{bmatrix} c6 & 0 & s6 \\ 0 & 1 & 0 \\ -s6 & 0 & c6 \end{bmatrix} \begin{bmatrix} c7 & -s7 & 0 \\ s7 & c7 & 0 \\ 0 & 0 & 1 \end{bmatrix} \tag{3.14}$$

We can see that equations (3.12) and (3.14) are the same rotation matrix with which the value of $\theta_5, \theta_6, \theta_7$ can be calculated. So, for a specific destination matrix and the elbow angle, solution of $Q = [\theta_1 \quad ... \quad \theta_7]^T$ can be get.

3.2.3. Calculation of the Center of Mass of the Whole Arm

Technical data can be found about the manipulator and its brackets in [13]. Motor's weight and connector's weight are showed in Table 2.5 and Table 2.7, respectively. And also, the center of mass of the motors and the center of mass of the connectors relative to their local frames are showed in Table 2.6 and 2.8. The center of mass of the whole arm can be estimated as equation (3.15).

$$COM = \frac{\sum_{i=1}^{7} CMm_i Mm_i + \sum_{i=1}^{7} CMc_{(i-1)(i)} Mc_{(i-1)(i)}}{\sum_{i=1}^{7} Mm_i + \sum_{i=1}^{7} Mc_{(i-1)(i)}} \tag{3.15}$$

where; *COM* is the center of mass of whole arm, CMm_i is the center of mass of i^{th} motor relative to base frame, Mm_i is mass of i^{th} motor, $CMc_{(i-1)(i)}$ is the center of mass of the connector between motors *(i-1)* and *(i)* relative to base frame, $Mc_{(i-1)(i)}$ is the mass of the i^{th} connector between motors *(i-1)* and *(i).*

Transformation of each motor's local coordinates to base frame can be written as:

$$CMm_i^0 = A_i^0 CMm_i \ , \tag{3.16}$$

In equations (3.16), CMm_i^0 denotes the center of mass of the i^{th} motor relative to their local frames. By using the same definition, transformation of each connector's local coordinates to base frame can be written as:

$$CMc_i^0 = A_i^0 CMc_i^{i-1} \tag{3.17}$$

In equation (3.17), CMc_i^0 is the center of mass of the i^{th} connector relative to their local frames. Total mass of motors and total center of mass of motors can be written as a form of equation (3.18) and equation (3.19), respectively.

$$T_{CM_{motors}} = \sum_{i=1}^{7} CM_{M_i} M_{M_i} \tag{3.18}$$

$$T_{M_{motors}} = \sum_{i=1}^{7} M_{M_i} \tag{3.19}$$

Total mass of connectors and total center of mass of connectors can be written as a form of equation (3.20) and equation (3.21), respectively.

$$T_{CM_{connectors}} = \sum_{i=1}^{7} CM_{C_{(i-1)(i)}} M_{C_{(i-1)(i)}} \tag{3.20}$$

$$T_{M_{Connectors}} = \sum_{i=1}^{7} M_{C_{(i-1)(i)}} \tag{3.21}$$

According to equations (3.18), (3.19), (3.20) and (3.21), the equation (3.3) can be written as a new form which equation is in below (3.22).

$$CM_{LWA3} = \frac{T_{CM_{motors}} + T_{CM_{connectors}}}{T_{M_{motors}} + T_{M_{Connectors}}} \tag{3.22}$$

3.2.4. Kinetic and Potential Energy of the LWA3

The kinetic energy of the rigid body can be written as common form as seen in (3.23)

$$K = \frac{1}{2} m v^T v + \frac{1}{2} \omega^T \mathcal{I} \omega \tag{3.23}$$

where m is the total mass of the object, v and ω are the linear and angular velocity vectors, respectively. $\mathcal{I}$ denotes the inertia tensor which is symmetric 3x3 matrix.

3.2.4.1. The Inertia Tensor

It is understood that the above linear and angular velocity vectors, v and w, respectively, are expressed in the inertial frame. In this case, we know that w is found from the skew symmetric matrix [5, 7].

$$S(w) = \dot{R} R^T \tag{3.24}$$

where R is the orientation transformation from the body attached frame and the inertial frame [5]. It is therefore necessary to express the inertia tensor, $\mathcal{I}$, also in the inertial frame in order to compute the triple product $\omega^T \mathcal{I} \omega$. The inertia tensor relative to the inertial reference frame will depend on the configuration of the object [5, 7, 17]. If we denote as I the inertia tensor expressed instead in the body attached frame, then the two matrices are related via a similarity transformation according to

$$\mathcal{I} = R I R^T \tag{3.25}$$

The inertia matrix expressed in the body attached frame is a constant matrix independent of the motion of the object and easily computed [5]. Let the mass density of the object be represented as a function of position, $p(x, y, z)$ [5, 7]. Then the inertia tensor in the body attached frame is computed as

$$I = \begin{bmatrix} I_{xx} & I_{xy} & I_{xz} \\ I_{yx} & I_{yy} & I_{yz} \\ I_{zx} & I_{zy} & I_{zz} \end{bmatrix} \tag{3.26}$$

Where

$$I_{xx} = \iiint (y^2 + z^2) p(x, y, z) dx\, dy\, dz \tag{3.27}$$

$$I_{yy} = \iiint (x^2 + z^2) p(x, y, z) dx\, dy\, dz \tag{3.28}$$

$$I_{zz} = \iiint (x^2 + y^2) p(x, y, z) dx\, dy\, dz \tag{3.29}$$

And

$$I_{xy} = I_{yx} = -\iiint xyp(x, y, z) dx\, dy\, dz \tag{3.30}$$

$$I_{xz} = I_{zx} = -\iiint xzp(x, y, z) dx\, dy\, dz \tag{3.31}$$

$$I_{yz} = I_{zy} = -\iiint yzp(x, y, z) dx\, dy\, dz \tag{3.32}$$

The diagonal elements of the inertia tensor, I_{xx}, I_{yy}, I_{zz} are called the principal moments of inertia about the *x*, *y*, and *z* axes, respectively [5]. The off-diagonal terms I_{xy}, I_{xz}, I_{yz} are called the cross products of inertia [5]. If the mass distribution of the body is symmetric with respect to the body attached frame, then the cross products of inertia are identically zero.

3.2.4.2. Kinetic Energy for a 7DOF Robot Arm

Linear and angular velocities of any point on any link can be expressed in terms of the Jacobian matrix and the derivatives of the joint variables [5]. Since, in our case,

the joint variables are indeed generalized coordinates, it follows that, for appropriate Jacobian matrices J_{v_i} and J_{w_i}, we have

$$v_i = J_{v_i}(q)\dot{q} \tag{3.33}$$

$$w_i = J_{w_i}(q)\dot{q} \tag{3.34}$$

Now, suppose the mass of link *i* is m_i and that the inertia matrix of link *i*, evaluated around a coordinate frame parallel to frame *i* but whose origin is at the center of mass, equals I_i. Overall kinetic energy of the manipulator can be written as:

$$K = \frac{1}{2}\dot{q}^T D(q)\dot{q} \tag{3.35}$$

$$M(q) = \sum_{i=1}^{7}\left\{m_i J_{v_i}(q)^T J_{v_i}(q) + J_{w_i}(q)^T R_i(q) I_i R_i(q)^T J_{w_i}(q)\right\} \tag{3.36}$$

M(q) is an nxn configuration dependent matrix called the mass-inertia matrix. The inertia matrix is symmetric and positive definite for any manipulator. Symmetry of *M(q)* is easily seen from equation (3.36).

3.2.4.3. Potential Energy for a 7DOF Robot Arm

In the case of rigid dynamics, the only source of potential energy is gravity [5, 7, 17]. The potential energy of the i^{th} link can be computed by assuming that the mass of the entire object is concentrated at its center of mass and is given by

$$P_i = m_i g^T r_{ci} \tag{3.37}$$

where *g* is the vector giving the direction of gravity in the internal frame and the vector r_{ci} gives the coordinates of the center of the mass of link *i*. The total potential energy of the 7 link robot is therefore

$$P = \sum_{i=1}^{7} P_i = \sum_{i=1}^{7} m_i g^T r_{ci} \tag{3.38}$$

3.2.4.4. Equations of Motion

First, the kinetic energy is a quadratic function of the vector $\dot{q}$ of the form

$$K = \frac{1}{2}\dot{q}^T M(q)\dot{q} = \sum_{i,j} d_{ij}(q)\dot{q}_i\dot{q}_j \tag{3.39}$$

where $d_{i,j}$ are the entries of the *nxn* inertia matrix *M(q)*, which is symmetric and positive definite for each $q \in \mathbb{R}^n$, and second, the potential energy $P = P(q)$ is independent of $\dot{q}$. We have already remarked that robotic manipulators satisfy these conditions [5].

The Euler-Lagrange equations for such a system can be derived as follows. Using equation (3.39) we can write the Lagrangian as

$$L = K - P = \frac{1}{2}\sum_{i,j} d_{ij}(q)\dot{q}_i\dot{q}_j - P(q) \tag{3.40}$$

The partial derivatives of the Lagrangian with respect to the k^{th} joint velocity is given by

$$\frac{\partial L}{\partial \dot{q}_k} = \sum_j d_{kj}\dot{q}_j \tag{3.41}$$

And therefore

$$\frac{d}{dt}\frac{\partial L}{\partial \dot{q}_k} = \sum_j d_{kj}\ddot{q}_j + \sum_j \frac{d}{dt} d_{kj}\dot{q}_j = \sum_j d_{kj}\ddot{q}_j + \sum_{i,j} \frac{\partial d_{kj}}{\partial q_i}\dot{q}_i\dot{q}_j \tag{3.42}$$

Similarly the partial derivative of the Lagrangian with respect to the k^{th} joint position is given by

$$\frac{\partial L}{\partial \dot{q}_k} = \frac{1}{2}\sum_{i,j} \frac{\partial d_{ij}}{\partial q_k}\dot{q}_i\dot{q}_j - \frac{\partial P}{\partial q_k} \tag{3.43}$$

Thus, for each *k=1, …, n*, the Euler-Lagrange equations can be written as

$$\sum_j d_{kj}\ddot{q}_j + \sum_{i,j}\left\{\frac{\partial d_{kj}}{\partial q_i} - \frac{1}{2}\frac{\partial d_{ij}}{\partial q_k}\right\}\dot{q}_i\dot{q}_j + \frac{\partial P}{\partial q_k} = \tau_k \tag{3.44}$$

By interchanging the order of summation and taking advantage of symmetry, one can show that

$$\sum_{i,j}\left\{\frac{\partial d_{kj}}{\partial q_i}\right\}\dot{q}_i\dot{q}_j = \frac{1}{2}\sum_{i,j}\left\{\frac{\partial d_{kj}}{\partial q_i}+\frac{\partial d_{ki}}{\partial q_j}\right\}\dot{q}_i\dot{q}_j \tag{3.45}$$

Hence

$$\sum_{i,j}\left\{\frac{\partial d_{kj}}{\partial q_i}-\frac{1}{2}\frac{\partial d_{ij}}{\partial q_k}\right\}\dot{q}_i\dot{q}_j = \sum_{i,j}\frac{1}{2}\left\{\frac{\partial d_{kj}}{\partial q_i}+\frac{\partial d_{ki}}{\partial q_j}-\frac{\partial d_{ij}}{\partial q_k}\right\}\dot{q}_i\dot{q}_j \tag{3.46}$$

$$\sum_{i,j}\left\{\frac{\partial d_{kj}}{\partial q_i}-\frac{1}{2}\frac{\partial d_{ij}}{\partial q_k}\right\}\dot{q}_i\dot{q}_j = \sum_{i,j}c_{ijk}\dot{q}_i\dot{q}_j \tag{3.47}$$

Where we define

$$c_{ijk} = \frac{1}{2}\left\{\frac{\partial d_{kj}}{\partial q_i}+\frac{\partial d_{ki}}{\partial q_j}-\frac{\partial d_{ij}}{\partial q_k}\right\} \tag{3.48}$$

The terms of c_{ijk} in equation (3.48) are known as Christoffel symbols [5]. For a fixed *k*, we have $c_{ijk}=c_{jik}$, which reduces the effort involved in computing these symbols by a factor of about one half. Finally, if we define

$$g_k = \frac{\partial P}{\partial q_k} \tag{3.49}$$

Then we can write the Euler-Lagrange equations as

$$\tau_k = \sum_{j=1}^{7} d_{kj}(q)\ddot{q}_j + \sum_{i=1}^{7}\sum_{j=1}^{7} c_{ijk}(q)\dot{q}_i\dot{q}_j + g_k(q) \tag{3.50}$$

In the above equations, there are three types of terms. The first type involves the second derivative of generalized coordinates. The second type involves quadratic terms in the first derivatives of q, where the coefficients may depend on q. These latter terms are further classified into those involving a product of the type $\dot{q}_i^2$ and those involving a product of the type $\dot{q}_i\dot{q}_j$ where $i \neq j$. Terms of the type $\dot{q}_i^2$ are called centrifugal, while

terms of the type $\dot{q}_i\dot{q}_j$ are called Coriolis terms. The third types of terms are those involving only q but not its derivatives. This third type arises from differentiating the potential energy. It is common to write equation (3.50) in matrix form as

$$\tau = M(q)\ddot{q} + C(q,\dot{q})\dot{q} + g(q) \tag{3.51}$$

In equation (3.51), friction and other disturbance forces are neglected. (3.51) is dynamic forces' equation in ideal condition. We can add friction terms and other as a new term into the (3.51). Now, we have

$$\tau = M(q)\ddot{q} + C(q,\dot{q})\dot{q} + g(q) + F(\dot{q}) + T_d \tag{3.52}$$

Where, τ is the 7*x1* vector of joint torques supplied by actuators, and q is the 7*x1* vector of joint positions, with $q=[\ \theta_1, \theta_2\ , \theta_3, \theta_4\ , \theta_5, \theta_6, \theta_7\ ]^T$. *M(q)* is an 7*x7* matrix, called mass matrix of the manipulator. The vector $C(q,\dot{q})$ represents torques arising from centrifugal and Coriolis forces [5, 10]. The vector $F(\dot{q})$ represents torques due to friction acting at the manipulator joints. *g(q)* represents torque due to gravity [9,10] with $g(q)=[g_1(q), \ldots, g_7(q)]^T$. T_d is a vector of unknown signals due to un-modeled dynamics and external dynamics [5].

In equation (3.52), the $(k,j)^{th}$ element of the matrix $C(q,\dot{q})$ is defined as

$$c_{kj} = \sum_{i=1}^{7} c_{ijk}(q)\dot{q}_i$$

$$c_{kj} = \sum_{i=1}^{7} \frac{1}{2}\left\{\frac{\partial d_{kj}}{\partial q_i} + \frac{\partial d_{ki}}{\partial q_j} - \frac{\partial d_{ij}}{\partial q_k}\right\}\dot{q}_i \tag{3.53}$$

3.2.5. Dynamics

The manipulator is modeled as a set of 7 moving rigid bodies connected in a serial chain with one end fixed to the ground and the other end free[1, 5-7]. The bodies are joined together with revolute joints; there is a torque actuator and friction acting at each joint. The Euler-Lagrange equations are used to define dynamic model [5]. The vector equation of motion of such a device can be written in the form of equation (3.54)[9, 10].

$$\tau = M(q)\ddot{q} + C(q,\dot{q}) + g(q) + F(\dot{q}) + T_d \tag{3.54}$$

In equation (3.4), τ is the 7*x1* vector of joint torques supplied by actuators, and q is the 7*x1* vector of joint positions, with $q=[\theta_1,\theta_2,\ \theta_3,\ \theta_4,\ \theta_5,\theta_6,\theta_7\ ]^T$. *M(q)* is an 7*x7* matrix, called mass matrix of the manipulator. The vector $C(q,\dot{q})$ represents torques arising from centrifugal and Coriolis forces [5, 10]. The vector $F(\dot{q})$represents torques due to friction acting at the manipulator joints. *g(q)* represents torque due to gravity[9,10]. T_d is a vector of unknown signals due to un-modeled dynamics and external dynamics [5]. The dynamic equations of the manipulators can be written as compact form (3.55):

$$\tau = M(q)\dot{q} + Q(q,\dot{q}) + T_d \tag{3.55}$$

where the vector $Q(q,\dot{q})$represents torques arising from centrifugal, Coriolis, gravity, and friction forces[5]. The j^{th} element of (3.55) can be written in the SOP form[5].

$$\tau_j = \sum_{i=1}^{u_j} m_{ji}\, f_{ji}(q,\dot{q}) + \sum_{i=1}^{v_j} q_{ji}\, g_{ji}(q,\dot{q}) + T_{d_j} \tag{3.56}$$

3.2.6. Friction Model

Friction is a complex nonlinear force that is difficult to model accurately [17], it has effects on robot dynamics. This situation was examined and proved experimentally in many studies [9-12, 17]. The effects of friction can also be modeled as a generalized

force applied to the joints of the arm [17]. Components of friction are examined using the following frictional force model for each joint:

$$b_k(\dot{q}) = b_k^v \dot{q}_k + sgn(\dot{q}_k)\left[b_k^d + (b_k^s - b_k^d)e^{\frac{-|\dot{q}_k|}{\epsilon}}\right] \tag{3.57}$$

where; sgn denotes the signum or sign function. b_k^v, b_k^d and b_k^s is viscous friction, dynamic friction and static friction coefficients of the joint k, respectively. ϵ is a small positive parameter. According to (3.57), total friction of whole arm can be expressed as:

$$F(\dot{q}) = \sum_{k=1}^{n} b_k(\dot{q}) \tag{3.58}$$

In equation (3.57) and (3.58), the frictional force approaches $\pm b_k^s$ when $\dot{q}_k \to 0$. Each joint of the LWA3 is directly driven. Hence, coefficients of friction are very small. Friction effects can be neglected because of this reason. In this study, total friction force is added to the dynamic model as a small disturbance.

3.2.7. Control Design

The end-effector trajectory tracking experiment is performed for verification of dynamic model of the LWA3. The structure of control law is shown in Figure 3.6.

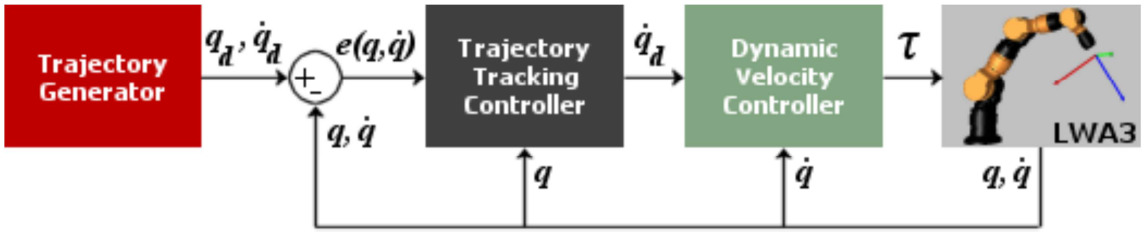

Figure 3.6. Control Law Structure

The trajectory of the end-effector was configured as equation (3.59). The trajectory is given by

$$T_{ef} = \begin{bmatrix} x \\ y \\ z \end{bmatrix} = \begin{bmatrix} 1 + \sin t \\ t \\ 2 + cost \end{bmatrix} \tag{3.59}$$

where, t denotes time and T_{ef} is a trajectory vector. All joints of the manipulator are moved when the end-effector tracks selected trajectory. Thus, changes of torques can be observed for all joints. The implemented control law is chosen the simplest form to verify the dynamic model. A control signal was designed in the form of

$$u = K_D(\dot{q}_d - \dot{q}) + K_p(q_d - q) \tag{3.60}$$

where, *u* is a control signal. Finally, an inverse dynamic controller was applied to (3.60) in the form of (3.61).

$$\tau = M(q)u + C(q, \dot{q})u + g(q) + F(\dot{q}) + T_d \tag{3.61}$$

In Equation (3.61), *u* is a control signal which is produced by PD controller. K_P and K_D are 7x7 diagonal positive definite matrices of gains. *M* and *C* matrices of the dynamic model were defined in equation (3.54). q_d and $\dot{q}_d$ are desired position and velocity, respectively.

3.2.8. Models Verification

PD controller and trajectory generator were developed by using C#.Net. q_d and $\dot{q}_d$ commands were send from developed interface to the RoboWork which is robotic simulation tool developed by Newtonium Research Group[18]. Communication between RoboWorks and C#.Net is supported by RoboTalk communication protocol [18]. Desired trajectory and end-effector trajectory tracking performance are illustrated in Figure 3.7.

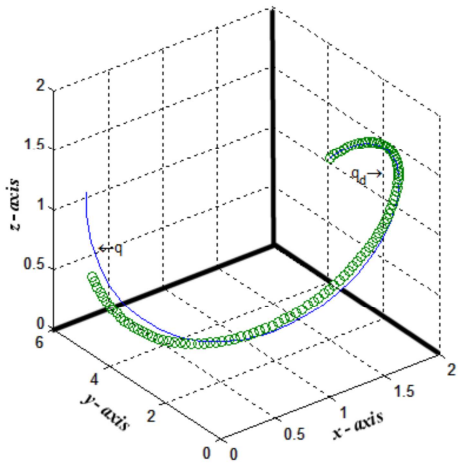

Figure 3.7. Desired trajectory and end-effector trajectory tracking performance

Calculated q and $\dot{q}$ were gathered from simulation tool by using C#. Experiment results are shown in Figure 3.9 -3.14 when end-effector tracked generated trajectory which was formulated in (3.59). According to simulation results, accuracy of developed model-based controller can be seen graphically in Figure 3.9 to 3.14.

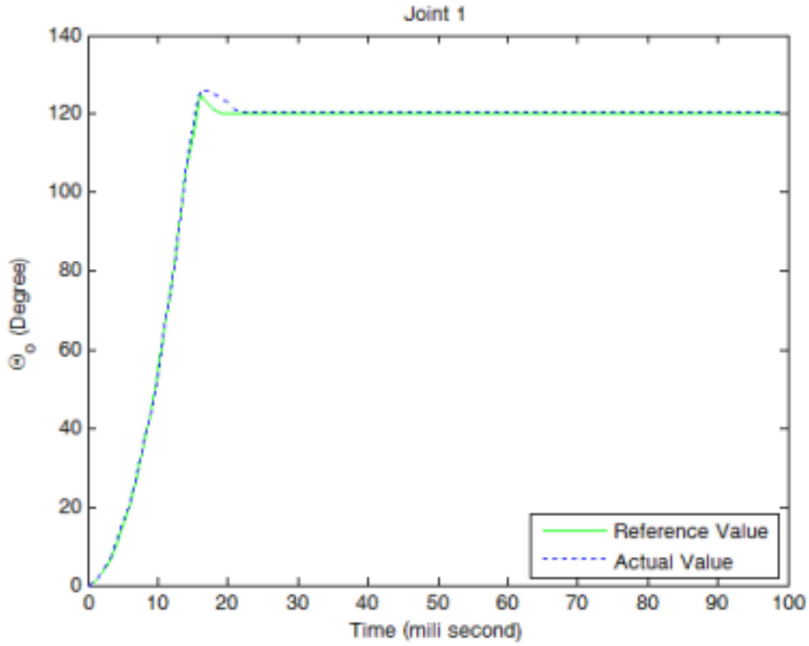

Figure 3.8. Joint angle of joint 1

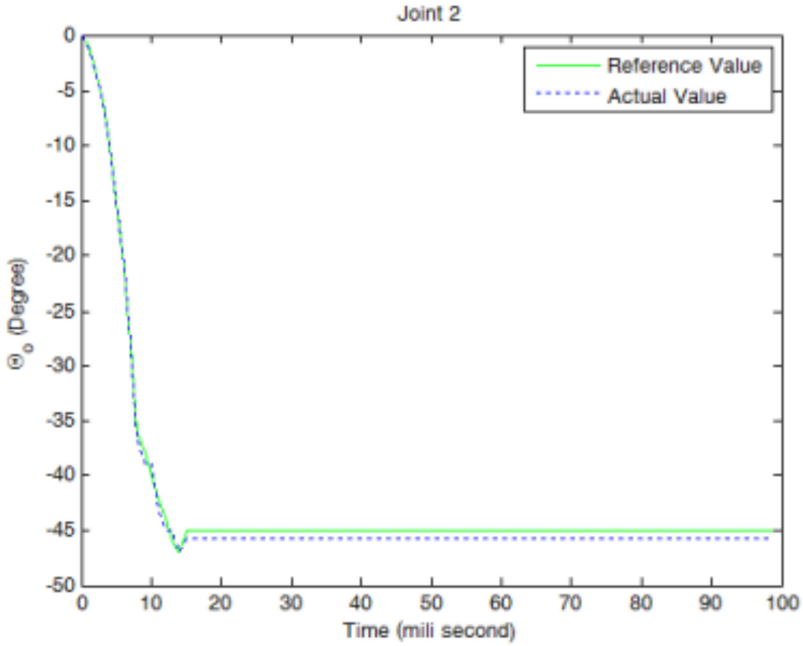

Figure 3.9. Joint angle of joint 2

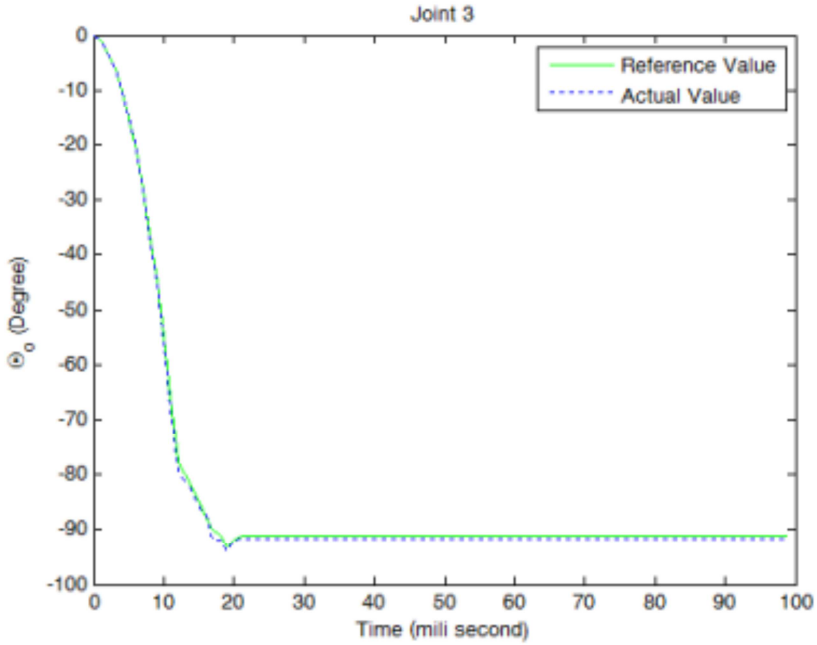

Figure 3.10. Joint angle of joint 3

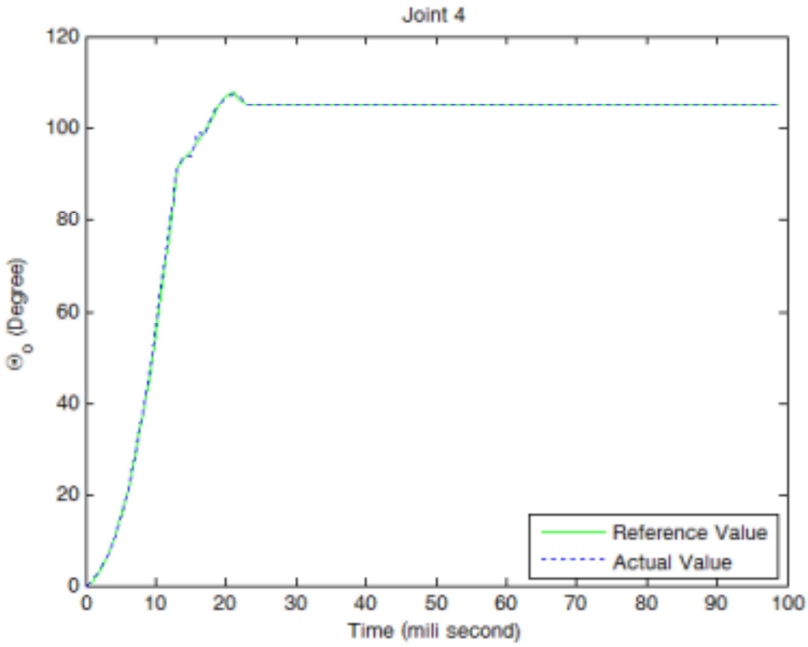

Figure 3.11. Joint angle of joint 4

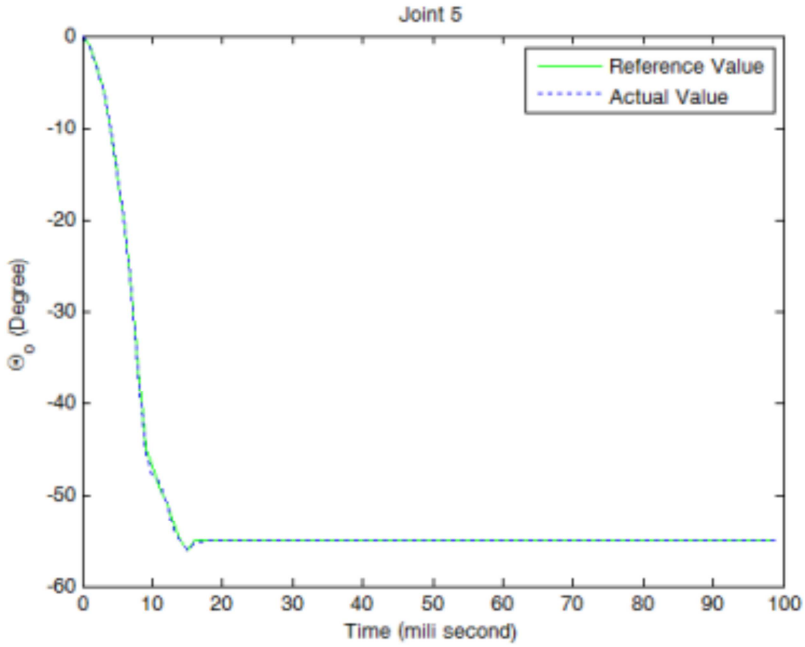

Figure 3.12. Joint angle of joint 5

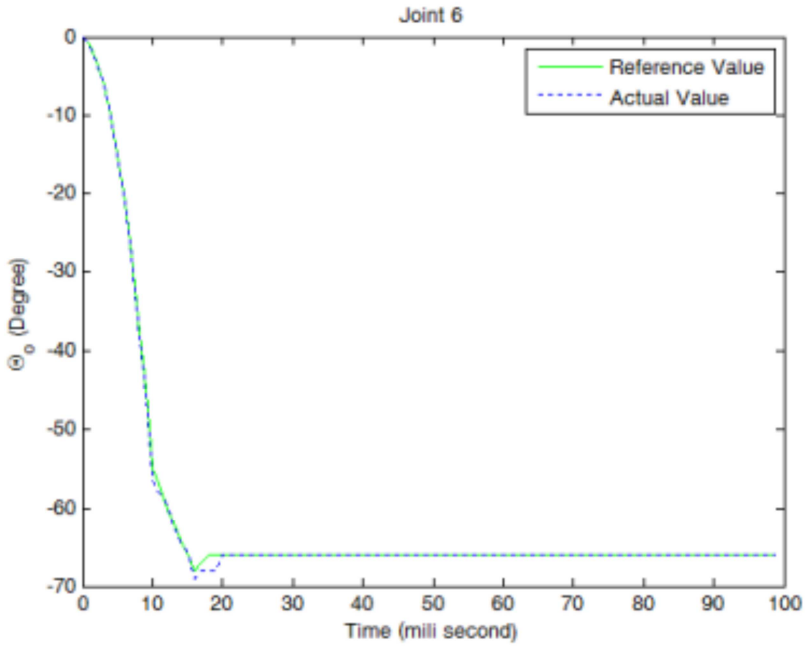

Figure 3.13. Joint angle of joint 6

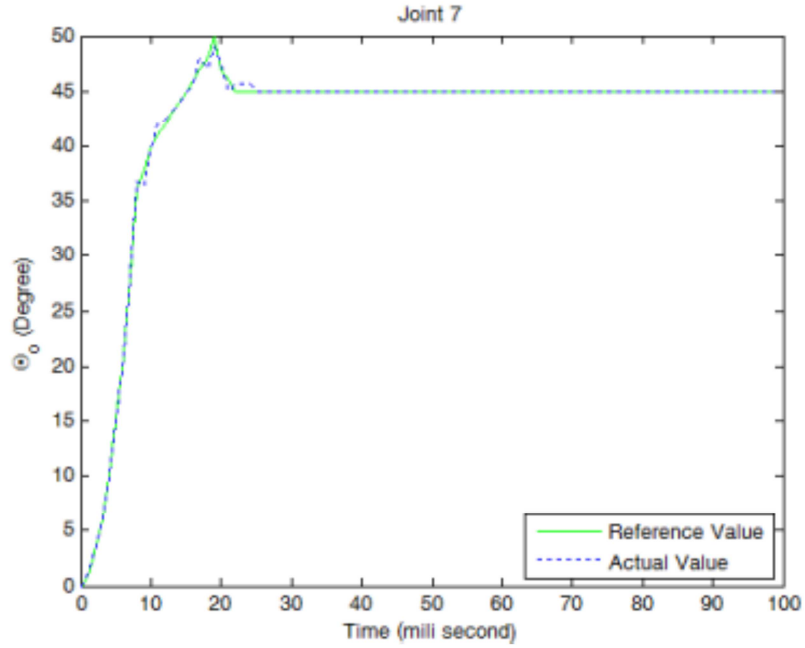

Figure 3.14. Joint angle of joint 7

In this section, dynamic modeling, control and analysis of the LWA3 was performed in simulation environment. Friction forces were modeled and were added to dynamical model as a disturbance. The parameters of the dynamic model were defined

in detail and grouped. A model-based PD controller was developed and it was used to evaluate the identified dynamic model with trajectory tracking experiment. Accuracy of proposed model was verified in this experiment. According to Figure 3.5, stability of each joint can be observed. Consequently, developing dynamic model-based controller for the LWA3 is high importance. Because, the Schunk LWA3 redundant 7-DOF manipulator is used not only scientific researches but also industrial applications. There are not enough researches in literature about this kind of manipulators. Simulation results verify that dynamic model of the manipulator is used accurately.

3.3. The 4 Wheel – Drive Skid – Steering Mobile Robot (4WD-MR)

In this section, a mathematical model of the skid-steering four wheel drive mobile robot (SSMR) moving on a planar surface is described which is shown in Figure 3.15. Free body diagram of the SSMR is shown in Figure 3.16. In this study, Segway RMP400 (RMP400) skid-steering mobile robot is used for SSMR. Technical details of RMP400 were explained in detail in Chapter 2.

Figure 3.15. The Segway RMP400 Mobile Robot

Now, kinematic and dynamic models of RMP400 are formulated. And then, the closed-loop control system for control of RMP400 will be described. The aim of this section is to analyze the characteristic behavior of SSMR and to develop the closed-loop controller for RMP400. According test results, RMP400's main characteristics are observed as stability, sensitivity, maneuverability, and accuracy.

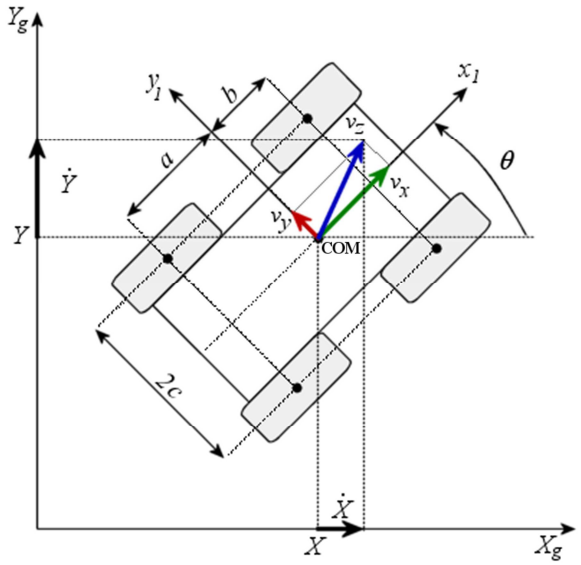

Figure 3.16. Free body diagram of the SSMR

General approach to analysis and to develop control for SSMR is divided into three parts including electrical drive subsystem, kinematics and dynamics [21-22]. This approach is commonly used to analyze mobile robots which are powered by electrical motors [21-23]. Block diagram of an electrically driven mobile robot is shown in Figure 3.17.

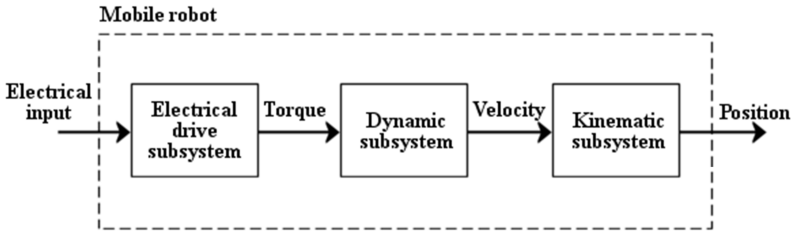

Figure 3.17. Block diagram of an electrically driven mobile robot

As seen in Figure 3.17, first electrical input is converted from voltage to torque by electrical drive subsystem. And then, torque is converted to velocity by dynamic subsystem. Finally, kinematic subsystem converts velocity to position.

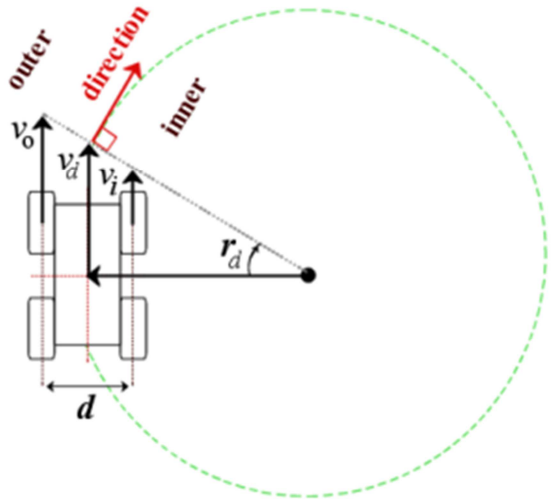

Figure 3.18. Turning model of the SSMR

The radius of the turn can be calculated from similarities of triangles [21] as seen in Figure 3.18.

$$r_d = \frac{V_o + V_i}{V_o + V_i} . \frac{d}{2} \tag{3.62}$$

$$v_d = \frac{V_o + V_i}{2} \tag{3.63}$$

In (3.62) and (3.63), r_d and v_d denote the desired radius and speed, respectively. V_o and V_i are the desired outer and inner wheel speeds, respectively. d is a distance between the right and the left wheels. r_d and v_d are the inputs of the simulation. After entering simulation inputs, the inner and outer speed can be calculated from (3.62) and (3.63) [21].

3.3.1. Modeling of Electrical Drive Subsystem of the RMP400

In this section, drive model of RMP400 is formulated. It is assumed that the robot is driven by four DC brushed motors with mechanical gears [23]. 4WD skid-steering electric vehicles are driven by four separate induction motors in each wheel. Configuration of right side of motorized wheels of RMP400 is shown in Figure 3.19.

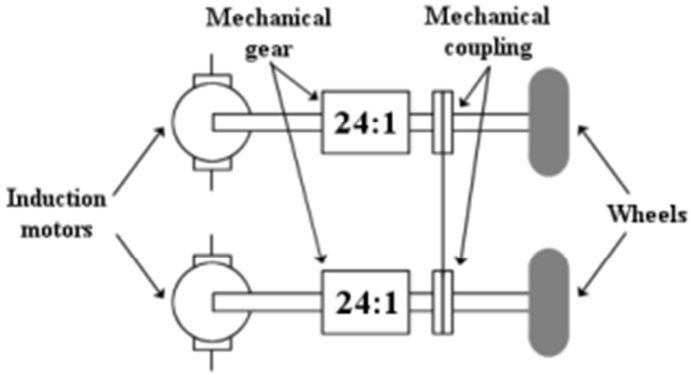

Figure 3.19. Configuration of right side of Segway RMP 400

Considering only one drive and assuming for simplicity that the torque τ_{mi} produced by the i^{th} motor is linearly dependent on the rotor current i_{ai}, τ_{mi} can be expressed as [23]:

$$\tau_{mi} = k_i i_{ai} \tag{3.63}$$

where, k_i is a motor torque constant. The voltage equation of the armature can be expressed by the following linear relationship [23]:

$$u_{iva} = L_a \frac{d}{dt} i_{ai} + R_a i_{ai} + k_e \omega_{mi} \tag{3.64}$$

where, L_a and R_a denote the series inductance and resistance of the rotors, respectively. k_e is the electromotive force coefficient, while ω_{mi} is the angular velocity of the rotor[23]. Since the i^{th} actuator is equipped with gears characterized by a ratio $n > 1$ [23], (3.63) and the angular velocity can be rewritten as

$$\tau_i = n k_i i_{ai} \tag{3.65}$$

$$\omega_{mi} = n \omega_i \tag{3.66}$$

In (3.65) and (3.66), some dynamic effects of inertia and backlash of gears have been neglected. As seen in Fig. 3.10, a new input control signal u_{va} on the voltage level is defined as

$$u_{va} = \begin{bmatrix} u_{vaL} \\ u_{vaR} \end{bmatrix} \tag{3.67}$$

Where, u_{vaL} and u_{vaR} are motor voltage signals on the left and right side of the vehicle, respectively. Since, each pair of motors is electrically and mechanically coupled, we have

$$\begin{bmatrix} u_{vaL} \\ u_{vaR} \end{bmatrix} = \begin{bmatrix} u_{va1} + u_{va2} \\ u_{va3} + u_{va4} \end{bmatrix} \tag{3.68}$$

and

$$\begin{bmatrix} \omega_L \\ \omega_R \end{bmatrix} = \frac{1}{n}\begin{bmatrix} \omega_{m1} \\ \omega_{m3} \end{bmatrix} = \frac{1}{n}\begin{bmatrix} \omega_{m2} \\ \omega_{m4} \end{bmatrix} \tag{3.69}$$

Assuming that all motors and gears have the same parameters and using (3.63)-(3.69), the following voltage-current equations can be written as:

$$\tau = 2k_i n i_a \tag{3.70}$$

$$u_{va} = 2L_a \frac{d}{dt} i_a + 2R_a i_a + 2k_e n \omega_m \tag{3.71}$$

3.3.2. Kinematics

To consider the kinematic model of the RMP400, it is assumed that the robot is placed on a plane surface with the internal orthonormal basis (X_g, Y_g, Z_g). A local coordinate frame denoted by (x_1, y_1, z_1) is assigned to the robot at its center of mass (COM). The coordinates of COM in the internal frame can be written as $COM = (X, Y, Z)$. Since in this section, the plane motion is considered only, the z-coordinate of COM is constant.

Suppose that the robot moves on a plane with linear velocity expressed in the local frame as

$$v = [v_x \quad v_y \quad 0]^T \tag{3.72}$$

and rotates with an angular velocity vector.

$$\omega = [0 \quad 0 \quad \omega]^T \tag{3.73}$$

If,

$$q = [X \quad Y \quad \theta]^T \tag{3.74}$$

is the state vector describing generalized coordinates of the robot, then

$$\dot{q} = [\dot{X} \quad \dot{Y} \quad \dot{\theta}]^T \tag{3.75}$$

denotes the vector of generalized velocities. From Figure 3.7, it can be noted that the variables $\dot{X}$ and $\dot{Y}$ are related to the coordinates of the local velocity vector as follows

$$\begin{bmatrix} \dot{X} \\ \dot{Y} \end{bmatrix} = \begin{bmatrix} cos\theta & -sin\theta \\ sin\theta & cos\theta \end{bmatrix} \begin{bmatrix} v_x \\ v_y \end{bmatrix} \tag{3.76}$$

Furthermore, because of the planar motion, one can write $\dot{\theta} = \omega$.

It is obvious that equation (3.76) does not impose any restrictions on the SSMR plane movement, since it describes free-body kinematics only. Therefore it is necessary to analyze the relationship between velocities and local velocities.

Suppose that the i^{th} wheel rotates with an angular velocity ω_i *(t)*, where i = 1, ...4, which can be seen as a control input. For simplicity, the thickness of the wheel is neglected and is assumed to be in contact with the plane at point P_i as illustrated in Figure 3.20. In contrast to most wheeled vehicles, the lateral velocity of the SMRR, v_{iy}, is generally nonzero. This property comes from the mechanical structure of the SSMR that makes lateral skidding necessary if the vehicle changes its orientation. Therefore the wheels are tangent to the path only if ω = 0, i.e., when the robot moves along a straight line.

In this description, we consider only a simplified case of the SSMR movement for which the longitudinal slip between the wheels and the surface can be neglected. According to this assumption, the following relation can be developed:

$$v_{ix} = r_i \omega_i \tag{3.77}$$

where v_{ix} is the longitudinal component of the total velocity vector vi of the i^{th} wheel expressed in the local frame and r_i denotes the so-called effective rolling radius of that wheel.

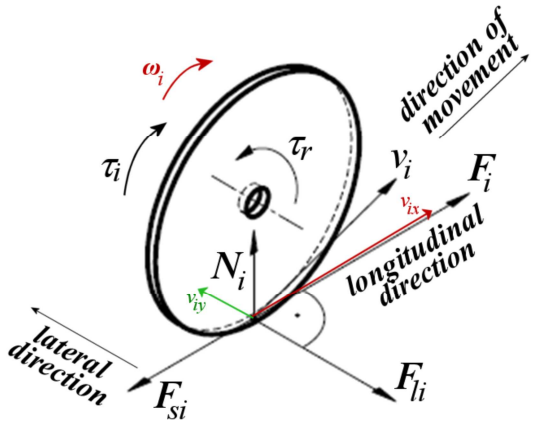

Figure 3.20. Velocities and forces of one Wheel

To develop a kinematic model, it is necessary to take into consideration all wheels together. In Figure 3.21, the radius vectors $d_i = [d_{ix} \quad d_{iy}]^T$ and $d_C = [d_{Cx} \quad d_{Cy}]^T$ are defined with respect to the local frame from the instantaneous center of rotation (ICR). Consequently, based on the geometry of Figure 3.21, the following expression can be deduced:

$$\frac{\|v_i\|}{\|d_i\|} = \frac{\|v\|}{\|d_C\|} = \|\omega\| \tag{3.78}$$

or, in a more detailed form:

$$\frac{v_{ix}}{-d_{iy}} = \frac{v_x}{-d_{Cy}} = \frac{v_{iy}}{d_{ix}} = \frac{v_y}{d_{Cx}} = \omega \tag{3.79}$$

where, the symbol $\|.\|$ denotes the Euclidian norm.

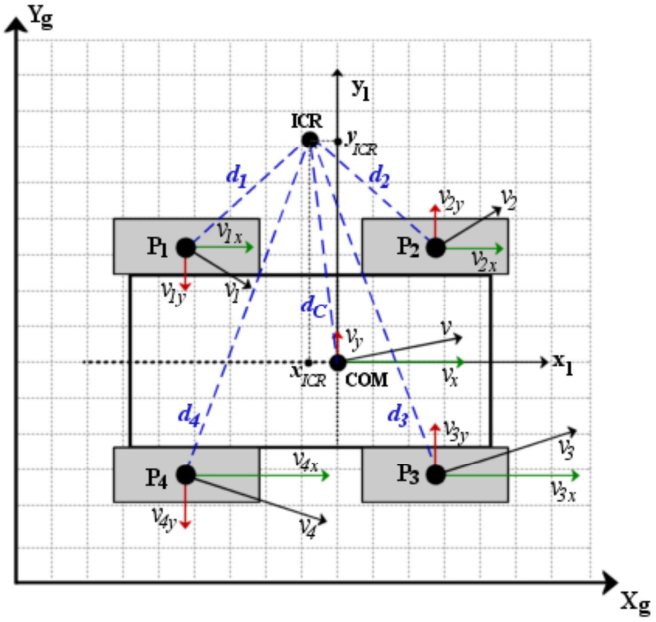

Figure 3.21. Wheel velocities

Defining the coordinates of the ICR in the local frame as

$$ICR = (x_{ICR}, y_{ICR}) = \left(-d_{xC}, -d_{yC}\right) \tag{3.80}$$

Allows us to rewrite equation (3.79) as follows:

$$\frac{v_x}{y_{ICR}} = \frac{v_y}{x_{ICR}} = \omega \tag{3.81}$$

From Figure 3.21, it is clear that the coordinates of vectors d_i satisfy the following relationships:

$$\begin{aligned} d_{1y} &= d_{2y} = d_{Cy} + c, \\ d_{3y} &= d_{4y} = d_{Cy} - c, \\ d_{1x} &= d_{4x} = d_{Cx} - a, \\ d_{2x} &= d_{3x} = d_{Cx} + b, \end{aligned} \tag{3.82}$$

where a, b and c are positive kinematic parameters of the robot depicted in Figure 3.16. After combining Equations (3.79) and (3.82), the following relationships between wheel velocities can be obtained:

$$
\begin{aligned}
v_L &= v_{ix} = v_{2x}, \\
v_R &= v_{3x} = v_{4x}, \\
v_F &= v_{2y} = v_{3y}, \\
v_B &= v_{1y} = v_{4y},
\end{aligned}
\tag{3.83}
$$

where v_L and v_R denote the longitudinal coordinates of the left and right wheel velocities, v_F and v_B are the lateral coordinates of the velocities of the front and rear wheels, respectively.

Using (3.79)–(3.83) it is possible to obtain the following transformation describing the relationship between the wheel velocities and the velocity of the robot:

$$
\begin{bmatrix} v_L \\ v_R \\ v_F \\ v_B \end{bmatrix} = \begin{bmatrix} 1 & -c \\ 1 & c \\ 0 & -x_{ICR} + b \\ 0 & -x_{ICR} - a \end{bmatrix} \begin{bmatrix} v_L \\ \omega \end{bmatrix} \tag{3.84}
$$

In accordance with (3.77) and (3.83), assuming that the effective radius is $r_i = r$ for each wheel, we can write

$$
\omega_w = \begin{bmatrix} \omega_L \\ \omega_R \end{bmatrix} = \frac{1}{r} \begin{bmatrix} v_L \\ v_R \end{bmatrix} \tag{3.85}
$$

where ω_L are ω_R are the angular velocities of the left and right wheels, respectively. Combining (3.84) and (3.85), the following approximated relations between the angular wheel velocities and the velocities of the robot can be developed:

$$
\eta = \begin{bmatrix} v_x \\ \omega \end{bmatrix} = r \begin{bmatrix} \dfrac{\omega_L + \omega_R}{2} \\ \dfrac{-\omega_L + \omega_R}{2c} \end{bmatrix} \tag{3.86}
$$

where, η is a new control input introduced at the kinematic level.

From the last equation it is clear that, theoretically, the pair of velocities ω_L and ω_R can be treated as a control kinematic input signal as well as velocities v_x and ω. However, the accuracy of the relation (3.86) mostly depends on the longitudinal slip and

can be valid only if this phenomenon is not dominant. In addition, the parameters *r* and *c* may be identified experimentally to ensure a high validity of the determination of the angular robot velocity with respect to the angular velocities of the wheels.

To complete the kinematic model of the SSMR, the following velocity constraint introduced in [30] from (3.81) can be considered:

$$v_y + x_{ICR}\dot{\theta} = 0 \tag{3.87}$$

The last equation is not integrable. In consequence, it describes a nonholonomic constraint which can be rewritten in the Pfaffian form:

$$[-sin\theta \quad cos\theta \quad x_{ICR}][\dot{X} \quad \dot{Y} \quad \dot{\theta}]^T = A(q)\dot{q} = 0 \tag{3.88}$$

where, Equation (3.76) has been used. Since the generalized velocity $\dot{q}$ is always in the null space of *A*, we can write

$$\dot{q} = S(q)\eta \tag{3.89}$$

where

$$S^T(q)A^T(q) = 0 \tag{3.90}$$

and

$$S(q) = \begin{bmatrix} cos\theta & x_{ICR}sin\theta \\ sin\theta & -x_{ICR}cos\theta \\ 0 & 1 \end{bmatrix} \tag{3.91}$$

It should be noted that since $\dim(\eta) = 2 < \dim(q) = 3$, Eqn. (3.89) describes the kinematics of the robot, which is under actuated. Additionally, this is a nonholonomic system because of the constraint described by (3.87). It is interesting to see that the analyzed kinematic model of the SSMR is quite similar to the kinematics of the two-wheel mobile robot presented by [23].

From (3.71) and (3.74) it can be seen that control of the v_y and v_{yi} velocity coordinates is not possible without the knowledge of the x_I-axis projection of the ICR. Therefore, considering the linear velocity v_x and the angular velocity ω as control

signals seems to have an advantage over the previous propositions presented by [23] and [30] where instead of ω, the velocity v_y is used.

3.3.3. Dynamics

In this section the dynamic properties of the SSMR are described, since the dynamic effects play an important role for such vehicles [24]. It is caused by unknown lateral skidding ground interaction forces. First, the wheel forces depicted in Figure 3.11 are examined. The active force F_i and reactive force N_i are related to the wheel torque and gravity, respectively. It is clear that that F_i is linearly dependent on the wheel control input τ_i, namely,

$$F_i = \frac{\tau_i}{r} \tag{3.92}$$

According to [23-26], we assume that the vertical force N_i acts from the surface to the wheel. To consider the four wheels of the vehicle (Figure 3.22) and neglecting additional dynamic properties, we obtain the following equations of equilibrium:

$$\begin{aligned} N_1 a &= N_2 b, \\ N_4 a &= N_3 b, \\ \textstyle\sum_{i=1}^{4} N_i &= mg, \end{aligned} \tag{3.93}$$

where m denotes the vehicle mass and g is the gravity acceleration. Since there is symmetry along the longitudinal midline, we obtain

$$\begin{aligned} N_1 = N_4 &= \frac{b}{2(a+b)} mg, \\ N_2 = N_3 &= \frac{a}{2(a+b)} mg \end{aligned} \tag{3.94}$$

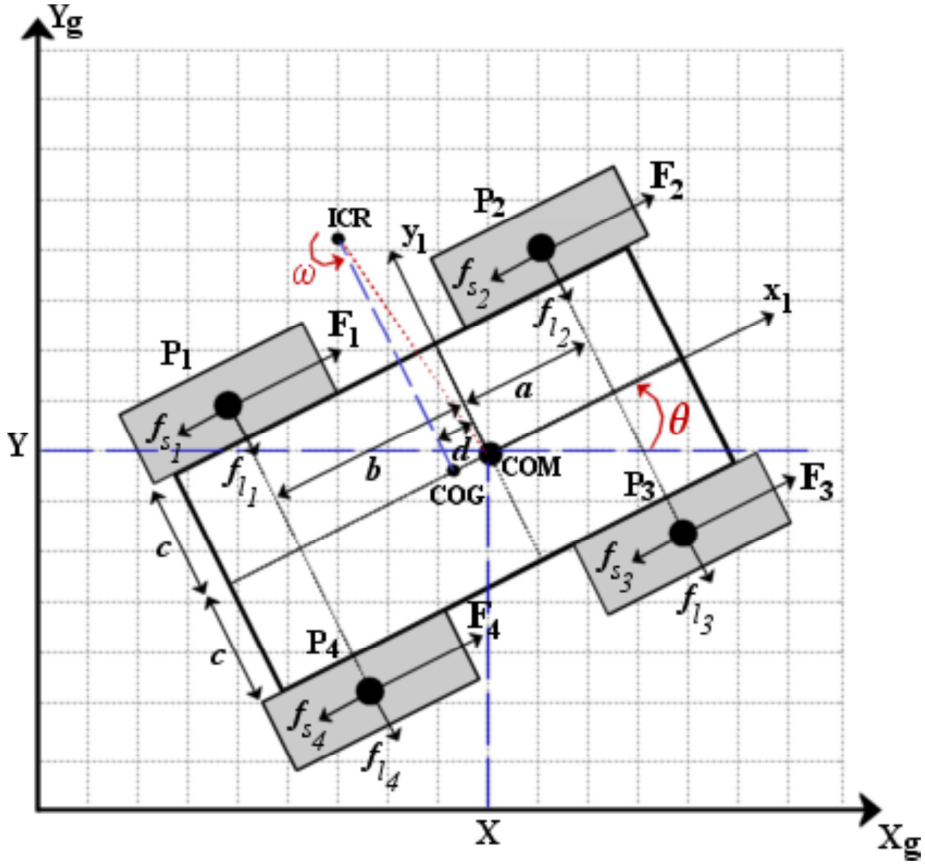

Figure 3.22. Active and Resistive Forces of the RMP400

Assume that the vector F_{si} results from the rolling resistant moment τ_{ri} and the vector F_{li} denotes the lateral reactive force. Based on [23-26] these reactive forces can be regarded as friction ones. However, it is important to note that friction modeling is quite complicated since it is highly nonlinear and depends on many variables. Therefore, in most cases only a simplified approximation describing the friction F_f as a super- position of Coulumb and viscous friction is considered. It can be written as

$$F_f(\sigma) = \mu_C N sgn(\sigma) + \mu_v \sigma \tag{3.95}$$

where σ denotes the linear velocity, N is the force perpendicular to the surface, while μ_c and μ_v denote the coefficients of Coulumb and viscous friction, respectively. Since for the SSMR the velocity σ is relatively low, especially during lateral slippage, the relation $\mu_c N \gg |\mu_v \sigma|$ is valid, which allows us to neglect the term $\mu_v \sigma$ to simplify the model. It is very important to note that the function (3.95) is not smooth when the velocity σ equals zero, because of the sign function *sgn(σ)*. It is obvious that this function is not

differentiable at $\sigma = 0$. Since a continuous and time differentiable model of the SSMR should be obtained, the following approximation of this function is proposed:

$$\widehat{sgn}(\sigma) = \frac{2}{\pi}\arctan(k_s\sigma) \tag{3.96}$$

where $k_s \gg 1$ is a constant which determines the approximation accuracy according to the relation

$$\lim_{k_s\to\infty} \frac{2}{\pi}\arctan(k_s\sigma) = sgn(x). \tag{3.97}$$

Based on the previous deliberations, the friction forces for one wheel can be written as

$$F_{li} = \mu_{lci} mg\widehat{sgn}(v_{yi}) \tag{3.98}$$

$$F_{si} = \mu_{sci} mg\widehat{sgn}(v_{xi}). \tag{3.99}$$

where μ_{lci} and μ_{sci} denote the coefficients of the lateral and longitudinal forces, respectively.

Using the Lagrange-Euler formula with Lagrange multipliers to include the nonholonomic constraint (3.87), the dynamic equation of the robot can be obtained. Next, it is assumed that the potential energy of the robot *PE(q)=0* because of the planar motion. Therefore the Lagrangian *L* of the system equals the kinetic energy:

$$L(q, \dot{q}) = T(q, \dot{q}). \tag{3.100}$$

Considering the kinetic energy of the vehicle and neglecting the energy of rotating wheels, the following equation can be developed:

$$T = \frac{1}{2} m v^T v + \frac{1}{2} \mathcal{I}\omega^2 \tag{3.101}$$

where *m* denotes the mass of the robot and $\mathcal{I}$ is the moment of inertia of the robot about the COM. For simplicity, it is assumed that the mass distribution is homogeneous.

Since $v^T v = v_x^2 + v_y^2 = \dot{X}^2 + \dot{Y}^2$, equation (3.101) can be written in the following form:

$$T = \frac{1}{2}m(\dot{X}^2 + \dot{Y}^2) + \frac{1}{2}I\dot{\theta}^2 \tag{3.102}$$

After calculating the partial derivative of kinetic energy and its time-derivative, the inertial forces can be obtained as

$$\frac{d}{dt}\left(\frac{\partial E_k}{\partial \dot{q}}\right) = \begin{bmatrix} m\ddot{X} \\ m\ddot{Y} \\ I\ddot{\theta} \end{bmatrix} = M\ddot{q} \tag{3.103}$$

Where

$$M = \begin{bmatrix} m & 0 & 0 \\ 0 & m & 0 \\ 0 & 0 & I \end{bmatrix} \tag{3.104}$$

Consequently, the forces which cause the dissipation of energy are considered. According to Figure 3.22, the following resultant forces expressed in the inertial frame can be calculated:

$$F_{rx}(\dot{q}) = cos\theta \sum_{i=1}^{4} F_{si}(v_{xi}) - sin\theta \sum_{i=1}^{4} F_{li}(v_{yi}), \tag{3.105}$$

$$F_{ry}(\dot{q}) = sin\theta \sum_{i=1}^{4} F_{si}(v_{xi}) + cos\theta \sum_{i=1}^{4} F_{li}(v_{yi}), \tag{3.16}$$

The resistant moment around the COM, M_r can be obtained as

$$M_r(\dot{q}) = -a \sum_{i=1,4} F_{li}(v_{yi}) + b \sum_{i=2,3} F_{li}(v_{yi}) + c\left[-\sum_{i=1,2} F_{si}(v_{xi}) + \sum_{i=3,4} F_{si}(v_{xi})\right] \tag{3.107}$$

To define generalized resistive forces, the vector

$$R(\dot{q}) = [F_{rx}(\dot{q}) \quad F_{ry}(\dot{q}) \quad M_r(\dot{q})]^T \tag{3.108}$$

is introduced. The active forces generated by the actuators which make the robot move can be expressed in the inertial frame as follows:

$$F_x = cos\theta \sum_{i=1}^{4} F_i \tag{3.109}$$

$$F_y = sin\theta \sum_{i=1}^{4} F_i \tag{3.110}$$

The active torque around the COM is calculated as

$$M = c(-F_1 - F_2 + F_3 + F_4) \tag{3.111}$$

In consequence, the vector F of active forces has the following form:

$$F = \begin{bmatrix} F_x \\ F_y \\ M \end{bmatrix} \tag{3.112}$$

Using (3.82), (3.109)-(3.111) and assuming that the radius of each wheel is the same, we get

$$F = \frac{1}{r}\begin{bmatrix} cos\theta \sum_{i=1}^{4} \tau_i \\ sin\theta \sum_{i=1}^{4} \tau_i \\ c(-F_1 - F_2 + F_3 + F_4) \end{bmatrix} \tag{3.113}$$

To simplify the notation, a new torque control input τ is defined as

$$\tau = \begin{bmatrix} \tau_L \\ \tau_R \end{bmatrix} = \begin{bmatrix} \tau_1 + \tau_2 \\ \tau_3 + \tau_4 \end{bmatrix} \tag{3.114}$$

where τ_L and τ_R denote the torques produced by the wheels on the left and right sides of the vehicle, respectively. Combining (3.112) and (3.113), we get

$$F = B(q)\tau \tag{3.115}$$

where B is the input transformation matrix defined as

$$B(q) = \frac{1}{r}\begin{bmatrix} cos\theta & cos\theta \\ sin\theta & sin\theta \\ -c & c \end{bmatrix} \tag{3.116}$$

Next, using (3.103), (3.109) and (3.115), the following dynamic model is obtained:

$$M(q)\ddot{q} + R(\dot{q}) = B(q)\tau \tag{3.117}$$

It should be noted that (3.117) describes the dynamics of a free body only and does not include the nonholonomic constraint (3.82). Therefore a constraint has to be imposed on (3.117). To this end, a vector of Lagrange multipliers, λ, is introduced as follows [20-26, 34-37]:

$$M(q)\ddot{q} + R(\dot{q}) = B(q) + A^T(q)\lambda \tag{3.118}$$

For control purposes it would be more suitable to express (3.118) in terms of the internal velocity vector η. Therefore, (3.118) is multiplied from the left by $S^T(q)$, which results in

$$S^T(q)M(q)\ddot{q} + S^T(q)R(\dot{q}) = S^T(q)B(q) + S^T(q)A^T(q)\lambda \tag{3.119}$$

After taking the time derivative of (3.89), we obtain

$$\ddot{q} = \dot{S}(q)\eta + S(q)\dot{\eta} \tag{3.120}$$

Next, using (3.120) and (3.89) in (3.118), the dynamic equations become

$$\bar{M}\dot{\eta} + \bar{C}\eta + \bar{R} = \bar{B}\tau \tag{3.121}$$

Where

$$\bar{C} = S^T M\dot{S} = mx_{ICR}\begin{bmatrix} 0 & \dot{\theta} \\ -\dot{\theta} & \dot{x}_{ICR} \end{bmatrix} \tag{3.122}$$

$$\bar{M} = S^T MS = \begin{bmatrix} m & 0 \\ 0 & mx_{ICR}^2 + I \end{bmatrix} \tag{3.123}$$

$$\bar{R} = S^T R = \begin{bmatrix} F_{rx}(\dot{q}) \\ x_{ICR}F_{ry}(\dot{q}) + M_r \end{bmatrix} \tag{3.124}$$

$$\bar{B} = S^T B = \frac{1}{r}\begin{bmatrix} 1 & 1 \\ -c & c \end{bmatrix} \tag{3.125}$$

3.3.4. Control Algorithm

Common approach to define mathematical model of the electrically driven mobile robots is to divide system into three parts [21-28]. These are electrical driven, kinematic and dynamic subsystems. Motion control of the RMP400 is often regarded as trajectory tracking control. Here, we regard it as the motion control system that has two sub-systems, that is, trajectory tracking controller at kinematic level and velocity controller at dynamic level [25]. Such a control system is illustrated in Figure 3.17.

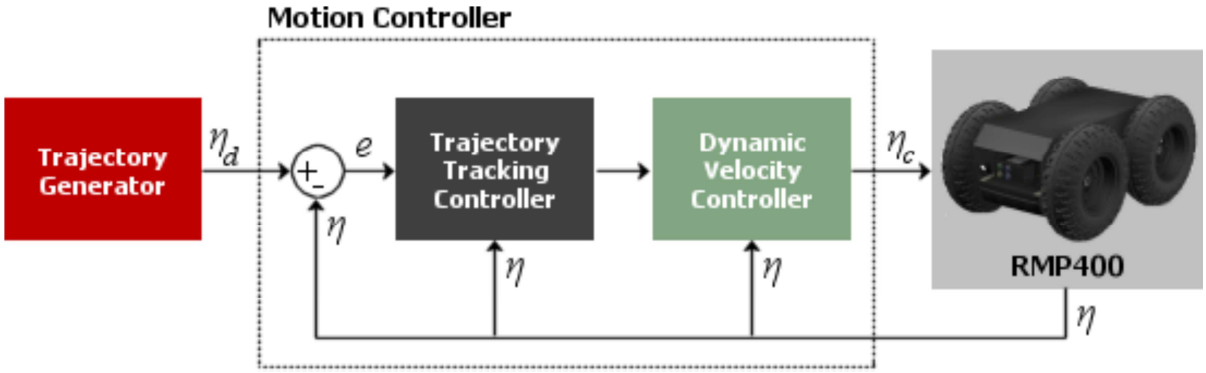

Figure 3.23. Motion control for the RMP400

The control objective is to asymptotically stabilize the tracking error at origin. Here we restrict the input trajectories to be persistently exciting and admissible. Let the reference trajectory be denoted by q_d then the trajectory tracking error is $e(t) \triangleq q_d(t) - q(t)$. Now define the admissible local velocity error $\eta_d(t) \triangleq [v_d(t) \quad \omega_d(t)]^T$ then the so-called persistently exciting reference trajectory is defined as

$$\dot{q}_d(t) \triangleq S\big(q_d(t)\big)\eta_d(t) \tag{3.126}$$

where $v_d(t) > 0$. The trajectory control problem is to find a smooth velocity control [25].

$$\eta_c(t) = f(e, \eta_d, K) \tag{3.127}$$

Such that $e(t) \to 0$ as $t \to \infty$, where K is the controller design parameters vector.

3.3.5. Models Verification

The designed adaptive tracking control system for the 4-wheel drive vehicle is simulated in MATLAB. The desired trajectory is chosen a sine curve along x axis, as shown in Figure 3.24. The speed along x axis is chosen as a constant of 0.1 m/s. The trajectories for each of the three states x, y and θ are shown in Figure 3.25. separately.

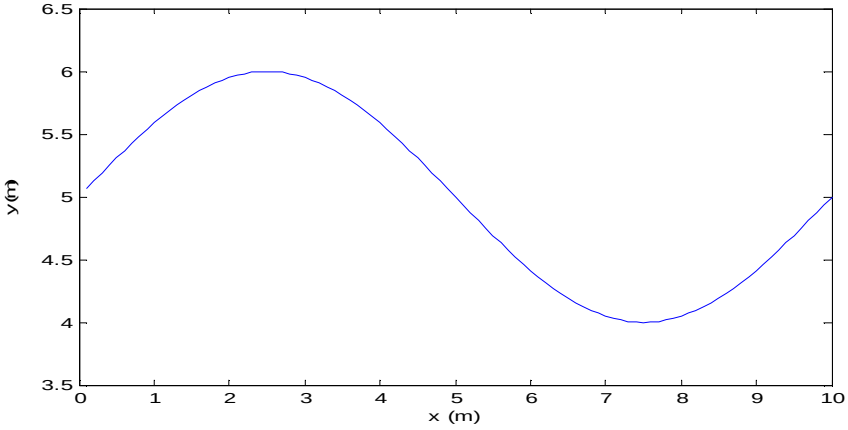

Figure 3.24. Desired trajectory on the vehicle

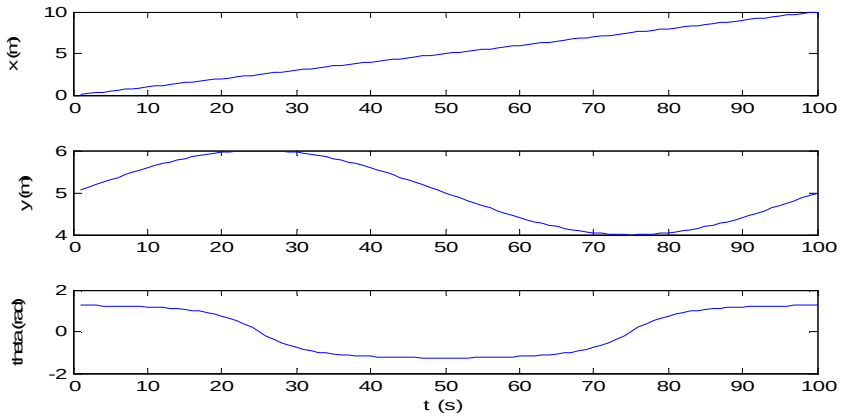

Figure 3.25. Desired trajectories of the three states

In the simulation, the mass m and inertia moment I of the vehicle are assumed to be unknown. The real value of them are set as 150 kg and 4.25 $kg \cdot m^2$. With implementing the model reference adaptive control laws, gradient algorithm based parameter estimation and nonlinear feedback control law, the simulated tracking results are shown in Figures 3.20 – 3.23 . The tracking results and tracking errors for all the three stats are in Figure 3.20 and 3.21, separately. The parameter convergence result for the two unknown vehicle parameters is shown in Figure 3.28. The Step response for x with estimated parameters is shown in Figure 3.29. From these results, we can see that the designed adaptive tracking controller can make the three states track the desired

trajectories very well as time increasing and all the tracking errors approach to zero asymptotically fast as time goes to zero. Besides, the estimation laws can make the estimated values approach to the real values of the two parameters asymptotically as time increasing, and once the values reaches the real values, they will remain unchanged any more. At last, from the step response of x with the estimated parameters, we can see that the settling time is smaller than 2 s and percentage overshoot is smaller than 5%. Thus the requirements of the single controller for each state are also satisfied.

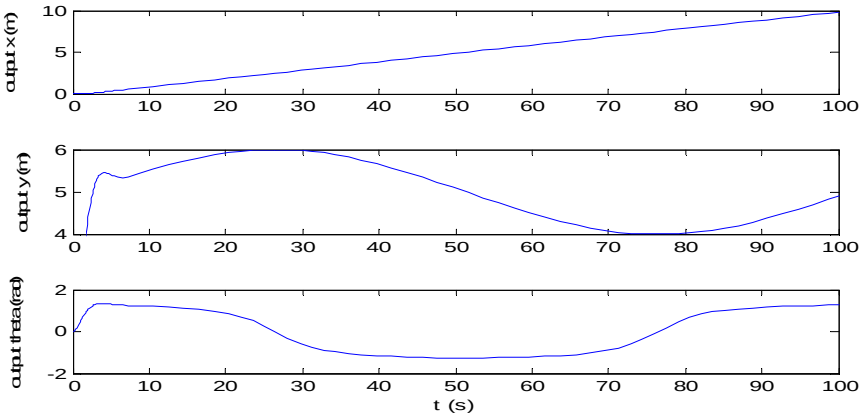

Figure 3.26. Tracking results of the three states

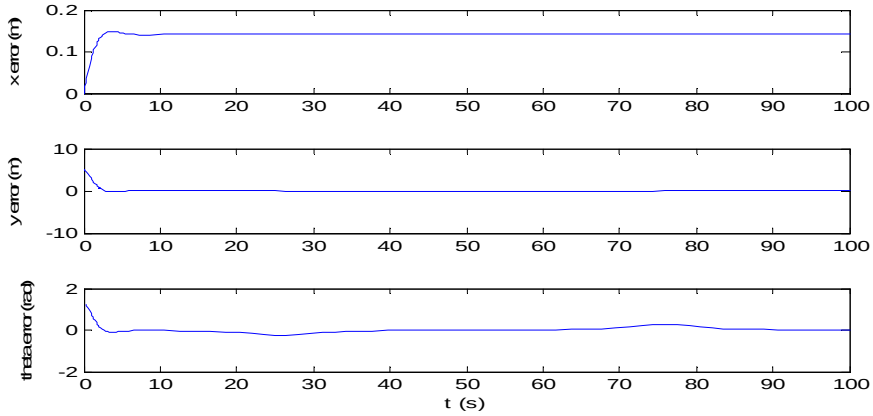

Figure 3.27. Tracking errors of the three states

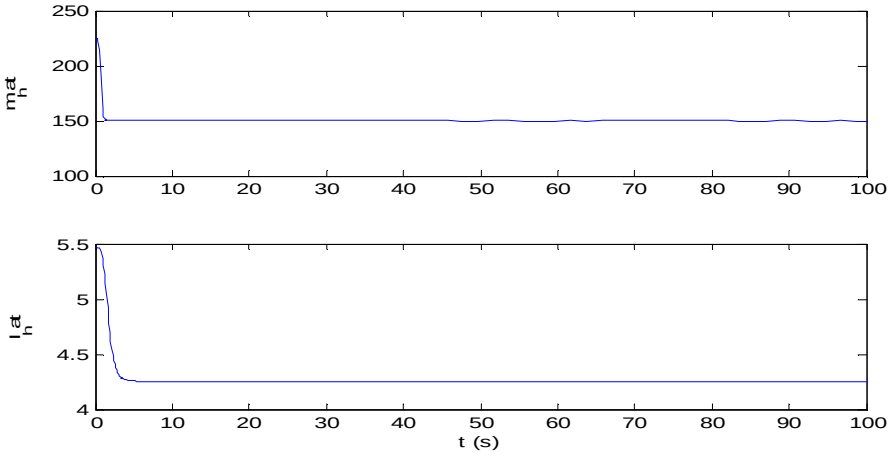

Figure 3.28. Parameter convergence result

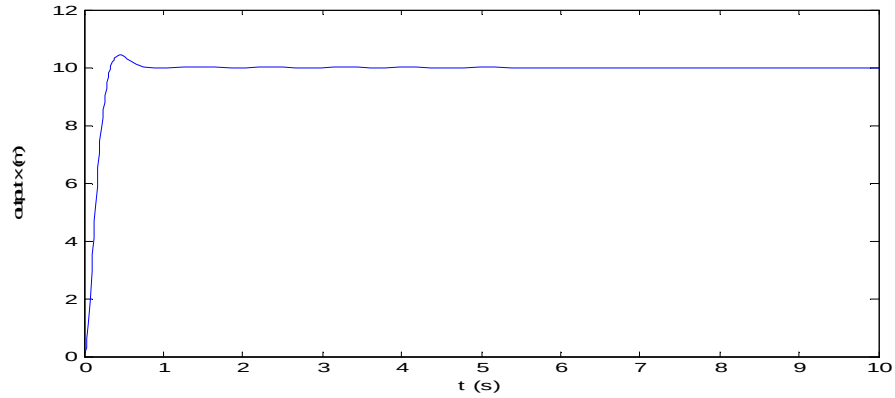

Figure 3.29. Step response of x with estimated parameters

The proposed adaptive control law was investigated with different road condition and different reference input. Figure 3.29 shows when the road condition was changed, the wheel angular speed is still able to track the reference speed by adapting the driving torque input. The speed error between the actual speed and the reference speed converged to zero eventually.

Aforementioned analysis and discussion is all about one wheel control. When it comes to the whole vehicle (four wheel driven robots), the driving torque input on each wheel cannot just depends on the torque command from the individual controller for each wheel. For the purpose of simple illustration, Figure 3.29 is the simulation result of a 4WD drive vehicle. When the road friction coefficient on the left side wheel was

reduced at fifty seconds, the maximum road friction torque was reduced to smaller value, which was even smaller than the command torque. In order to keep the left wheel from slipping, the torque input on the left wheel must be reduced. While the maximum road friction torque on the right wheel did not change. In order to keep the vehicle right on the track, or from deviation, the torque output on the right wheel was also reduced to a certain value.

3.4. The Nonholonomic Manipulator

The mobile manipulator with a 7-DOF manipulator (LWA3) and a 4WD mobile base is shown in Figure 1.3. We can see that every joint of this manipulator is a revolute joint and any two adjacent joints are perpendicular to each other. A gripper is mounted on the end of the seventh link.

The control procedure is described as follows [21, 22, 41]. The 4WD MM receives the six dimensional position and orientation commands of the end-effector from the controller. Then the actual values are gathered and send them to the mobile manipulator at the same time. Then, with the information and the commands, the mobile manipulator controller finds out the best motion path and makes the mobile manipulator respond to implement the task [41]. The feedback data is important for adaptive control to have the ability to perform the redundancy resolution autonomously, which can reduce the burden of the controller effectively [41].

3.4.1. Redundancy Resolution

The coordinate frame of every link is established according to the classical DH representation which is shown in Table 3.1 in order to build the forward kinematic model. The configuration vector of the 7-DOF manipulator can be written as

$$q_a = [q_1 \quad \cdots \quad q_7]^T \tag{3.128}$$

where $q_i (i = 1 \ldots 7)$ is the i[th] joint angle of the manipulator. The configuration vector of the nonholonomic mobile base can be written as

$$q_b = [x \quad y \quad \beta]^T \tag{3.129}$$

In equation (3.129), *x*, *y* are positions on plane axis and β is the orientation of the mobile base. The configuration vector of the mobile manipulator can be defined as

$$q = [q_b \quad q_a]^T \tag{3.130}$$

And the task vector can be written as

$$\xi = [x_e \quad y_e \quad z_e \quad \emptyset_e \quad \theta_e \quad \varphi_e]^T \tag{3.131}$$

In equation 3.131, x_e, y_e, z_e are the position of the end-effector, ϕ_e, θ_e, φ_e, are the orientation defined as Euler Angles. The transformation matrix of the mobile base coordinate frame is defined in equation (3.116) and (3.125) for the mobile manipulator. It can be re-written as

$$B = \begin{bmatrix} c\beta & -s\beta & 0 & x \\ s\beta & c\beta & 0 & y \\ 0 & 0 & 1 & 0 \\ 0 & 0 & 0 & 1 \end{bmatrix} \tag{3.132}$$

The transformation matrix A of the coordinate frame from the base to the end-effector is defined in equation (3.1) and (3.2). The task can be describes as

$$\xi = f(q) = f(q_b, q_a) \tag{3.133}$$

With the constraint of the rolling without slipping condition, the velocity input of this nonholonomic mobile base can be set as [41]

$$\eta_b = [v \quad \omega]^T \tag{3.134}$$

where *v* is the linear velocity and ω is the angular velocity. Therefore, the kinematic model of the mobile base is given as [41]

$$\dot{q}_b = \begin{bmatrix} \dot{x} \\ \dot{y} \\ \dot{\beta} \end{bmatrix} = \begin{bmatrix} c\beta & 0 \\ s\beta & 0 \\ 0 & 1 \end{bmatrix} [v \quad \omega] = G(q_b)\eta_b \tag{3.135}$$

Since the manipulator is a completely unconstrained system, the velocity input can be set as

$$\dot{q}_a = \eta_a \tag{3.136}$$

Then the velocity input for the nonholonomic mobile manipulator is given as

$$\eta = \begin{bmatrix} \eta_b \\ \eta_a \end{bmatrix} \tag{3.137}$$

Hence, the velocity kinematic for the nonholonomic mobile manipulator with respect to time can be calculated by

$$\dot{\xi} = J_n(q)\eta \tag{3.138}$$

where the 6x9 matrix J_n is the Jacobian of the nonholonomic mobile manipulator. For given task ξ, all solutions η to the velocity kinematics in equation (3.138) can be expressed as

$$\eta = J_n^+(q)\dot{\xi} + (I - J_n^+(q)J_n(q))\eta_s \tag{3.139}$$

where the $J_n^+ = J_n^T(J_n J_n^T)^1$ is the right psedue inverse of matrix J_n, $I - J_n^+ J_n$ is the null-space of J_n and η_s is an arbitrary vector.

The design of the velocity kinematic controller is based on the velocity kinematic model of the nonholonomic mobile manipulator in equation (3.139). The control law is a design based on the principle that the end-effector should reach the desired position and orientation within the minimum possible time [41, 21-22].

$$\eta_d = J_n^+(q_c)\left(\dot{\xi}_d - K\xi_{err}\right) + \left(I - J_n^+(q_c)J_n\left(S(T)\right)\right)\alpha\eta_s \tag{3.140}$$

where $\dot{\xi}_d = [\dot{x}_{ed} \quad \dot{y}_{ed} \quad \dot{z}_{ed} \quad \dot{\emptyset}_{ed} \quad \dot{\theta}_{ed} \quad \dot{\varphi}_{ed}]^T$ is the desired velocity of the end-effector, $\xi_{err} = \xi_d - \xi = [x_{err} \quad y_{err} \quad z_{err} \quad \emptyset_{err} \quad \theta_{err} \quad \varphi_{err}]^T$ is the vector of

error from the end-effector's current position and orientation to the desired target, q_c is the online sensor information, K and a are suitable constant gain factors and η_s is an arbitrary vector, which is designed to control the secondary task. Any value given to η_s will have effects on the internal structure of the manipulator only and will not affect the final control of the end-effector at all. By using this controller we can achieve secondary tasks, such as joint limit avoidance, singularity removing, maximum manipulability and obstacle avoidance.

3.4.2. Feedback Linearization of the Nonholonomic Mobile Manipulator

In the general case of an n-link manipulator the dynamic equations represent a multi-input nonlinear system. The conditions for feedback linearization of multi-input systems are more difficult to state, but the conceptual idea is the same as the single-input case. That is, one seeks coordinate systems in which the nonlinearities can be exactly canceled by one or more of the inputs. In the multi-input system we can also decouple the system, that is, linearize the system in such a way that the resulting linear system is composed of subsystems, each of which is affected by only a single one of the outer loop control inputs. Since we are concerned only with the application of these ideas to manipulator control we will not need the most general results in multi-input feedback linearization. Instead, we will use the physical insight gained by our detailed derivation of this result in the single-link case to derive a feedback linearizing control both for n-link rigid manipulators and for 7-link manipulators with elastic joints directly.

Since the generalized torques or forces $\tau_i (i = 1,2..n)$ are the function of the joint variables q, velocities $\dot{q}$, and accelerations $\ddot{q}$, i.e. ,

$$\tau_i = \tau_i(q, \dot{q}, \ddot{q}) \qquad (i=1,2, .. n) \quad (3.141)$$

where q $q = (q_1, q_2 ... q_n)'$, then the first expansion (i.e., linearization) of (3.1) or (3.141) is

$$\delta\tau_i = \sum_{j=1}^{n}\left[\left(\frac{\partial \tau_i}{\partial \ddot{q}_j}\right)^0 \delta\ddot{q}_j + \left(\frac{\partial \tau_i}{\partial \dot{q}_j}\right)^0 \delta\dot{q}_j + \left(\frac{\partial \tau_i}{\partial q_j}\right)^0 \delta q_j\right] \tag{3.142}$$

Throughout this part of the dissertation, a parameter denoted by a right superscript zero is evaluated about the nominal trajectory; δq_i denotes the perturbation of the joint variable q_i from the nominal trajectory $q_i^0, i.e., \delta q_i = q_i - q_i^0$ and $\delta\tau_i$ denotes the perturbation of the generalized force/torque τ_i from the nominal generalized force/torque $\tau_i^0, i.e., \delta\tau_i = \tau_i - \tau_i^0$.

In (5.2), we define

$$A_{ij} = \frac{\partial \tau_i}{\partial \ddot{q}_j}\ ,\ B_{ij} = \frac{\partial \tau_i}{\partial \dot{q}_j}/2\ ,\ C_{ij} = \frac{\partial \tau_i}{\partial q_j} \tag{3.143}$$

By using (3.142) and (3.143) can be easily changed into the following vector form:

$$\delta\tau = A^0\delta\ddot{q} + 2B^0\delta\dot{q} + C^0\delta q \tag{3.144}$$

where $\delta\tau = (\delta\tau_1, \delta\tau_2, ..., \delta\tau_n)$ and $\delta q = (\delta q_1, \delta q_2, ..., \delta q_n)'$ and the *i*th row and *j*th column elements of matrices $A^0, B^0,$ and C^0 are $A_{ij}^0, B_{ij}^0,$ and C_{ij}^0 respectively. Because matrix A^0 is symmetric positive-definite, (3.144) can be further rewritten int the following state equation form:

$$\begin{bmatrix}\delta\dot{q}\\ \delta\ddot{q}\end{bmatrix} = \begin{bmatrix}0 & I_n\\ -(A^0)^{-1}C^0 & -2(A^0)^{-1}B^0\end{bmatrix}\begin{bmatrix}\delta q\\ \delta\dot{q}\end{bmatrix} + \begin{bmatrix}0\\ (A^0)^{-1}\end{bmatrix}\delta\tau \tag{3.145}$$

where I_n is the *nxn* identity matrix.

Thus the computational algorithm for deriving the complete linearized dynamic models of robot manipulators can be stated as follows [21-41]:

Function Begin

Input the parameters of each link: $\alpha_i, \theta_i, d_i, I_i, m_i, r_i, \bar{I}_i$ *for i=1, 2, .., n.*

Input the joint positions q*, velocities* $\dot{q}$ *and acceleration* $\ddot{q}$

Compute T_i *with backward recursion*

Compute M_i

Compute M_{ij}

Compute M_{ijk}

Compute M_{ijks}

Compute the inertial force-acceleration sensitivity terms

Compute the centrifugal and Coriolis force-velocity sensitivity terms

Compute the inertial force-position sensitivity terms

Compute the centrifugal and Coriolis force-position sensitivity terms

Compute the gravitational force-position sensitivity terms

Compute the generalized force-position sensitivity terms

Compute the generalized forces/torques τ_i

End.

4. ADAPTIVE CONTROL DESIGN FOR THE NON-HOLONOMIC MOBILE MANIPULATOR

4.1. Introduction

When the vehicle is running, because the load the vehicle varies when it is running, m is changing. Also because the configuration of the loads varies, like moving manipulator or putting loads in different locations, I is changing. Thus we have two dynamically changing and unknown parameters: m and I. This section will discuss how to design a dynamic controller to control the 4-wheel drive vehicle to track an assigned desired trajectory. Following steps which are shown in Figure 4.1 are designed to control nonholonomic mobile manipulator.

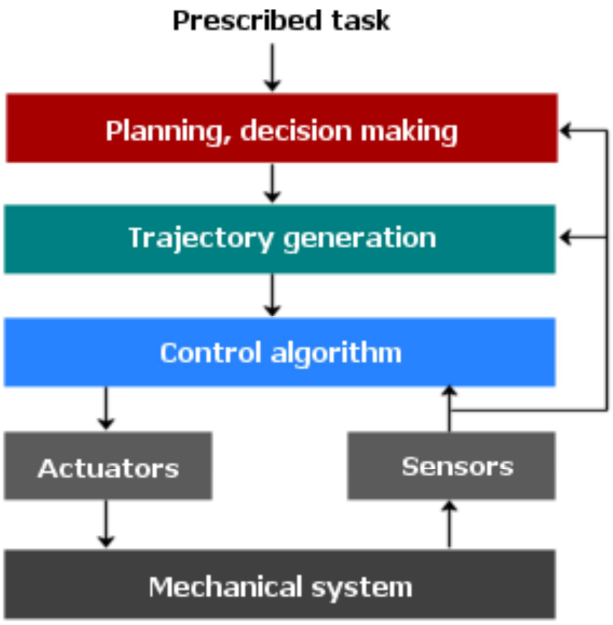

Figure 4.1. Block diagram of robot control

4.2. Model Reference Adaptive Control

To handle the unknown parameters m and I in the plant systems, model reference adaptive control method is used. The objective of the adaptive controller is to make the performance of each of states x, y and θ be as same as a predefined second-order reference model. Block diagram of model reference adaptive control [58 - 90] is shown in Figure 4.2.

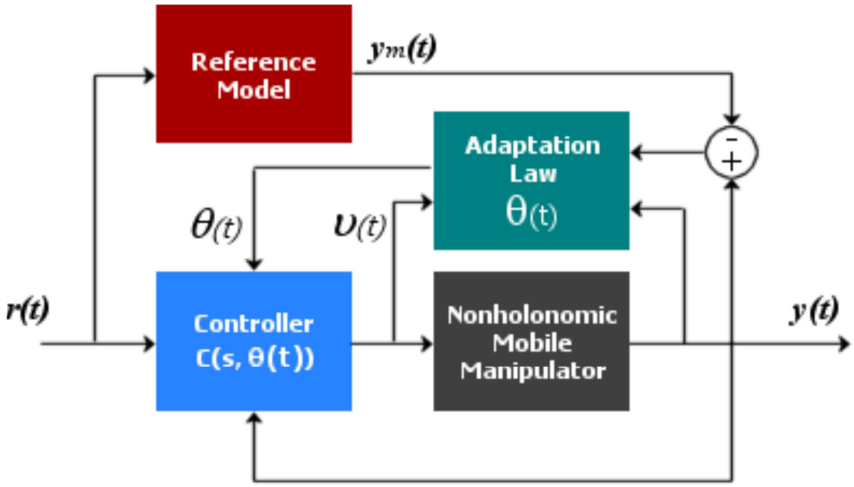

Figure 4.2. Block diagram of model reference adaptive control

The desired performance is chosen as settling time < 2 s and percentage overshoot < 5%. Thus choose $w_n = 10\ rad/s$ and $\zeta = 0.707$, we get the reference model as:

$$W_m(s) = \frac{y_m}{r} = \frac{100}{s^2 + 14.14s + 100} \tag{4.1}$$

We have three states and three independent linear plant systems, so we will have three independent adaptive control laws. Because the plant system and the reference system are both second order and the relative degrees are both 2. By using model reference adaptive control, the whole control system diagram with nonlinear feedback control law can be described in the figure below. For the model reference adaptive control part, the adaptive control laws for each state can be described as

$$u_x = \theta_{x_1}^* \frac{1}{s+1} u_x + \theta_{x_2}^* \frac{1}{s+1} x + \theta_{x_3}^* x + c_{x_0}^* r_x \tag{4.2}$$

$$u_y = \theta_{y_1}^* \frac{1}{s+1} u_y + \theta_{y_2}^* \frac{1}{s+1} y + \theta_{y_3}^* y + c_{y_0}^* r_y \tag{4.3}$$

$$u_\theta = \theta_{\theta_1}^* \frac{1}{s+1} u_\theta + \theta_{\theta_2}^* \frac{1}{s+1} \theta + \theta_{\theta_3}^* \theta + c_{\theta_0}^* r_\theta \tag{4.4}$$

where, θ* and c* are all unknown control parameters, and r_x, r_y and r_θ are the desired inputs for each state separately.

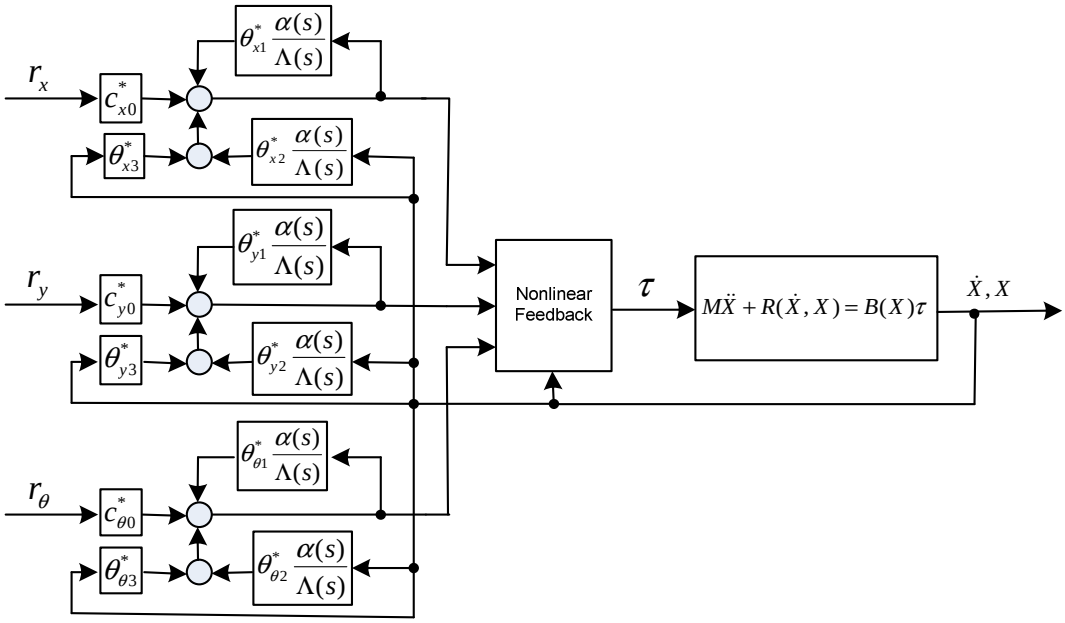

Figure 4.3. Adaptive tracking system diagram

Using model reference adaptive control, we usually have two choices: direct method and indirect method. Direct method means to determine the controller parameters directly by using some adaption laws and indirect method means to determine the internal unknown parameters by using some adaption laws first and then derive the controller parameters. If we use direct adaptive control, there will be totally 12 unknown parameters of θ^* and c^* to determine. This is too complicated and time-

consuming. As we know before, there are actually only two unknown parameters for the plant, so we try to find an indirect adaptive control law to estimate m and I first and then compute the 12 controller parameters.

Plug the adaptive control law into the three linear plant systems and make the transfer function of each of the closed-loop systems equal to the transfer function of the reference model$W_m(s)$, and then we get:

$$\theta_{x_1}^* = -14.14, \theta_{x_2}^* = -14.14m, \theta_{x_3}^* = -114.14m, c_{x_0}^* = 100m$$

$$\theta_{y_1}^* = -14.14, \theta_{y_2}^* = -14.14m, \theta_{y_3}^* = -114.14m, c_{y_0}^* = 100m$$

$$\theta_{\theta_1}^* = -14.14, \theta_{\theta_2}^* = -14.14I, \theta_{\theta_3}^* = -114.14I, c_{\theta_0}^* = 100I$$

These equations provide a relationship between the 12 unknown controller parameters and the two unknown parameters *m* and *I*. Once we have got the estimation of the two unknown parameters as $\hat{m}$ and $\hat{I}$, furthermore, by using the relationship above, we can therefore derive the new model reference adaptive control laws containing only the estimation of the two unknown parameters as

$$u_x = -\frac{14.14}{s+1}u_x + \hat{m}\left(\frac{14.14}{s+1}x - 114.14x + 100r_x\right) \tag{4.5}$$

$$u_y = -\frac{14.14}{s+1}u_y + \hat{m}\left(\frac{14.14}{s+1}y - 114.14y + 100r_y\right) \tag{4.6}$$

$$u_\theta = -\frac{14.14}{s+1}u_\theta + \hat{m}\left(\frac{14.14}{s+1}\theta - 114.14\theta + 100r_\theta\right) \tag{4.7}$$

4.3. Adaptive Tracking Control Design

4.3.1. Linearization and decupling

Because the dynamic model derived in Chapter 3 is a nonlinear and coupled multi-input-multi-output system, it is hard to design a controller for this kind of systems. Especially for using adaptive control method, we require some kind of single-

input-single-output systems as plants. Thus, we use the nonlinear feedback technique to linearize and decouple the dynamic system. The nonlinear feedback control law is designed as

$$A\dot{X} = 0 \tag{4.8}$$

$$\tau = B^*(u + R(\dot{X}, X)) \tag{4.9}$$

where, B^* is the pseudo inverse of *B*, and $u = [u_x \quad u_y \quad u_\theta]^T$ is the virtual internal input vector. Plug it into the dynamic model, we have,

$$M\ddot{X} = u \tag{4.10}$$

Therefore, we get three independent linearized and decoupled systems as

$$m\ddot{x} = u_x \tag{4.11}$$

$$m\ddot{y} = u_y \tag{4.12}$$

$$I\ddot{\theta} = u_\theta \tag{4.13}$$

By Laplacian transformation, we get the transfer functions of the three independent linear plant systems as,

$$G_x(s) = \frac{x}{u_x} = \frac{1}{ms^2} \tag{4.14}$$

$$G_y(s) = \frac{y}{u_y} = \frac{1}{ms^2} \tag{4.15}$$

$$G_\theta(s) = \frac{\theta}{u_\theta} = \frac{1}{Is^2} \tag{4.16}$$

where, m and I are the unknown parameters.

4.3.2. Parameter error convergence

This subsection will discuss the estimation the two unknown parameters m and I. From the transfer functions of each state, we have

$$u_x = m_1 s^2 x \tag{4.17}$$

$$u_y = m_2 s^2 y \tag{4.18}$$

$$u_\theta = I s^2 \theta \tag{4.19}$$

For implementation reason, the previous systems are divided by $(s+1)^2$ on both sides, and then we have

$$\frac{1}{(s+1)^2} u_x = m_1 \frac{s^2}{(s+1)^2} x \tag{4.20}$$

$$\frac{1}{(s+1)^2} u_y = m_2 \frac{s^2}{(s+1)^2} y \tag{4.21}$$

$$\frac{1}{(s+1)^2} u_\theta = I \frac{s^2}{(s+1)^2} \theta \tag{4.22}$$

Because u_x, u_y and u_θ are some virtual internal inputs and not measurable, we need to transform these variables to functions of some measurable variables. From the nonlinear feedback law equation (4.9), we have

$$u = B\tau - R(\dot{X}, X) \tag{4.23}$$

Thus, we have

$$u_x = \frac{\cos(\theta)}{r}(\tau_1 + \tau_2 + \tau_3 + \tau_4) - \cos(\theta)\sum_{i=1}^{4} \mu_{sci} mg \operatorname{sgn}(\dot{x}) - \sin(\theta)\sum_{i=1}^{4} \mu_{lci} mg \operatorname{sgn}(\dot{y}) \tag{4.24}$$

$$u_y = \frac{\sin(\theta)}{r}(\tau_1 + \tau_2 + \tau_3 + \tau_4) - \sin(\theta)\sum_{i=1}^{4} \mu_{sci} mg \operatorname{sgn}(\dot{x}) + \cos(\theta)\sum_{i=1}^{4} \mu_{lci} mg \operatorname{sgn}(\dot{y}) \tag{4.25}$$

$$u_\theta = -\frac{a}{r}(\tau_1+\tau_2)+\frac{c}{r}(\tau_3+\tau_4)$$
$$-a\sum_{i=1,4}\mu_{lci}mg\,\mathrm{sgn}(\dot{y})+b\sum_{i=2,3}\mu_{lci}mg\,\mathrm{sgn}(\dot{y})+c\left[-\sum_{i=1,2}\mu_{sci}mg\,\mathrm{sgn}(\dot{x})+b\sum_{i=3,4}\mu_{sci}mg\,\mathrm{sgn}(\dot{x})\right] \quad (4.26)$$

where, all variables are measurable. Therefore, we have the following SPMs:

$$z_1 = m_1\phi_1 \text{, where, } z_1 = \frac{1}{(s+1)^2}u_x \text{ and } \phi_1 = \frac{s^2}{(s+1)^2}x$$

$$z_2 = m_2\phi_2 \text{, where, } z_2 = \frac{1}{(s+1)^2}u_y \text{ and } \phi_2 = \frac{s^2}{(s+1)^2}y$$

$$z_3 = I\phi_3 \text{, where, } z_3 = \frac{1}{(s+1)^2}u_\theta \text{ and } \phi_3 = \frac{s^2}{(s+1)^2}\theta$$

With our priori knowledge, we have $100 \le m \le 250\,(kg)$ and $3.125 \le I \le 7.813\,(kg\cdot m^2)$. Thus we can choose the initial values of $\hat{m}$ and $\hat{I}$ as 225 kg and 5.469 $kg\cdot m^2$, which are the middle values of the two ranges. By using Gradient Algorithm with normalization and projection, we have the adaption laws as:

$$\dot{\hat{m}}_1 = \begin{cases} \gamma_1\varepsilon_1\phi_1, & \text{if } 100 \le \hat{m}_1 \le 250 \\ & \text{or if } \hat{m}_1 = 100 \text{ and } \varepsilon_1\phi_1 \ge 0 \\ & \text{or if } \hat{m}_1 = 250 \text{ and } \varepsilon_1\phi_1 \le 0 \\ 0, & \text{otherwise} \end{cases} \quad (4.27)$$

where, $\varepsilon_1 = \dfrac{z_1 - \hat{m}_1\phi_1}{(1+\phi_1^2)^2}$ and $\hat{m}_1(0) = 225$.

$$\dot{\hat{m}}_2 = \begin{cases} \gamma_2\varepsilon_2\phi_2, & \text{if } 100 \le \hat{m}_2 \le 250 \\ & \text{or if } \hat{m}_2 = 100 \text{ and } \varepsilon_2\phi_2 \ge 0 \\ & \text{or if } \hat{m}_2 = 250 \text{ and } \varepsilon_2\phi_2 \le 0 \\ 0, & \text{otherwise} \end{cases} \quad (4.28)$$

where, $\varepsilon_2 = \dfrac{z_2 - \hat{m}_2\phi_2}{(1+\phi_2^2)^2}$ and $\hat{m}_2(0) = 225$.

$$\dot{\hat{I}} = \begin{cases} \gamma_3 \varepsilon_3 \phi_3, & \text{if } 100 \le \hat{I} \le 250 \\ & \text{or if } \hat{I} = 100 \text{ and } \varepsilon_3 \phi_3 \ge 0 \\ & \text{or if } \hat{I} = 250 \text{ and } \varepsilon_3 \phi_3 \le 0 \\ 0, & \text{otherwise} \end{cases} \tag{4.29}$$

where, $\varepsilon_3 = \dfrac{z_3 - \hat{I}\phi_3}{(1+\phi_3^2)^3}$ and $\hat{I}(0) = 5.469$.

With the adaption laws above, we can get the unknown parameter estimates of $\hat{m} = \dfrac{\hat{m}_1 + \hat{m}_2}{2}$ and $\hat{I}$. Plug them into the control laws above, and we can get the complete model reference adaptive control laws.

4.3.3. Tracking control design

In the previous design, the reference signal tracking has been realized by using model reference adaptive control laws and nonlinear feedback law. Given a desired trajectory with respect to time, $X_d(t) = [x_d(t) \quad y_d(t) \quad \theta_d(t)]^T$, by using the derived adaptive control laws, we get the three virtual internal inputs as

$$u_x = -\frac{7.7}{s+1}u_x + \hat{m}\left(\frac{14.14}{s+1}x - 144.14x + 100mx_d(t)\right) \tag{4.30}$$

$$u_y = -\frac{7.7}{s+1}u_y + \hat{m}\left(\frac{14.14}{s+1}y - 144.14y + 100my_d(t)\right) \tag{4.31}$$

$$u_\theta = -\frac{7.7}{s+1}u_\theta + \hat{I}\left(\frac{14.14}{s+1}\theta - 144.14\theta + 100Ix_\theta(t)\right) \tag{4.32}$$

Furthermore, with the nonlinear feedback law equation (4.9), we can eventually get the four input torques of the vehicle for tracking the desired trajectory.

5. CASE STUDIES AND DISCUSSIONS

5.1. Simulation Validation and Results

The designed adaptive tracking control method for the 4-wheel drive mobile platform is implemented by simulation in MATLAB software. The desired trajectory is chosen a sine curve along x axis, as shown in Figure 5.1. The speed along x axis is chosen as a constant of 0.1 m/s. The trajectories of the three states, x, y and θ, are shown in Figure 5.2 separately.

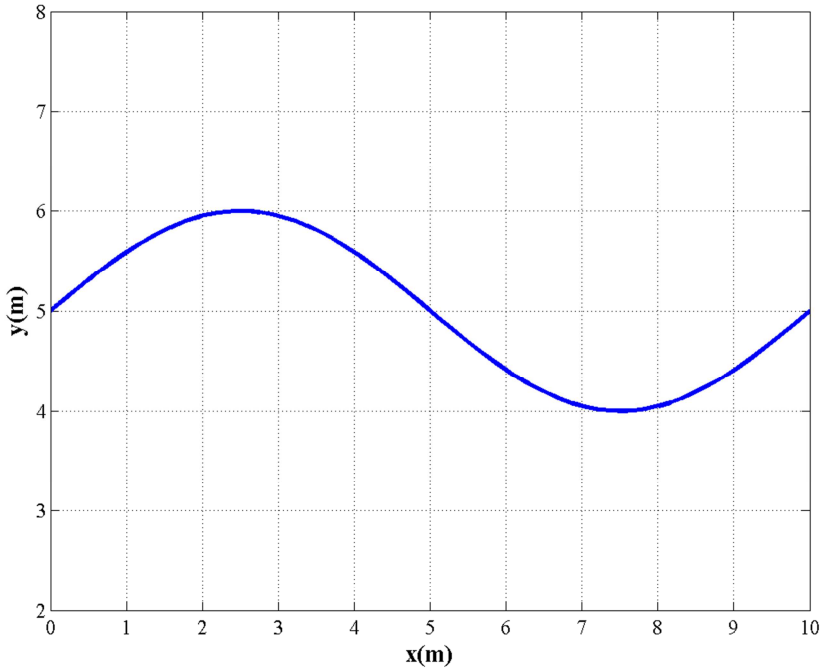

Figure 5.1. Desired trajectory on the 4WD ground vehicle

In the simulation, the mass m and inertia moment I of the 4WD ground vehicle are assumed to be unknown. The real value of them are set as 150 kg and 4.25 $kg \cdot m^2$. With implementing the model reference adaptive control laws, gradient algorithm based parameter estimation and nonlinear feedback control law, the simulated tracking results are shown in Figure 5.1 – 5.5. The desired trajectory and the tracking results errors for all the three states are shown in Figure 5.2. And also tracking errors for all the three states are shown in Figure 5.7. From these results, we can see that the designed adaptive tracking controller can make the three states track the desired trajectories very well as

time increasing and all the tracking errors approach to zero asymptotically fast as time goes to zero.

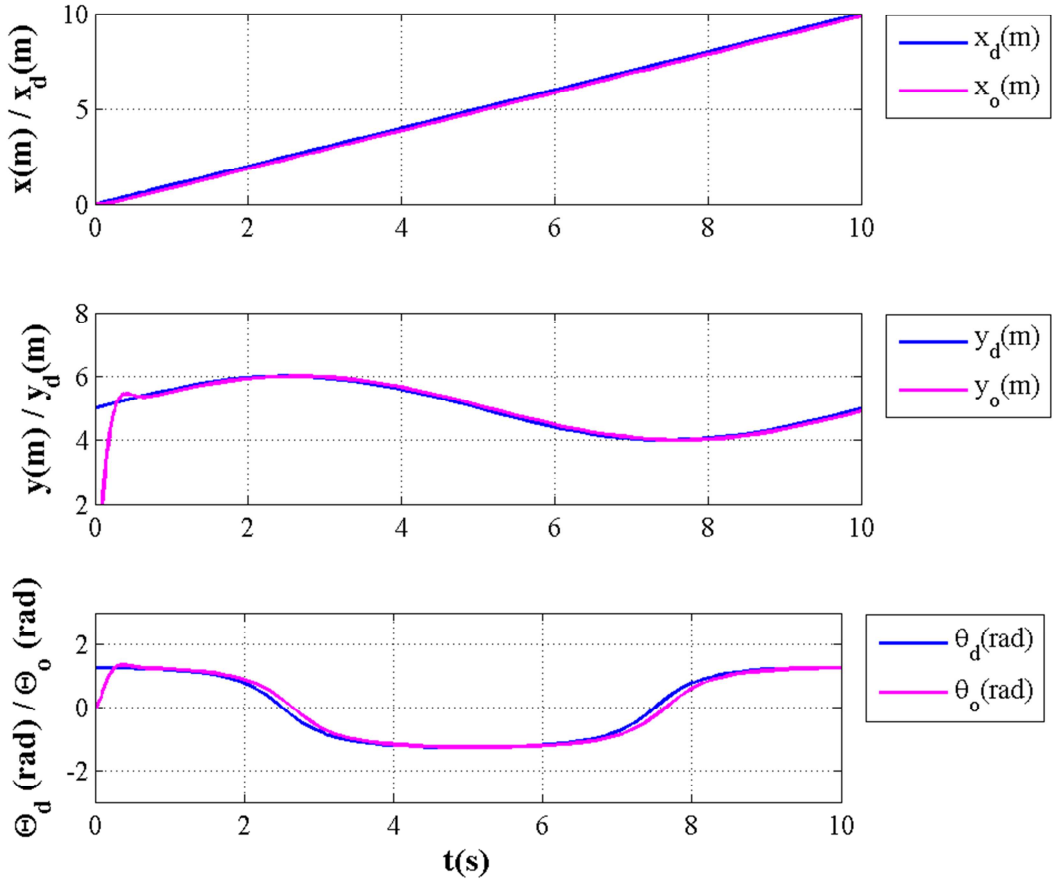

Figure 5.2. Desired trajectories and tracking results of the three states

The parameter convergence result for the two unknown 4WD ground vehicle parameters is shown in Figure 5.4. It is seen that the estimation laws can make the estimated values approach to the real values of the two parameters asymptotically as time increasing, and once the values reaches the real values, they will remain unchanged any more.

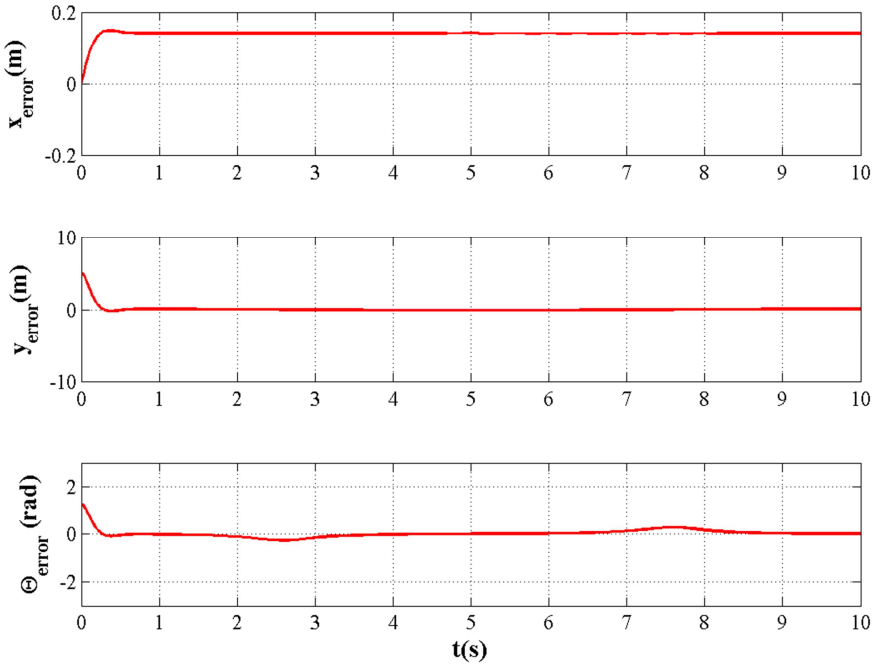

Figure 5.3. Tracking errors of the three states

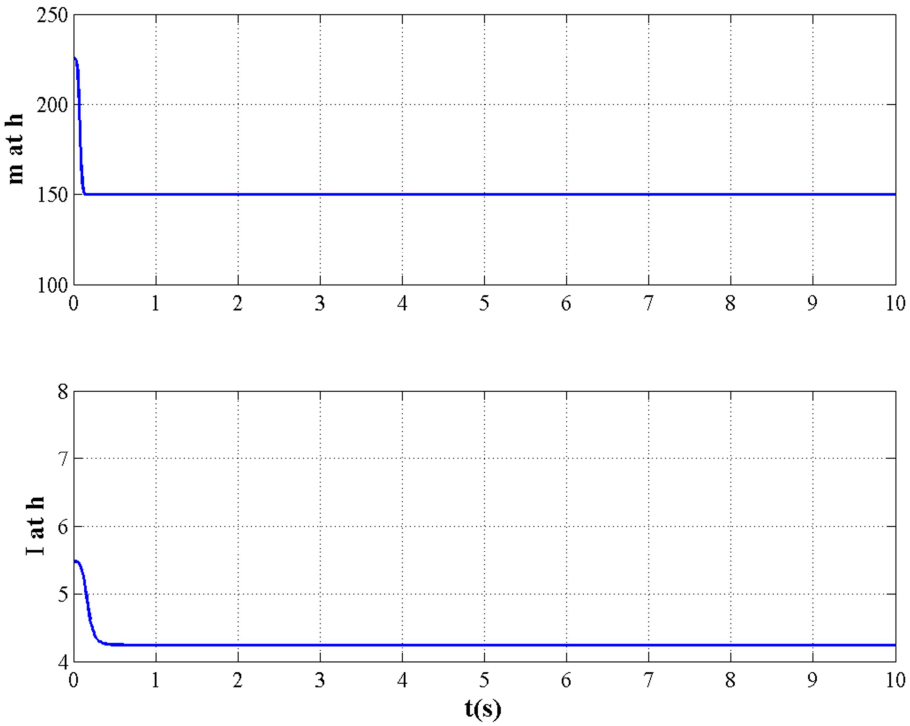

Figure 5.4. Parameter convergence result

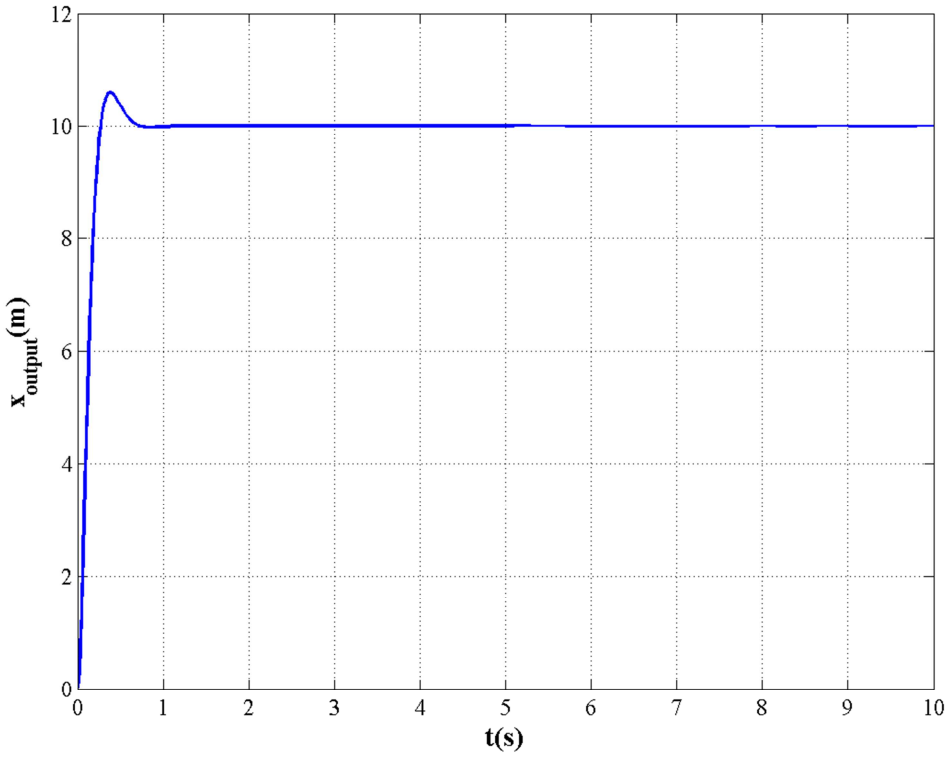

Figure 5.5. Step response of x with estimated parameters

The step response of the state x with estimated parameters is shown in Figure 5.5 from the step response plot, we can see that the settling time is smaller than 2 s and percentage overshoot is smaller than 5%. Thus the requirements of the adaptive controller are satisfied as well.

5.2. Real System Experiments

Videos of real system experiments can be found in Appendix. Some of screenshots of real system experiments are shown in Figure 5.6, 5.7, 5.8 and 5.9. Path tracking experiment is illustrated in Figure 5.6. In Figure 5.7 and Figure 5.8, position and precise trajectory planning experiments are demonstrated. Trajectory tracking experiment is illustrated in Figure 5.9.

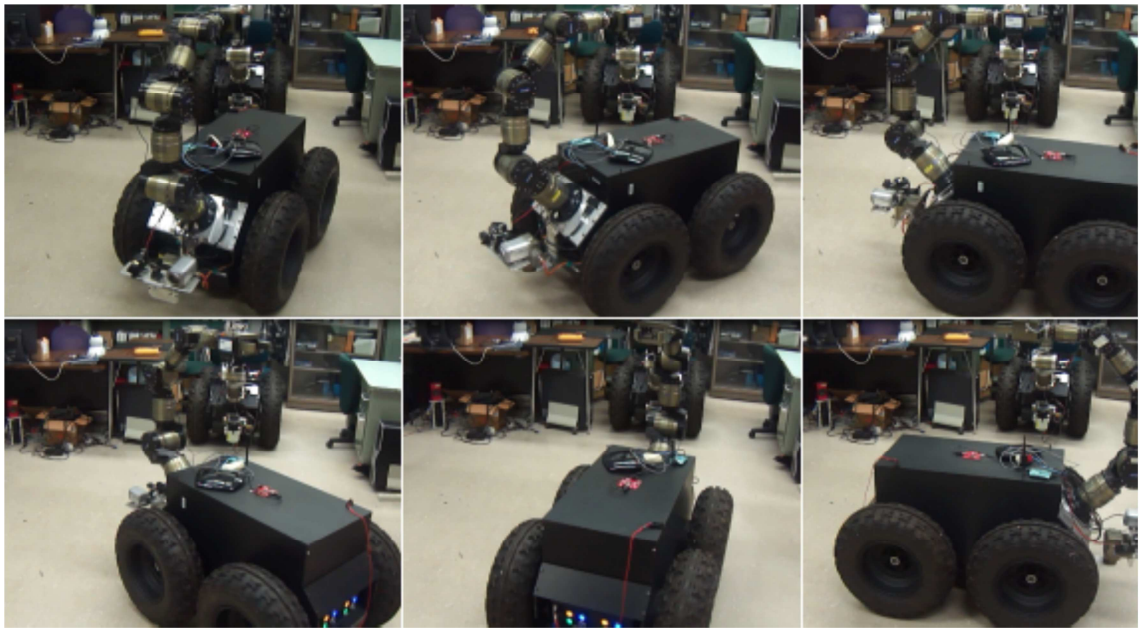

Figure 5.6. View from path tracking experiment

Figure 5.7. View from position and precise trajectory planning experiment 1

Figure 5.8. View from position and precise trajectory planning experiment 2

Figure 5.9. View from position and precise trajectory tracking experiment

5.3. Discussions

In this study, an adaptive tracking control method for a 4WD ground vehicle with unknown vehicle parameters has been studied. The dynamic model of the system with unknown vehicle parameters is derived. A nonlinear feedback law is used to linearize

and decouple the system into three independent and linear systems. A model reference adaptive control method with gradient algorithm based estimation is used to design the tracking controller under unknown mass and inertia moment of mobile manipulator. Simulation is implemented and the results show the designed controller can make the 4WD ground vehicle well track a desired trajectory and satisfy the predefined requirements with the unknown vehicle parameters. For future work, this method can be extended to cope with more complicated cases, such as variable parameters, unknown road conditions, etc. These new unknown parameters can be added and the road conditions can be modeled and involved into the system model. Then the proposed adaptive control method can be modified and applied to estimate these new unknown parameters and realize the tracking control under the new challenges.

6. CONCLUSIONS

In the first part of this study, dynamic modeling, control and analysis of the Schunk LWA3 was performed in simulation environment. The LWA3 is a high-accuracy robotic arm for precise manipulation tasks in both industrial applications and scientific researches. However, there are no enough technical details and information about the dynamic modeling of the Schunk LWA3 from literature review. Dynamic models of robots define the relationship between the motion of the robot and the actuator torques, which is very important for precise control of manipulators. This study is focused on the development of the dynamic model of the Schunk LWA3 robot arm, identification of unknown dynamics parameters and the dynamic control design for the arm. The dynamic model and desired dynamic controller are verified by a trajectory tracking test through simulation. Friction forces were modeled and were added to dynamical model as a disturbance. The parameters of the dynamic model were defined in detail and grouped. A model-based PD controller was developed and it was used to evaluate the identified dynamic model with trajectory tracking experiment. Accuracy of proposed model was verified in this experiment. According to Fig.5, stability of each joint can be observed. Consequently, developing dynamic model-based controller for the Schunk LWA3 is high importance. Because, the Schunk LWA3 redundant 7-DOF manipulator is used not only scientific researches but also industrial applications. There are not enough researches in literature about this kind of manipulators. Simulation results verify that dynamic model of the manipulator is used accurately. Developed controller will be tested in real environment. And then, simulation results and real environment test results will be compered as a future work.

In the second part of this study, an adaptive tracking control method for a 4WD ground vehicle with unknown vehicle parameters has been studied. The dynamic model of the system with unknown vehicle parameters is derived. A nonlinear feedback law is used to linearize and decouple the system into three independent and linear systems. A model reference adaptive control method with gradient algorithm based estimation is used to design the tracking controller under unknown mass and inertia moment of mobile manipulator. Simulation is implemented and the results show the designed controller can make the 4WD ground vehicle well track a desired trajectory and satisfy

the predefined requirements with the unknown vehicle parameters. For future work, this method can be extended to cope with more complicated cases, such as variable parameters, unknown road conditions, etc. These new unknown parameters can be added and the road conditions can be modeled and involved into the system model. Then the proposed adaptive control method can be modified and applied to estimate these new unknown parameters and realize the tracking control under the new challenges.

Mobile manipulators offer a dual advantage of mobility and dexterity of a mobile robot and a manipulator. They are composed of a manipulator and a mobile platform. Mobile manipulators have a much larger workspace than fixed–base manipulators. Also, they are more capable than mobile robots. While an on-board manipulator reaches out and performs manipulation tasks, the role of the mobile platform is to adjust a position of the mobile manipulator according to preferred configuration. Mobile manipulators can be used in various military and civilian areas including space exploration, military operations, auto-manufacturing and health-care, etc. In this study, an adaptive tracking controller for a mobile manipulator which consists of a 4-wheel drive(4WD) ground vehicle and a 7-DOF robot arm with unknown vehicle parameters is designed to track an assigned desired trajectory under unknown vehicle parameters. The simulation results are demonstrated the correctness and effectiveness of the performance of the proposed controller.

REFERENCES

[1] J. Swevers, W. Verdonck and J. DeSchutter (2007), "Dynamic Model Identification for Industrial Robots", IEEE Control Systems Magazine, pages 58-71.

[2] T.J. Tarn, Y. Wu, N. Xi and A. Isidori (1996), "Force Regulation and Contact Transition Control", IEEE Control System, Vol. 16, Issue 1, pp.32-40, 1996.

[3] O.Khatib (1987), "A Unified Approach for Motion and Force Control of Robot Manipulators: the Operational Space Formulation", IEEE Journal of Robotics and Automation, Vol. 3, Issue 1, pp. 43-53.

[4] Y. Wu, T.J Tarn, N. Xi and A. Isidori (1996), "On Robust Impact Control via Positive Acceleration Feedback for Robot Manipulators", IEEE International Conference on Robotics and Automation, Vol.2, pp.1891-1896.

[5] M.W. Spong, S. Hutchinson and M. Vidyasagar (2006), "Robot Dynamics and Control", John Wiley & Sons Publishing Co., Hoboken NJ, USA.

[6] J.Wu, J.Wang and Z. You (2010), "An Overview of Dynamic Parameter Identification of Robots", Robotics and Computer – Integrated Manufacturing, Vol. 26, pp.414-419.

[7] B. Siciliano, L. Sciavicco, L. Villan, and G. Oriolo (2010), "Robotics: Modeling, Planning and Control", Springer.

[8] H. Wang, Y Jia, N. Xi and J. Buether (2010), "An Online Motion Planning Algorithm for a 7DOF Redundant Manipulator", IEEE International Conference on Robotics and Biomimetics, pp.1057-1062.

[9] N.D. Voung and M. H. Ang Jr (2009), "Dynamic Model Identification for Industrial Robots", ActaPolytechnicaHungarica, Vol.6, Issue 5, pp.51-68.

[10] J.J. Craig (1988), "Adaptive Control of Mechanical Manipulators", Addison-Wesley Publishing Co.

[11] M. Shimizu, W.K. Yoon, and K. Kitagaki (2007), "A Practical Redundancy Resolution for redundant 7 DOF Manipulators with Joint Limits", IEEE International Conference on Robotics and Automation, pp.4510-4516.

[12] N.A. Bompos, P.K. Artemiadis, A.S. Oikonomopoulos and K.J. Kyriakopoulos (2007), "Modeling, Full Identification and Control of the Mitsubishi PA-10

Robot Arm", IEEE/ASME International Conference on Advanced Intelligent Mechatronics, pp.1-6.

[13] Schunk LWA3 Modular Manipulator Datasheet, 2007.

[14] R. Featherstone and D. Orin (2000), "Robot Dynamics: Equations and Algorithms", IEEE International Conference on Robotics and Automation, pp.826-835.

[15] K. J. Astrom, T. Hagglund (2001), "The Future of PID Control", Control Engineering Practice, Vol.9, pp.1163-1175.

[16] M. Stilman, J. Wang, K. Teeyapan and r. Marceau (2009), "Optimized Control Strategies for Wheeled Humanoids and Mobile Manipulators", 9th IEEE-RAS International Conference on Humanoid Robots, pp.568-573.

[17] R. J. Schilling (1990) , "Fundamentals of Robotics: Analysis and Control", Prentice Hall.

[18] http://www.newtonium.com (Access date: October 16, 2013)

[19] SEGWAY RMP400 Datasheet, (2010).

[20] S.B. Nokleby and R.P. Podhorodeski (2004), "Identifying Multi-DOF-Loss Velocity Degeneracies in Kinematically – Redundant Manipulators", Mechanism and Machine, Vol. 39, pages 201-213.

[21] G.Shuang, N.C. Cheung, K.W.E. Cheng, D. Lei, and L.Xiaozhong (2207), "Skid-Steering in 4-Wheel-Drive Electric Vehicle", 7th International Conference on Power Electronics and Drive Systems (PEDS '07), pages 1548-1553, Bangkok, Thailand.

[22] W. Yu, O.Y. Chuy, E.G. Collins, and P. Hollis (2010), "Analysis and Experimental Verification for Dynamic Modeling of A Skid-Steering Wheeled Vehicle", IEEE Transaction on Robotic, Vol. 26, No. 2, pages 340-353.

[23] K. Kozlowski and D. Pazderski (2004), "Modeling and Control of A 4-Wheel Skid-Steering Mobile Robot", International Journal of Applied Mathematics and Computer Science, Vol. 14, No. 4, pages 477-496.

[24] L. Caracciolo, A. De Luca, and S. Iannitti (1999), "Trajectory tracking control of a four-wheel differentially driven mobile robot", IEEE International Conference on Robotics and Automation, Detroit MI, USA, pages 2632–2638.

[25] S. Arslan and H. Temeltaş (2011), “Robust Motion Control of A Four Wheel Drive Skid-Steered Mobile Robot”, 7th International Conference on Electrical and Electronics Engineering (ELECO 2011), pages II-415-II-41, Bursa, Turkey.

[26] D. Pazderski, K. Kozlowski and M. Lawniczak (2004), “Practical Stabilization of 4WD Skid-Steering Mobile Robot”, 4th International Workshop on Robot Motion and Control, pages 175-180, Puszczykowo, Poland.

[27] Y. Wang, Y. Jia, X. Li and N. Xi (2011), “Dynamics modeling of a mobile manipulator for wheel slip avoidance”, IEEE International Conference on Robotics and Biomimetics (ROBIO 2011), pages 1621-1626, Phuket Island, Thailand.

[28] Mandow, J.L. Martinez, J. Morales, and J.L. Blanco (2007), “Experimental Kinematics for Wheeled Skid-Steer Mobile Robots”, IEEE/RSJ International Conference on Intelligent Robots and Systems (IROS 2007), pages 1222-1227, San Diego CA, USA.

[29] O. Chuy, E.G. Collins, W. Yu, and C. Ordonez (2009), “Power Modeling of a Skid Steered Wheeled Robotic Ground Vehicle”, IEEE International Conference on Robotics and Automation (ICRA 2009), pages 4118-4123, Kobe, Japan.

[30] V. Nazari and M. Naraghi (2008), “Sliding Mode Fuzzy Control of a Skid Steer Mobile Robot for Path Following”, 10th International Conference on Control, Automation, Robotics and Vision (ICARCV 2008), pages 549-554, Hanoi, Vietnam.

[31] W. Yu, O.Y. Chuy, E.G. Collins and P. Hollis (2009), “Dynamic Modeling of a Skid-Steered Wheeled Vehicle with Experimental Verification”, IEEE/RSJ International Conference on Intelligent Robots and Systems (IROS 2009), pages 4212-4219, St. Louis MO, USA.

[32] E. Maalouf, M. Saad, and H.Saliah (2006), “A Higher Level Path Tracking Controller for A Four-Wheel Differentially Steered Mobile Robot”, Robotics and Autonomous Systems, Vol. 54, pages 23-33.

[33] G.K. Fourlas (2013), “Theoretical approach of model based fault diagnosis for a 4-wheel skid steering mobile robot”, 21st Mediterranean Conference on Control & Automation (MED 2013), pages 597-602, Crete, Greece.

[34] M. Shimizu, H. Kakuya and W.K. Yoon (2008), “Analytical Inverse Kinematic Computation for 7 DOF Redundant Manipulators with Joint Limits and Its Application to Redundancy Resolution”, IEEE Transaction on Robotic, Vol. 24, No. 5, pages 1131-1142.

[35] M.G. Marcos, J.A.T. Machado and T.P.A. Perdicoulis (2009), “Trajectory Planning of Redundant Manipulators Using Genetic Algorithms”, Communication Nonlinear in Nonlinear Science and Numerical Simulation”, Vol. 14, pages 2858-2869.

[36] H. Wang, Y. Jia and N. Xi (2012), “Sensor-Based Redundancy Resolution for a Nonholonomic Mobile Manipulator”, IEEE/RSJ International Conference on Intelligent Robots and Systems (IROS 2012), pages 5327 - 5332, Vilamoura, Portugal.

[37] S. Yahya, M. Moghavvemi and H.A.F. Mohamed (2011), “Geometrical Approach of Planar Hyper-Redundant Manipulators: Inverse Kinematics, Path Planning and Workspace”, Simulation Modeling Practice and Theory, Vol. 19, pages 406 – 422.

[38] S. Sastry and M. Bodson (2011), “Adaptive Control: Stability, Convergence and Robustness”, Dover Publications Inc., Mineola NY, USA.

[39] K.J. Astrom (1987), “Adaptive Feedback Control”, Proceeding of IEEE , pages 185-209.

[40] S. Bharadwaj, A.V. RAo and K.D. Mease (1998), “Entry Trajectory Tracking Law via Feedback Linearization”, Journal of Guidance, Control and Dynamics, Vol. 21, No. 5, pages 726-732.

[41] H. Zhang, Y. Jia, Y.Guo, K. Qian, A. song and N. Xi (2013), “Online Sensor Information and Redundancy Resolution Based Obstacle Avoidance for High DOF Mobile Manipulator Teleoperation”, International Journal of Advanced Robotic Systems, Vol. 10, pages 1-9.

[42] V. Andaluz, F. Roberti and R. Carelli (2010), “Robust Control with Redundancy Resolution and Dynamic Compensation for Mobile Manipulators”, 2010 IEEE International Conference on Industrial Technology (ICIT2010), pages 1469-1474, Vina del Mar, Chile.

[43] Z. Li, S.S. Ge and A. Ming (2007), “Adaptive Robust Motion/Force Control of Holonomic-Constrained Nonholonomic Mobile Manipulators”, IEEE Transaction on Systems, Man, and Cybernetics Part B: Cybernetics”, Vol. 37, no. 3, pages 607 – 616.

[44] A. De Luca, G. Oriolo and P.R. Giordano (2006), “Kinematic Modeling and Redundancy Resolution for nonholonomic Mobile Manipulators”, 2006 IEEE International Conference on Robotics and Automation (ICRA 2006), pages 1867-1873, Orlando FL, USA.

[45] J.H. Chung and S.A. Velinsky (1999), “Robust Interaction Control of a Mobile Manipulator – Dynamic Model Based Coordination”, Journal of Intelligent and Robotic Systems, Vol. 26, pages 47 – 63.

[46] Y. Fujimoto and T. Murakami (2010), “A realization of wheelchair pushing operation considering high tracking performance and ride quality improvement by mobile manipulator”, 11th IEEE International Workshop on Advanced Motion Control, pp. 732 – 737.

[47] T.I.J. Tsay, Lai, Y. F. and Hsiao, Y. L. (2010), “Material handling of a mobile manipulator using an eye-in-hand vision system”, 2010 IEEE/RSJ International Conference on Intelligent Robots and Systems, pp. 4743 – 4748.

[48] G. Scaglia, A. Rosales, L. Quintero, V. Mut and R. Agarwal (2010), "A linear-interpolation-based controller design for trajectory tracking of mobile robots", Control Engineering Practice, Vol. 18, pp.318–329.

[49] C.Y. Chen, T.H S. Li, Y.C Yeh and C.C Chang (2009), "Design and implementation of an adaptive sliding-mode dynamic controller for wheeled mobile robots", Mechatronics, Vol. 19, pp.156–166.

[50] J. Wang and Y. Li (2009), "Dynamic Control and Analysis of a Nonholonomic Mobile Modular Robot", Lecture Notes in Computer Science-Intelligent Robotics and Applications, Volume 5928, pp.776-791.

[51] H. Khaloozadeh, M. A. Nekoui, and F. Shahni (2010), "Adaptive Tracking and Asymptotic Rejection of Unknown but Bounded Disturbances in Nonlinear MIMO Systems", International Journal of Control, Automation, and Systems, Vol. 8, Issue 3, pp.527-533.

[52] K. Shojaei, A.M. Shahri and A. Tarakameh (2011), "Adaptive feedback linearizing control of nonholonomic wheeled mobile robots in presence of parametric and nonparametric uncertainties", Robotics and Computer-Integrated Manufacturing, Vol. 27, pp.194–204.

[53] F. Yang and C. Wang (2012), "Adaptive tracking control for uncertain dynamic nonholonomic mobile robots based on visual servoing", Journal of Control Theory and Applications, Vol.10, Issue 1, pp.56-63.

[54] J. Cheong, W. Eom and J. Lee (2009), "Cornering stability improvement for 4 wheel drive hybrid electric vehicle", IEEE International Symposium on Industrial Electronics, pp. 853 – 858.

[55] M. Akar (2006), "Yaw rate and sideslip tracking for 4-wheel steering cars using sliding mode control", 2006 IEEE International Symposium on Intelligent Control, pp. 1300 – 1305.

[56] M. Barreras, C. Villegas, M. Garcia-Sanz and J. Kalkkuhl (2006), "Robust QFT tracking controller design for a car equipped with 4-wheel steer-by-wire Computer Aided Control System Design", 2006 IEEE International Conference on Control Applications, pp. 1312 – 1317, 2006.

[57] Y.K. Tham, H. Wang and E.K. Teoh (1998), "Adaptive state estimation for 4-wheel steerable industrial vehicles", Proceedings of the 37th IEEE Conference on Decision and Control, pp. 4509 – 4514.

[58] T. Nakakuki, T. Shen, and K. Tamura (2008), "Adaptive control approach to uncertain longitudinal tire slip in traction control of vehicle", Asian Journal of Control, Vol. 10, Issue 1, pp. 67-73.

[59] J. Yi, L. Alvares, R. Horowitz and C. Canudas (2000), "Adaptive emergency braking control using a dynamic tire/road friction model", Proceedings of the 39th IEEE Conference on Decision and Control, pp. 456 – 461.

[60] V. Andaluz, F. Roberti and R. Carelli (2010), "Adaptive Control with Redundancy Resolution of Mobile Manipulators", Proceedings of the 36th Annual Conference of the IEEE Industrial Electronics Society, pp.1436 – 1441.

[61] L.A.Z. Aviles, J.C.P. Ortega, and E.G. Hurtado (2012), "Experimental Study of the Methodology for the Modelling and Simulation of Mobile Manipulators", International Journal of Advanced Robotic Systems, Vol 9, pp. 1-10.

[62] V.T. Dinh, H. Nguyen, S.M. Shin, H.K. Kim, S.B. Kim, and G.S. Byun (2012), "Tracking Control of Omnidirectional Mobile Platform with Disturbance Using Differential Sliding Mode Controller", International Journal of Precision Engineering and Manufacturing, Vol. 13, No. 1, pp. 39-48.

[63] J.H. Chung and S.A. Velinsky (1998), "Modeling and control of a mobile manipulator", Robotica, Vol. 16, pp. 607-613.

[64] Gang Tao (2003), "Adaptive Control Design and Analysis", John Wiley & Sons Publishing Co., Hoboken NJ, USA.

[65] K. Astrom and B.Wittenmark (2008), Dover Publications Inc., Mineola NY, USA.

[66] Peter Corke (2011), "Robotics, Vision and Control Fundamental Algorithms in MATLAB®", Springer-Verlag Berlin Heidelberg, Berlin, Germany.

[67] D.C. Karnopp, D.L. Margolis and R.C. Rosenberg(2012), "System Dynamics: Modeling, Simulation, and Control of Mechatronic Systems", John Wiley & Sons Publishing Co., Hoboken NJ, USA.

[68] R. E. Parkin (1991), “Applied Robotic Analysis”, Prentice Hall, Upper Saddle River NJ, USA.

[69] S. B. Niku (2001), “Introduction to robotics Analysis, Systems, Applications”, Prentice Hall, Upper Saddle River NJ, USA.

[70] B. Siciliano, O. Khatib (2008), “Springer Handbook of Robotics”, Springer, Berlin, Germany.

[71] P. Mellodge, P. Kachroo (2009),”Model Abstraction in Dynamical Systems: Application to Mobile Robot Control”, Springer, Berlin, Germany.

[72] E. Dombre, W. Khalil (2007), “Modeling, Performance Analysis and Control of Robot Manipulators “, ISTE Ltd., Londan UK.

[73] T. Bajd, M. Mihelj, J. Lenarcic, A. Stanovnik, M. Munih (2010), “Robotics”, Springer, Berlin, Germany.

[74] R. Featherstone (2008), “Rigid Body Dynamics Algorithms“, Springer, Berlin, Germany.

[75] T. Kröger, F. M. Wahl (2009), “Advances in Robotics Research: Theory, Implementation, Application”, Springer, Berlin, Germany.

[76] F. Fahimi (2009), “Autonomous Robots: Modeling, Path Planning, and Control”, Springer, Berlin, Germany.

[77] E. Layer, K. Tomczyk (2010), “Measurements, Modelling and Simulation of Dynamic Systems”, Springer, Berlin, Germany.

[78] R.V. Patel, F. Shadpey (2005), “Control of Redundant Robot Manipulators: Theory and Experiments”, Springer, Berlin, Germany.

[79] T. Narikiyo, M. Kawanishi, T. Mizumo and Y. Hanada (2010), “Robust Adaptive Position/Force Control of Mobile Manipulators: Theory and Experiments”, SICE Annual Conference, pp.1326-1331.

[80] R. Colbaugh, E. Barany, and K. Glass (1998), “Adaptive Control of Nonholonomic Robotic Systems”, Journal of Robotic Systems, Vol.15, Issue 7, pp.365-393.

[81] Z. Li, Y. Yang, and J. Li (2010), “Adaptive Motion/Force Control of Mobile Under-Actuated Manipulators with Dynamics Uncertainties by Dynamic Coupling and Output Feedback”, IEEE Tran. on Control Systems Technology, Vol. 18, Issue 5.

[82] Y. Li, Y. Liu and S. Yan (2005), “Adaptive Neural-Network Control for Redundant Nonholonomic Mobile Modular Manipulators”, Lecture Notes in Computer Science Volume 3498, 2005, pp 271-276, Springer Berlin Heidelberg.

[83] Z. Xie, A. Ming and Z. Li (2007), “Adaptive Robust Trajectory and Force Tracking Control of Constrained Mobile Manipulators”, 2007 IEEE International Conference on Mechatronics and Automation, pp.1351-1355.

[84] A. Karray and M. Feki (2010), “Adaptive Tracking Control of a Mobile Manipulator”, 2010 7th International Multi-Conference on Systems, Signals and Devices, pp.1-7.

[85] N. Chen, F. Song, G. Li, X. Sun and C. Ai (2013), “An Adaptive sliding Mode Backstepping Control for the Mobile Manipulator with nonholonomic Constraints”, Communications in Nonlinear Science and Numerical Simulation, Vol.18, pp.2885-2899.

[86] R. Fierro and F. L. Lewis (1997), “Control of a Nonholonomic Mobile Robot: Backstepping Kinematics into Dynamics”, Journal of Robotic Systems, Vol.14, Issue 13, pp.149-163.

[87] M. Boukattaya, T. Damak and M. Jallouli (2011), “Robust Adaptive Control for Mobile Manipulators”, International Journal of Automation and Computing, Vol.8, Issue 1, pp.8-13.

[88] Y. Liu and Y. Li (2006), “Sliding Mode Adaptive Neural-Network Control for Nonholonomic Mobile Modular Manipulators”, Journal of Intelligent and Robotic Systems, Vol.44, pp.203–224.

[89] G. Zhong, Y. Kobayashi, Y. Hoshino and T. Emaru (2013), “System Modeling and Tracking Control of Mobile Manipulator Subjected to Dynamic Interaction and Uncertainty”, Nonlinear Dynamics, Vol.73, pp.167-182.

[90] A. Mazur and K. Arent (2006), “Trajectory Tracking Control for Nonholonomic Mobile Manipulators”, Robot Motion and Control LNCIS 335, pp.55-71, Springer-Verlag London Limited.

CURRICULUM VITAE

Name Surname **:** Gökhan Erdemir

Birth of Place and Date of Birth **:** İstanbul, January 2, 1981

Foreign Language **:** English (fluent)

Email **:** goerdemir@gmail.com

Education

Degree	Department	University / High School	Graduation Year
High School	Computer Programming	Sisli Technical High School, Istanbul, Turkey	1998
Bachelor	Computer and Control Teaching	Marmara University, Istanbul, Turkey	2003
Master	Computer and Control Education	Marmara University, Istanbul, Turkey	2006

Work Experience

Year	Company	Position
Sep. 2012 to Current	Istanbul Aydin University, Istanbul, Turkey Department of Mechatronics Engineering	Lecturer
Jan. 2012 Sep. 2012	University of Michigan, Ann Arbor MI, USA Health Management and Research Center	Senior Analyst Programmer (Part-Time)
Feb. 2011 Sep. 2012	Michigan State University, East Lansing MI, USA Robotics – Automation Laboratory	Research Scholar
Sep. 2006 Feb. 2011	Istanbul Aydin University, Istanbul, Turkey Department of Computer Programming	Lecturer

Publications

International Referred Journals

- KUZUCUOGLU A.E., ERDEMİR G., "Development of a Web-Based Control and Robotic Applications Laboratory for Control Engineering Education", Information Technologies and Control (ISSN: 1392-124X), Vol.40, Issue 4, p.352-358, 2011, DOI: 10.5755/j01.itc.40.4.985.
- GUNAY B., ERDEMİR, G., "Lateral Analysis of Longitudinal Headways in Traffic Flow", International Journal of Engineering and Applied Sciences (IJEAS), Vol.3, Issue 2, p. 90-100, 2011 (ISSN: 1309 – 7997).
- GUNAY B., ERDEMİR, G., "Using Wavelet Transforms for Better Interpretation of Traffic Simulation", Traffic Engineering and Control 50(10) p. 450-453, 2009 (ISSN: 0041 – 0683).

International/National Referred Conferences

- ASLAN Z., ERDEMIR G., TOKGOZLU A., "Analyses of Climate Change Impacts on Wind Speed and Energy Potential by Using ANN", the 7th International Congress on Industrial and Applied Mathematics (ICIAM 2011), July 18 – 22, Vancouver, BC, Canada.
- ERDEMİR G., GÜNAY B., "Analysing Neighbouring Lane Effects on Car Following Headways Using Wavelets", The Fifth International Symposium on Wavelets Applications to World Problems IWW2010, June 7 - 8, Istanbul, Turkey, 2010.
- GUNAY B., ERDEMİR, G., "A Two-Dimensional Adjustment Factor for Better Realism in Multilane Traffic Flow Modeling", the 12th World Conference on Transport Research WCTR2010, Lisbon, Portugal, 2010.
- ERDEMİR G., GÜNAY B., "Scenario Analysis of Microscopic Traffic Simulation Using Wavelets", the 4th International Workshop on Applications of Wavelets to Real World Problems: IWW2009, Kocaeli, Turkey, 2009.

- KAPTANOGLU E., ERDEMİR G., “Internet Based Monitoring of Multivariable Control Using A Quadruple-Tank System for Mechatronics Education”, MECHANICS'08, Kaunas, Lithuania, 2008.
- ERDEMİR G., KUZUCUOĞLU A.E., “Remote-Access Process Control Laboratory for Liquid Level and Flow System”, the 2007 World Congress in Computer Science, Computer Engineering, and Applied Computing (WORLDCOMP'07), Las Vegas NV, USA, 2007.

Projects

- Advisor (2012-2013): “Digital Dermatoscopy and Total Body Mapping System”. This project was supported by TUBITAK.
- Research Scholar (2011-2012): “RGB Color Sensor with Analog/Digital Output”. This project was supported Ministry of Science, Industry and Technology.
- Research Scholar (2008-2009): “Intelligent Color Recognition for Paint Mixture Machine”. This project was supported TUBITAK.

Memberships

1. Institute of Electrical and Electronics Engineers (IEEE)
2. IEEE Control Systems Society
3. IEEE Robotics & Automation Society
4. IEEE Vehicular Technology Society
5. International Society of Automation (ISA)
6. Intelligent Transportation Society of America (ITSA)

Awards and Honors:

1. TUBITAK (The Scientific and Technological Research Council of Turkey) Scholarship, 2010.
2. National Instruments 2007 NI Virtual Instrumentation Applications Paper Contest Second Place winner, 2007.